

Spring 2005

# Biosensing with microcantilever-based sensors

Xiaodong Yan  
*Louisiana Tech University*

Follow this and additional works at: <https://digitalcommons.latech.edu/dissertations>



Part of the [Biomedical Engineering and Bioengineering Commons](#), and the [Electrical and Computer Engineering Commons](#)

---

## Recommended Citation

Yan, Xiaodong, "" (2005). *Dissertation*. 610.  
<https://digitalcommons.latech.edu/dissertations/610>

This Dissertation is brought to you for free and open access by the Graduate School at Louisiana Tech Digital Commons. It has been accepted for inclusion in Doctoral Dissertations by an authorized administrator of Louisiana Tech Digital Commons. For more information, please contact [digitalcommons@latech.edu](mailto:digitalcommons@latech.edu).

# **BIOSENSING WITH MICROCANTILEVER-BASED SENSORS**

By

Xiaodong Yan, M. S.

A Dissertation Presented in Partial Fulfillment  
of the Requirement for the Degree  
Doctor of Philosophy in Engineering

COLLEGE OF ENGINEERING AND SCIENCE  
LOUISIANA TECH UNIVERSITY

March 2005

UMI Number: 3164470

### INFORMATION TO USERS

The quality of this reproduction is dependent upon the quality of the copy submitted. Broken or indistinct print, colored or poor quality illustrations and photographs, print bleed-through, substandard margins, and improper alignment can adversely affect reproduction.

In the unlikely event that the author did not send a complete manuscript and there are missing pages, these will be noted. Also, if unauthorized copyright material had to be removed, a note will indicate the deletion.

**UMI**<sup>®</sup>

---

UMI Microform 3164470

Copyright 2005 by ProQuest Information and Learning Company.

All rights reserved. This microform edition is protected against unauthorized copying under Title 17, United States Code.

ProQuest Information and Learning Company  
300 North Zeeb Road  
P.O. Box 1346  
Ann Arbor, MI 48106-1346

LOUISIANA TECH UNIVERSITY

THE GRADUATE SCHOOL

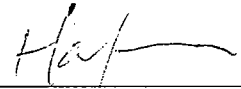
March 1, 2005

Date

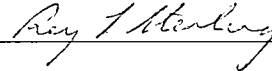
We hereby recommend that the dissertation prepared under our supervision  
by Xiaodong Yan

entitled Biosensing with Microcantilever Sensors

be accepted in partial fulfillment of the requirements for the Degree of  
Doctor of Philosophy in Engineering



(Supervisor of Dissertation Research

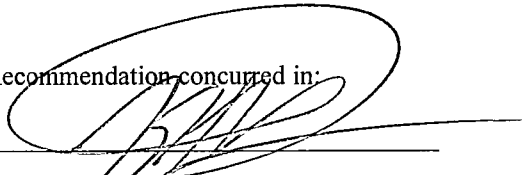


Head of Department

PhD in Engineering

Department

Recommendation concurred in:

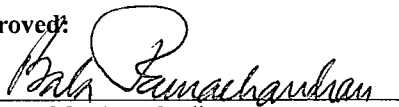


Yurii Luov

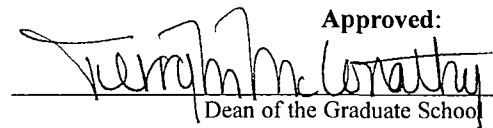
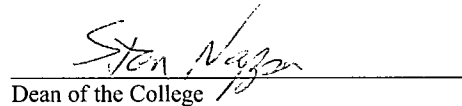
Advisory Committee



Approved:

  
Director of Graduate Studies

Approved:

  
Dean of the Graduate School  
Dean of the College

## ABSTRACT

Microcantilevers provide an ideal platform for biosensors. The micron-sized transducer brings several advantages, such as high sensitivity, small sample quantity for analysis, portability, implantability, and the ability to be mass produced and integrated into standard microelectronic processing technologies like complementary metal oxide semiconductors (CMOS).

The objective of this research is to investigate and develop modification methods of microcantilevers for biosensing applications.

Two microcantilever modification methods were investigated. They are the self-assembly monolayer method and the layer-by-layer method. A fundamental procedure for modification of microcantilevers using the layer-by-layer approach was developed for the first time in this research. These modification methods for microcantilevers provide practical ways for immobilization of recognition specifics, such as enzymes and antibodies, on the surface of the microcantilever. The modifications allow for detection of corresponding targets.

In this research, the following results have been obtained: 1) Development of a glucose sensor using microcantilever with layer-by-layer nano assembly containing glucose oxidase. The sensor has a response time in the range of seconds. 2) Development of a hydrogen peroxide sensor using the microcantilever with layer-by-layer nano assembly containing hydrogen peroxides. The detection limit for this sensor is  $10^{-9}$ M. 3)

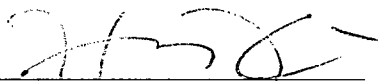
Development of a sensor for detection of biowarfare agents. For the measurement of Tularemia, this sensor reached the detection limit of  $10^3$  organism/ml. 4) Development of a sensor for detection of chemical warfare agents with sensitivity of  $10^{-7}$ M for organophosphates.

The results obtained from this research have demonstrated that the microcantilever-based biosensors can be developed for detection of various biomolecules or monitoring different processes. The glucose sensor developed in this research has great potential to be used as an implantable glucose sensor for continuous blood glucose monitoring, which is critical in diabetes care. And the sensor for detection of biowarfare agents could be used for homeland security, which is one of the most important issues of the nation.

## APPROVAL FOR SCHOLARLY DISSEMINATION

The author grants to the Prescott Memorial Library of Louisiana Tech University the right to reproduce, by appropriate methods, upon request, any or all portions of this Dissertation. It is understood that "proper request" consists of the agreement, on the part of the requesting party, that said reproduction is for his personal use and that subsequent reproduction will not occur without written approval of the author of this Dissertation. Further, any portions of the Dissertation used in books, papers, and other works must be appropriately referenced to this Dissertation.

Finally, the author of this Dissertation reserves the right to publish freely, in the literature, at any time, any or all portions of this Dissertation.

Author   
Date 2/25/05

## TABLE OF CONTENTS

	PAGE
LIST OF FIGURES .....	x
ACKNOWLEDGMENTS .....	xiii
CHAPTER ONE INTRODUCTION.....	1
1.1 Microcantilever Sensors.....	1
1.2 Review of Microcantilever-Based Biosensors.....	3
1.2.1 DNA-Based Microcantilever Biosensors.....	4
1.2.2 Antibody-Based Microcantilever Biosensors .....	13
1.2.3 Enzyme Immobilization Microcantilever Biosensors.....	19
1.3 Objective of This Dissertation .....	19
1.4 Organization of This Dissertation.....	20
CHAPTER TWO DETECTION OF ORGANOPHOSPHATES USING AN ACETYL CHOLINESTERASE (ACHE) COATED MICROCANTILEVER .....	21
2.1 Introduction.....	21
2.2 Self-Assembly Monolayer (SAM).....	22
2.2.1 Introduction.....	22
2.2.2 Preparation .....	23
2.2.3 Mixed SAMs.....	24
2.2.4 Characteristic .....	26
2.3 Experiment Material .....	29
2.4 Microcantilever Modification .....	30
2.5 Experiment Setup.....	31
2.6 Results and Discussion .....	33
2.6.1 Enzyme Immobilization.....	33
2.6.2 Microcantilever Deflection Due to AChE Inhibition by Paraoxon .....	35
2.6.3 Sensing Mechanism .....	36
2.7 Summary .....	37



CHARTER THREE MOLECULAR RECOGNITION OF BIOWARFARE AGENTS USING MICROCANTILEVER SENSORS.....	39
3.1 Introduction.....	39
3.1.1 Antibody-Antigen .....	40
3.2 Experimental Material .....	44
3.3 Microcantilever Modification .....	45
3.4 Experiment Setup.....	48
3.5 Results and Discussions.....	49
3.6 Summary .....	51
CHAPTER FOUR  MICROCANTILEVER MODIFICATION WITH LAYER-BY-LAYER TECHNIQUES .....	52
4.1 Introduction to Layer-by-Layer Technique .....	52
4.1.1 Polyanion / Polycation Alternate Assembly .....	53
4.1.2 Standard Assembly Procedure .....	53
4.1.3 Kinetics of Polyion Adsorption .....	56
4.1.4 First Layers and Precursor Film.....	58
4.1.5 Multilayer Structure .....	59
4.2 Objective of Research.....	59
4.3 Experiment Material and Procedure .....	60
4.4 Results and Discussions.....	61
4.4.1 Contact Angle Measurement.....	61
4.4.2 Microcantilever Deflection .....	62
4.5 Summary .....	65
CHAPTER FIVE  MODIFICATION OF MICROCANTILEVER WITH LAYER-BY-LAYER NANO-ASSEMBLY FOR GLUCOSE MEASUREMENT.....	66
5.1 Introduction.....	66
5.2 Experiment Materials.....	67
5.3 Experiment Setup.....	67
5.4 Microcantilever Layer-by-Layer GOx Surface Immobilization Process.....	68
5.5 Results and Discussions.....	71
5.5.1 Selective Modification of Microcantilever .....	71
5.5.2 Flow Rate and Measurement Accuracy .....	72
5.5.3 Deflection Amplitude vs the Concentration of Glucose .....	79
5.5.4 Microcantilever Deflection in a Saline Solution.....	80
5.5.5 Selectivity and Lifetime.....	80
5.5.6 Number of GOx Layers in the Mutilayer Assembly.....	82
5.5.7 Deflection Mechanism .....	82
5.5.7.1 Thermal Effect .....	86
5.5.7.2 pH Change in the Film.....	89
5.5.7.3 Conformation Change of Glucose Oxidase .....	90

5.5.7.4 Hydrogen Peroxide .....	93
5.6. Summary .....	93
CHAPTER SIX MICROCANTILEVER MODIFICATION BY HORSERADISH PEROXDIASE (HRP) INTERCALATED NANO-ASSEMBLY FOR HYDROGEN PEROXIDE DETECTION .....	95
6.1 Introduction.....	95
6.2 Experimental Material .....	96
6.3 Microcantilever Modification .....	97
6.4 Experiment Setup and Procedure.....	98
6.5 Results and Discussion .....	98
6.5.1 Typical Deflection of Microcantilever upon Exposure to Hydrogen Peroxides Solution .....	98
6.5.2 Deflection of Microcantilever upon Exposure to Different Concentration of Hydrogen Peroxides .....	100
6.5.3 Selectivity .....	101
6.5.4 Sensing Mechanism .....	101
6.6 Summary .....	102
CHAPTER SEVEN CONCLUSIONS AND FUTURE WORK.....	104
7.1 Conclusions.....	104
7.2 Future Work for This Research.....	105
7.3 Future Work for Microcantilever-based Biosensor Development.....	105
REFERENCES .....	108

## LIST OF FIGURES

Figure 1-1 Electron micrographs of microcantilevers fabricated in IfM The sizes of cantilevers on the right vary from 5 $\mu\text{m}$ to 200 $\mu\text{m}$ in extent from the support .....	1
Figure 1-2 Inkjet printing of individual droplets onto a cantilever array (a) as a scheme and (b) as seen by a video camera. A positioning system allows accurate placement of single droplets onto selected cantilevers. When deposited with a small pitch, the droplets merge into a continuous layer covering the entire cantilever length. For demonstration, three droplets of water are deposited onto selected cantilevers. Owing to the oblique view of the camera, only the central cantilever is in focus.....	6
Figure 1-3 Schematic of the digestion and ligation experiments. DNA on the cantilever surface incorporating a <i>Hind</i> III site was first cut with <i>Hind</i> III endonuclease, leaving a single-stranded end. Then DNA with a compatible end was ligated to the DNA on the cantilever, producing a longer DNA on the cantilever surface. X's and Y's represent base pairs not involved in the digestion/ligation site. Subscripts denote that a variable number of uninvolved base pairs could be used.....	8
Figure 1-4. The sensor and reference cantilevers are supported by L-shaped thick structures that connect them to the die. The die is placed in a stainless steel fluidic chamber. The differential bending is measured directly using interferometry.....	12
Figure 1-5. Schematic for the concept of the magneto-mechanical analysis of biorecognition processes on functional cantilever in presence of an external magnetic field .....	13
Figure 1-6 Microcantilever resonator for detection of single cell and single virus. <b>A</b> , a single E coli cell on a microcantilever, <b>B</b> , a single vaccine virus particle on a microcantilever .....	16
Figure 1-7 <b>A</b> , SEM micrograph showing <i>Salmonella</i> attached to the cantilever surface functionalized with the antibody. No <i>Salmonella</i> was observed in the unfunctionalized areas. <b>B</b> , Close up of <i>Salmonella</i> on cantilever.....	18
Figure 2-1 Preparation of SAMs. The substrate, Au on Si, is immersed into an ethanol solution of the desired thiol(s). Initial adsorption is fast (seconds); then an organization phase follows which should be allowed to continue for >15 h for best results. A schematic of a fully-assembled SAM is shown to the right .....	24
Figure 2-2 Schematic illustration of the preparation of two-component alkanethiolate gradients. (a) The two different thiols, represented	

by X and O, are injected into glass filters. (b) They diffuse slowly through the polysaccharide gel and attach to the gold substrate. (c) Top view showing the placement of the gold substrate between the filters. (d) Schematic illustration of a fully assembled gradient .....	25
Figure 2-3 A schematic model of the $(\sqrt{3}) \times (\sqrt{3}) R30^\circ$ overlayer structure formed by alkanethiolate SAMs on Au(111).....	26
Figure 2-4. IRAS spectrum of a hexadecanethiolate SAM in the CH stretching region. The most prominent vibrations are indicated. d+ and d- are the symmetric and antisymmetric CH <sub>2</sub> stretches; r+ and r- are the symmetric and antisymmetric CH <sub>3</sub> stretches, respectively. At the measurement temperature used (82 K), the ra- and rb-components of the r- peak are resolved.....	28
Figure 2-5 A SEM picture of a silicon microcantilever.....	29
Figure 2-6 The modification procedure of an AChE covered microcantilever .....	30
Figure 2-7 A schematic of the experimental setup used in this work.....	31
Figure 2-8 The change of UV absorption of a 1mg/ml AChE solution in 0.01M phosphate buffer solution in a UV-transparent cuvet before and after exposure to a glutaraldehyde activated microcantilever at certain hours. The cuvet (BrandTech Scientific Inc.) is transparent between 220 nm and 900 nm. No UV absorption change was observed to an AChE solution in the cuvet in the presence of a bare gold coated microcantilever (figure not shown). This control experiment suggests that AChE does not adsorb onto the wall of cuvet and the gold surface of a microcantilever .....	32
Figure 2-9 Changes in the UV absorption intensity at 278 nm of a 1mg/ml AChE solution in 0.01M phosphate buffer solution to a glutaraldehyde activated microcantilever versus the exposure time .....	34
Figure 2-10 Bending response as a function of time, t, for a silicon microcantilever with AChE enzyme coated on its gold side after injection of $10^{-4}$ M paraoxon in 0.01 M phosphate buffer solution at pH = 7.2. The microcantilever was preequilibrated in a 0.01M phosphate buffer solution before injection of the paraoxon solution.....	35
Figure 2-11 Maximum deflection of a silicon microcantilever coated with AChE enzyme on its gold side as a function of the concentration of paraoxon in 0.01M phosphate buffer solution at pH = 7.2.....	36
Figure 3-1 Structure of a typical immunoglobulin (antibody) protein. Two identical heavy chains are connected by disulfide linkages. The antigen-combining site is composed of the variable regions of the heavy and light chains, whereas the effector site of the antibody (which controls whether it agglutinates antigens) is determined by the amino acid sequence of the heavy chain constant region .....	41
Figure 3-2 Illustration of antigen-antibody recognition by complementary shape .....	41

Figure 3-3 Bending response as a function of time for an antibody immobilized microcantilever and a microcantilever modified by the same procedure except the final antibody attaching step upon injection of a $1 \times 10^6$ organisms/mL solution of <i>F. Tularensis</i> in 0.1M phosphate-buffered saline buffer (pH=7.3).....	47
Figure 3-4 Bending response as a function of time for antibody immobilized microcantilevers upon injection of different concentration (organisms/mL) solutions of <i>F. Tularensis</i> in 0.1M phosphate-buffered saline buffer (pH=7.3).....	48
Figure 3-5 Deflection rate for antibody modified microcantilevers after exposure to <i>F. Tularensis</i> vs. the concentration of <i>F. Tularensis</i> .....	49
Figure 4-1 Schematic picture of polycation/polyanion multilayer, neighbor layers interpenetrate on about 30%, so that only first and third layers are well separated.....	54
Figure 4-2 Common polyions used in LbL assembly .....	55
Figure 4-3 Schematics of the microcantilever modification procedure.....	60
Figure 4-4 Contact angles of water on the gold and silicon surface of a microcantilever during the procedure of layer-by-layer formation.....	62
Figure 4-5 Contact angles of water on the TTS treated silicon surface and MES coated gold surface of a microcantilever during the procedure of layer-by-layer formation.....	63
Figure 4-6 Bending response as a function of time for a TTS and MES treated silicon microcantilever upon alternate injection of a $10^{-2}$ M solution of PDDA and PSS in $10^{-2}$ M PBS buffer (pH=6.5) at a constant 4ml/h flow rate.....	63
Figure 4-7 Bending response as a function of time for a unmodified coated silicon microcantilever upon alternate injection of a $10^{-2}$ M solution of PDDA and PSS in PBS buffer (pH=6.5) at a constant 4ml/h flow rate .....	64
Figure 5-1 LbL nano assembly with immobilized enzyme on MCL surface .....	70
Figure 5-2 Selective modification of microcantilever .....	71
Figure 5-3 The bending response for a microcantilever-A and a microcantilever-B to a $8 \times 10^{-3}$ M glucose solution in 0.01M NaCl, respectively .....	72
Figure 5-4 a) Deflection of MCL when exposure to 10mM glucose. b) Calculated glucose concentration in the reaction cell after injection of 10mM glucose solution. ....	73
Figure 5-5 Microcantilever deflection at a different flow rate when exposed to 10mM glucose solution.....	74
Figure 5-6 Reproducibility experiment with one microcantilever exposed to 10mM glucose solution for 10 times .....	76
Figure 5-7 Microcantilever deflection upon exposure to glucose solution from 2 to 50 mM.....	76
Figure 5-8 Microcantilever deflection upon exposure to glucose solution from 50 to 2 mM .....	77

Figure 5-9 Linear relationship between the magnitude of microcantilever deflection and the concentration of tested glucose solution .....	78
Figure 5-10. Bending response of a microcantilever-A to a $10^{-2}$ M glucose solution from a $4 \times 10^{-3}$ M glucose solution in a 0.01M NaCl solution.....	79
Figure 5-11 MCL deflection with exposure to glucose, mannose, fructose, and galactose at concentration of 4mM .....	80
Figure 5-12 Deflection of microcantilever modified with different layers of GOx .....	81
Figure 5-13 Dimensions of the commercial microcantilever used in the research.....	83
Figure 5-14 Deflection of microcantilever upon exposure to 10mM at different temperature .....	85
Figure 5-15 pH effect on microcantilever.....	87
Figure 5-16 Overall topology of glucose oxidase holoenzyme [89].....	88
Figure 5-17 Subunit structure of GOX showing FAD (red spacefill) [89].....	89
Figure 5-18 pH variation of L-glucose and D-glucose solution upon exposure to glucose oxidase.....	91
Figure 5-19 Microcantilever deflection upon exposure to 10mM D-glucose and L-glucose .....	92
Figure 6-1 Schematic of microcantilever modification. The final nano-assembly on the gold side of silicon microcantilevers were MES/(PEI/PSS) <sub>3</sub> /(HRP/PSS) <sub>3</sub> .....	97
Figure 6-2 Deflection of microcantilevers upon exposure to a 1mM hydrogen peroxide solution. The microcantilevers were modified with a) (PEI/PSS) <sub>3</sub> / (PSS/HRP) <sub>3</sub> and b) (PEI/PSS) <sub>6</sub> ... ..	99
Figure 6-3 The average maximum deflection of (PEI/PSS) <sub>3</sub> /(HRP/PSS) <sub>3</sub> modified microcantilevers at different hydrogen peroxide concentrations. ....	100
Figure 6-4 Deflection of (PEI/PSS) <sub>3</sub> /(HRP/PSS) <sub>3</sub> modified microcantilevers to a $1 \times 10^{-6}$ M solution of hydrogen peroxide and $1 \times 10^{-5}$ M concentration of different acid solutions .....	101

## ACKNOWLEDGMENTS

First I thank Dr. Hai-Feng Ji for leading me into this wonderful microcantilever technology field, and his kindness, guidance, encouragement, and support to me during my pursuing my Ph.D. degree here at IfM. I am very fortunate to have such a great mentor in this important period of my life.

I thank Dr. Kody Varahramyan, Dr. Yuri Lvov, Dr. Bill Elmore, and Dr. Sidney Sit for being members of my advisory committee, and their valuable advice for the improvement of this dissertation.

The author would like to thank his all current and former group members for their cooperation, understanding, and support of this research. It's been an honor and pleasure to work with these colleagues. The author especially thanks the following group members for their valuable opinions, their sharing of knowledge and expertise, and the help they provided: Dr. Yanjun Tang, Hao Xu, Yifei Zhang, Yuming Yang, Yu Feng, Jing Zhang, Ke Liu, Min Wang, Xiaolei Shi, Vemana Purushotham, Venkata Chivukula, Priya Rao, Swepta Kondu, Chandana Karnati, Kilsha Hill, and Jesscia Thibodeaux.

The author acknowledges the support from the following people of associated with the Institute for Micromanufacturing (IfM): Dr. Mike McShane, Dr. Karen Xu, Ji Fang, Dr. Weisong Wang, Dr. Qun Gu, Dr. Zonghuan Lu, Dr. Jingshi Shi, John McDonald, and Scott Williams. The author also wishes to thank the following people of

associated with the Chemistry Program: Dr. Dale Snow, Dr. Upali Siriwardane, and Danny Eddy. Their help made it possible for this dissertation research to go smoothly.

I thank my parents, Professors Yu Yan and Weixiang He, for their love, understanding, and support. They always had their faith in me, even when things did not seem to be going in my way. I thank my brothers, Xin Yan and Chen Yan, for their caring and encouragements.

The last, but the most important, I thank my wife, Qiongying Ye, for her love, understanding, and encouragement, and for taking care of my life so that I can better concentrate on my research. This dissertation wouldn't be possible without her support.



# CHAPTER ONE

## INTRODUCTION

### 1.1 Microcantilever Sensors

Since the publication of three pioneer papers in 1994 [1-3], microcantilever sensor technology has boomed and become a promising sensor technology. Microcantilever sensors have several advantages over many other sensor technologies, including faster response time, lower cost of fabrication, the possibility of sensor arrays with small overall dimensions, the ability to explore microenvironments, and improved portability for field applications. SEM pictures of microcantilevers are shown in Figure 1-1.

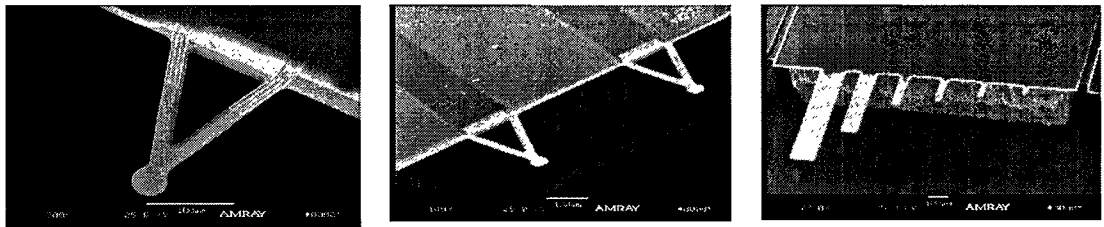


Figure 1-1 Electron micrographs of microcantilevers fabricated in IfM. The sizes of cantilevers on the right vary from 5  $\mu\text{m}$  to 200  $\mu\text{m}$  in extent from the support.

Cantilever resonance responses, such as frequency, deflection, Q-factor, and amplitude, undergo changes due to adsorption or changes in environment. In theory, cantilevers could be modified and optimized for sensitive and interference-free detection of chemicals and physical quantities.

Resonance frequency. The resonance frequency,  $f$ , of an oscillating cantilever can be expressed as

$$f = \frac{1}{2\pi} \sqrt{\frac{K}{m^*}} \quad (1.1)$$

where  $K$  is the spring constant of the lever and  $m^*$  is the effective mass of the microcantilever. The effective mass can be related to the mass of the beam,  $m_b$ , through the relation:  $m^* = nm_b$ , where  $n$  is a geometric parameter. It is clear that the resonance frequency can change due to changes in mass as well as changes in spring constant.

Microcantilever bending. Resonance frequency of a microcantilever can be used to detect chemical species in air. When the target is loaded on the microcantilever, the resonance frequency of microcantilever is going to change. However, that change is not going to show up because the frequency of is damped in aqueous solution. One of the unique characteristics of microcantilevers is that the device can be made to undergo bending due to molecular adsorption by confining the adsorption to one side of the cantilever. This bending is due to adsorption-induced differential stress on the cantilever. Using Stoney's formula [4], the radius of curvature of bending of the cantilever due to adsorption can be written as:

$$\frac{1}{R} = \frac{6(1-\nu)}{Et^2} \delta s \quad (1.2)$$

where  $R$  is the radius of curvature for the cantilever,  $\nu$  and  $E$  are Poisson's ratio and Young's modulus for the substrate, respectively, and  $t$  is the thickness of the cantilever, and  $\delta s$  is the film stress.

Microcantilever bendings are generally induced by adsorption-induced surface stress change or film volume change. Adsorption of chemicals on the microcantilever surface changes the surface stress because of the repulsion or attraction of the molecules on the surface. The swelling or shrinking of the polymer film on the cantilever upon exposure to specific analytes could generally bend the microcantilever significantly.

### 1.2 Review of Microcantilever-Based Biosensors

Biosensors have attracted considerable interest in the last few years since the monitoring of a specific substance is central in many applications ranging from clinic analysis to environmental control and the monitoring of many industrial processes. Biosensors offer many advantages in comparison to many conventional analytical approaches in terms of simplicity and lower detection limits. The simplicity of many biosensor formats often allows for their use by untrained personnel such as by patients for home monitoring of, for example, glucose within blood or urine or, alternatively, within a doctor's surgery – so negating the need for samples to be returned to pathology laboratories or other centralized clinical biochemistry laboratory facilities. One of the greatest advantages that biosensors frequently enjoy is their specificity due to their exploitation of biological molecules such as enzymes or antibodies. Analyses *via* biosensors may frequently be performed without the need for formal training, and for this reason many human sources of error may often be eliminated.

Microcantilever-based biosensors offer new, exciting opportunities in developing microscopic biomedical analysis systems with unique characteristics. Current microcantilever-based biosensors can be generally grouped into the following types:

DNA-based sensor, antibody-based sensor and enzyme-based sensors. This section summarizes the up-to-date development of microcantilever-based biosensors in the above areas.

### 1.2.1 DNA-Based Microcantilever Biosensors

The first experiment about DNA hybridization on microcantilevers [5] confirmed that ssDNA modified microcantilevers respond to the DNA hybridization. For the hybridization experiments, synthetic thio-modified oligonucleotides with different base sequences were covalently linked on the gold-covered side of the cantilevers. This process is done by inserting the two cantilever arrays into two separate reservoirs, which were then filled with solution of different oligonucleotides. The functionalization of one cantilever with a 12-mer oligonucleotide and the other with a 16-mer oligonucleotide was performed in parallel under identical conditions. The arrays were equilibrated in hybridization buffers until the differential signal became stable. Then, the complementary 16-mer oligonucleotide solution was injected into the liquid cell followed by injection of complementary 12-mer oligonucleotide solution. The injections led to hybridization of oligonucleotides in solution with the matching oligonucleotides immobilized on the cantilever surfaces. This process resulted in a difference in surface stress between the functionalized gold and the nonfunctionalized Si surface, which bent the cantilever. During hybridization, the number of charges in the molecular layer from the sugar-phosphate backbone of the oligonucleotides and their surrounding counterions is increased. Simultaneously, the chain packing of oligonucleotides on the surface also increases. Both interactions, electro-static as well as steric, are repulsive and produce compressive surface stress during hybridization.

Based on the above work, an MC array system was developed for multiple quantitative DNA tests [6]. The experiment was carried out on a cantilever array of eight identical silicon cantilevers. The incubation of individual gold-coated cantilevers was performed in microcapillaries, each containing a different thiolated probe DNA. After injection of target DNA into the solution, they will hybridize sequence-specifically to their complementary partner immobilized on a particular cantilever. Researchers proposed that steric hindrance effects are the major reason causing the compressive surface stress thus the bending. The testing limit is 75nm of DNA concentration in solution.

In another independent work [7], the DNA hybridization-induced microcantilever bending was explained by the changes in configurational entropy and intermolecular energetic induced by specific biomolecular interactions. By controlling entropy change during DNA hybridization, the direction of cantilever motion can be manipulated. These thermodynamic principles were also used to explain the origin of motion generated from protein–ligand binding.

Hansen et al. [8] demonstrated that the discrimination of DNA mismatches can be done using an elegantly simple microcantilever-based optical deflection assay, without the need for external labeling. Another work on DNA hybridization [9] showed similar results.

A. Bietsch et al [10] introduced a new method for rapid functionalization of cantilever arrays with DNA or protein by inkjet printing. The inject printer is an MD-P-705-L inkjet dispensing system (Microdrop, Norderstedt, Germany), and was equipped with a three-axis micropositioning system having an accuracy of 10  $\mu\text{m}$  and piezo-driven

autopipettes with 70  $\mu\text{m}$  nozzle diameters. The piezo-pipettes were filled from the front side, allowing the use of small sample volumes of 5–25  $\mu\text{l}$ . A stroboscopic camera system provided visual control to adjust piezo voltages and pulse durations for reliable droplet ejection and to avoid satellite drops. Single droplet with diameters in air of 60–80  $\mu\text{m}$  corresponding to volumes of 0.1–0.3 nl was ejected on demand. Figure 1-2 shows a schematic overview and illustrates how water droplets were deposited onto Si cantilevers. When droplets were spotted with pitches smaller than 0.1 mm, they merged and formed continuous films. The vertical separation between the nozzle and the sample was typically 0.4 mm.

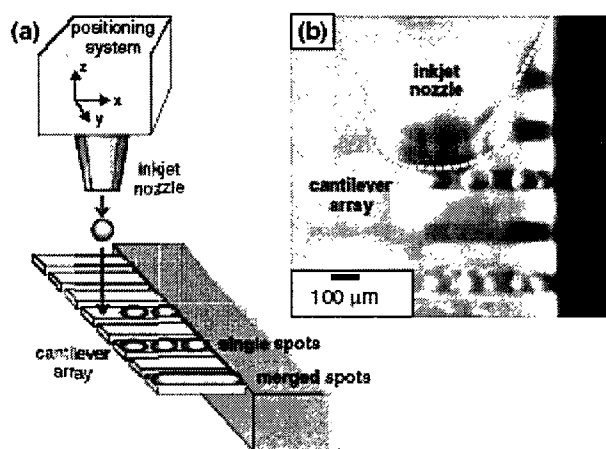


Figure 1-2 Inkjet printing of individual droplets onto a cantilever array (a) as a scheme and (b) as seen by a video camera. A positioning system allows accurate placement of single droplets onto selected cantilevers. When deposited with a small pitch, the droplets merge into a continuous layer covering the entire cantilever length. For demonstration, three droplets of water are deposited onto selected cantilevers. Owing to the oblique view of the camera, only the central cantilever is in focus.

The uniformity of DNA layers deposited by inkjet was verified by a selective wet etching method developed by the same research group [11]. In the selective wet etching, the etch bath was composed of a water solution of  $\text{Fe}(\text{NO}_3)_3$  and thiourea. When

cantilever arrays were immersed in the etch bath, the non-treated (bare surface) Au was clearly removed after 10-30 minutes. The residual Au structures reflected the integrity of deposited monolayer patterns and allowed microscopic inspection down to the nanometer scale. The functionality of ssDNA-coated cantilevers was verified in a sensor experiment. The data clearly demonstrated a specific response of the ssDNA-coated cantilever upon injection of the complementary ssDNA target. The reaction was reproducible as the target could be washed off successfully by cycles of the buffer solution. In an additional experiment where both sides of the cantilevers were coated with gold, the etch test showed that DNA can be printed onto one side of the cantilevers without contaminating the backside. This result suggests that the inkjet printing provides a very effective way to functionalize one side of microcantilever. Another advantage of this method is its fast process. Functional DNA probes can be printed by inkjet within a few seconds. The coating of an entire chip with different probe layers requires only one to five minutes.

In all the DNA-based microcantilever sensors discussed above, probe ssDNA was first immobilized on cantilever surface. A novel approach was to immobilize a double-stranded DNA on the cantilever surface through conjugation chemistry, then the cantilever was exposed to a *Hind* III enzyme, which cut the DNA on the cantilever at the specific recognition site, leaving a 5-base single-stranded “sticky end” that can be used to attach a piece of DNA with a complementary end [12]. Figure 1-3 shows a schematic of the digestion and ligation reactions.

Immobilization the DNA-oligo layer on gold surface is a crucial step in making DNA sensors. The adsorption kinetics of thiol-modified DNA-oligos on gold surface (Marie et al., 2002) suggested that the immobilization has three phases. Firstly (I), a single layer of

oligos self-assemble formed on the cantilever surface. Secondly (II), oligos begin to adsorb on top of the first oligo layer due to non-specific hydrogen bonds between the oligos. Finally (III), the loosely bound oligos are desorbed during rinse in DI water.

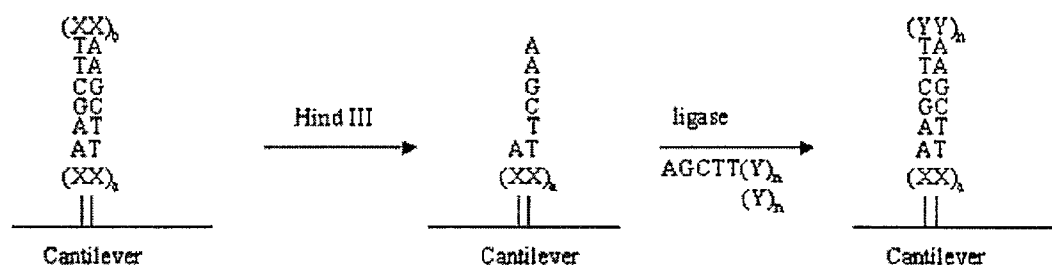


Figure 1-3 Schematic of the digestion and ligation experiments. DNA on the cantilever surface incorporating a *Hind* III site was first cut with *Hind* III endonuclease, leaving a single-stranded end. Then DNA with a compatible end was ligated to the DNA on the cantilever, producing a longer DNA on the cantilever surface. X's and Y's represent base pairs not involved in the digestion/ligation site. Subscripts denote that a variable number of uninvolved base pairs could be used.

M. Alvarez et al [13] studied the forces responsible for the bending motion during the formation of a monolayer of thiolated 27-mer single-stranded DNA on a microcantilever and during the subsequent hybridization with the complementary nucleic acid. The nanomechanical response was compared with data from surface plasmon resonance (SPR) and radiolabeling, to determine the surface coverage and to study the intermolecular forces. They concluded that the main source of surface stress during the immobilization is the covalent bond between the surface and gold atoms and the sulfur atoms of the thiol linker of the DNA probes, with a small contribution from the weak interactions between the nucleotide chain and the gold. In contrast, the only contribution to the surface stress during hybridization is the intermolecular forces between neighboring DNA molecules.



Simulation and modeling of the DNA hybridization processes were conducted to further explain the origin of nanomechanical bending. In a model proposed by Hagan, et al. [14], the forces determining equilibrium cantilever deflection can be divided into four basic categories. First, the conformational entropy of an adsorbed macromolecule is decreased by the presence of neighboring molecules. The molecules also energetically repel each other, due to solvent-mediated interactions as well as electrostatic repulsions. The electrostatic free energy is represented by  $F_{\text{ELEC}}$ , and the free energy resulting from macromolecular conformational entropy and nonelectrostatic interactions will be denoted by  $F_{\text{POLY}}$ . In addition, there is a free energy contribution associated with the osmotic pressure of the counterions localized in the region of the cantilever due to the charges on DNA molecules. This will be denoted by  $F_{\text{OSM}}$ . The free energy associated with these effects decreases as the intermolecular distances and volume occupied by counterions increase. In other words, adsorption on a curved surface leads to lower free energies for the same average distance between molecular graft points on the surface. In the cantilever experiments, these effects lead to a force that favors deflection. There is, however, a mechanical energy penalty associated with bending the cantilever, denoted by  $E_{\text{CANT}}$ . The balance between these two effects determines the cantilever deflection at equilibrium.

$E_{\text{CANT}}$  can be expressed as,  $E_{\text{CANT}} = \frac{C}{R^2}$ , where  $C$  depends on the thickness of the cantilever and the modulus of the material of construction and  $R$  denotes the radius of curvature of the shape adopted by the cantilever. The overall free energy,  $F$ , can now be written as,  $F = F_{\text{CANT}} + F_{\text{POLY}} + F_{\text{OSM}} + F_{\text{ELEC}}$ . If we are able to determine the dependence of the latter three terms on  $R$ , then the equilibrium radius,  $R_{\text{EQ}}$ , can be

calculated by minimizing  $F(R)$ . In the limit of small curvature, the optically measured

deflection ( $\delta$ ) is then given by  $\delta = \frac{d_2^2}{2R_{EQ}}$ , where  $d_2$  is the length of the cantilever.

Applying this model with results from Fritz et al. [5] and Wu et al. [7], it was found that hydration forces are the dominant factor determining cantilever deflections but not the electrostatics or conformational entropy. Using an empirical potential, derived from independent experiments, which accounts for these effects, they predicted deflections that are consistent with results in Wu et al. The researchers predict cantilever deflections for the adsorption of ssDNA that are smaller than those for dsDNA, which agrees with the observations in Fritz et al., but is not consistent with Wu et al. Their calculations showed that, if a more flexible cantilever is considered, experimentally relevant deflections can be achieved at interaction strengths and grafting densities for which conformational entropy is a significant factor. Under these conditions, deflections can be smaller upon hybridization, as seen in Wu et al. This result underscores the importance of considering the interplay between material properties and probe-target interactions during microdevice design. Their calculations highlighted the importance of grafting density in determining the magnitude of cantilever deflections. An important finding is that cantilever deflections are very sensitive to the morphology of the surface, as evidenced by the influence of disordered grafting points on deflection. This finding emphasizes that characterization and control of nanoscale self-assembly processes that determine probe molecule adsorption are imperative for reliable microdevice design.

In another model [15], the nanomechanical bending of the cantilever in the DNA sensor was explained by the flexoelectric effect, instead of conformational entropy force.

Based upon polyelectrolytes theory and the relation between concentration and electric potential, an apparent semi-microscopic relation between cantilever deflection, ssDNA length, and salt concentration was deduced. These results were in good agreement with the experimental observations of Wu et al.

Besides these DNA hybridization experiments, DNA aptamers have been immobilized on the cantilever for the detection of protein [16]. Aptamers are DNA or RNA molecules, which can form tertiary structures that recognize and bind to their respective targets. The aptamer receptors have been successfully produced against a wide range of targets, from small molecules to proteins to whole cells. The sensor utilizes two adjacent cantilevers that constitute a sensor/reference pair and allows direct detection of the differential bending between the two cantilevers [17] (Figure 1-4). One cantilever is functionalized with aptamers selected for Taq DNA polymerase while the other is blocked with single stranded DNA. The target-aptamer binding induces a change in surface stress, which causes a differential cantilever bending that ranges from 3 to 32 nm, depending on the ligand concentration. Protein recognition on the sensor surface is specific and is concentration dependent.

An alternative method for optical method of recording the deflection of microcantilever is piezoresistive/piezoelectric readout technique [18-19]. Piezoresistive stress sensors can be integrated inside a cantilever structure by using a Wheatstone bridge [20-21].

Piezoresistive detection, compared to the optical one, has several advantages: no macroscopic optical components and no laser alignment are needed; read-out electronics can in principle be integrated on the same silicon chip supporting the cantilevers using

the same CMOS fabrication technology. Optical techniques may be subjected to artifacts due to changes in the optical properties of the medium surrounding the cantilever, e.g., a change in the refracting index when the laser spot hits the photo detector surface. Piezoresistive detection does not suffer from this problem and can work in non-transparent solutions. These benefits make the piezoresistive detection technique one choice for developing portable or even implantable biosensors for *in vivo* measurement.

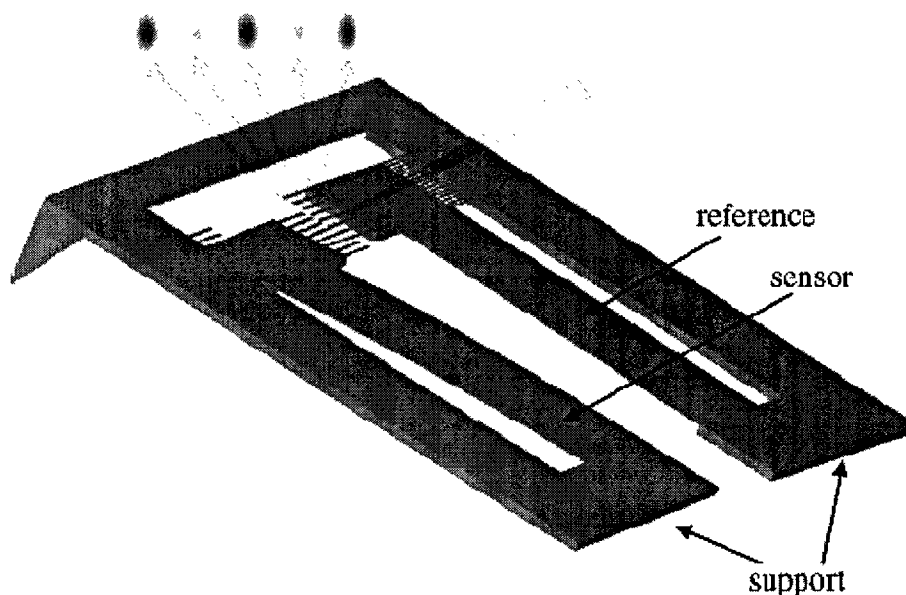


Figure 1-4. The sensor and reference cantilevers are supported by L-shaped thick structures that connect them to the die. The die is placed in a stainless steel fluidic chamber. The differential bending is measured directly using interferometry.

Another microcantilever-based DNA detection applied a new concept for the amplification of deflection amplitude. The method involves the association of magnetic particles that carry the biorecognition complex to the functionalized cantilever and the magneto-mechanical deflection of a cantilever in the presence of an external magnet (Figure 1-5). It was shown that this magneto-mechanical method could detect trace

amounts of extremely dilute biological samples, for example the sensitivity limit for M13ø DNA was  $7.1 \times 10^{-20}$  M [22].

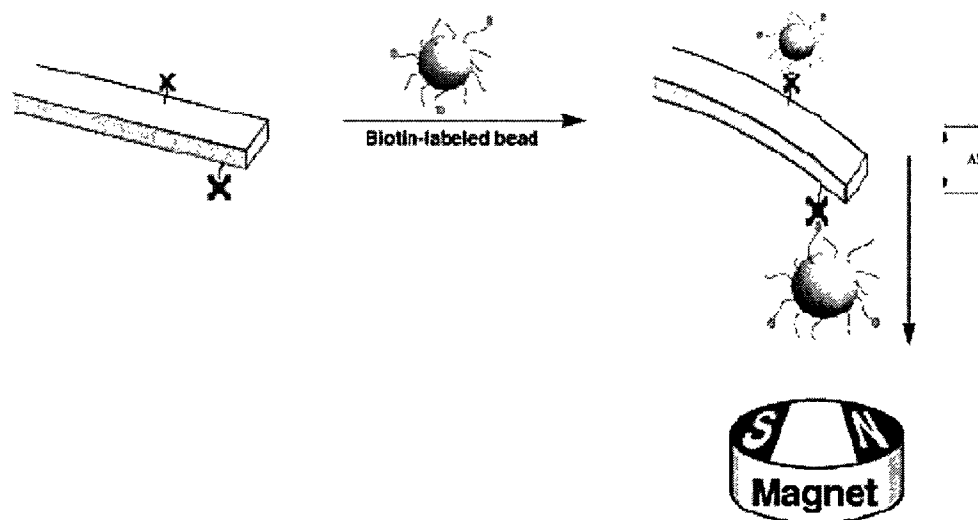


Figure 1-5. Schematic for the concept of the magneto-mechanical analysis of biorecognition processes on functional cantilevers in the presence of an external magnetic field.

### 1.2.2 Antibody-Based Microcantilever Biosensors

The first antibody-based microcantilever sensor was developed in 1999 for the detection of herbicide 2,4-dichloroethoxyacetic acid (2,4-D) [23]. In the experiments, a microcantilever was modified with herbicide 2,4-D, which was covalently attached to the microcantilever through the albumin linker. The cantilever deflected 50 nm when it is exposed to a 5 mg/ml solution of monoclonal antibody (MAb). The cantilever bent away from the coated side, which corresponded to a decrease of the surface stress. This bending is expected since a binding should lead to a decrease of the surface energy and hence, the surface stress.

Another two promising antibody-based microcantilever sensors may have applications in prostate cancer detection [24] and cardiac problems [25].

PSA that is detectable in serum has proved to be an extremely useful marker for early detection of prostate cancer and in monitoring patients for disease progression and the effects of treatment. The distinction between complex PSA (cPSA) and unbound or free PSA (fPSA) has become recognized as a clinically relevant feature of the PSA tests; the lower the fPSA in serum, the higher the chances of malignancy. Wu et al. have used a polyclonal anti-PSA antibody as a “ligand” covalently linked to the cantilever surface. The cantilever deflection due to specific fPSA binding with this antibody could detect fPSA concentrations from 0.2 ng/ml to 60  $\mu$ g/ml, which falls in the clinically relevant diagnostic PSA concentration range. The sensor could be able to detect fPSA even against the simulated background “noise” of unrelated human serum proteins such as HP and HSA or nonhuman serum protein such as bovine serum albumin (BSA), which was present at concentrations as high as 1 mg/ml.

Creatin kinase and myoglobin are two important cardiac biomarker proteins. As the development or absence of these proteins strongly predicts the individual mortality risk of a patient and has immediate therapeutic implications, continuous monitoring of a combination of these markers in real time would be very attractive. Arntz et al. [25] developed continuous label-free detection of these two cardiac biomarker proteins using an array of microfabricated cantilevers functionalized with covalently anchored anti-creatin kinase and anti-myoglobin antibodies. The results showed that the sensitivity achieved for myoglobin detection is below 20  $\mu$ g/ml. Both myoglobin and creatin kinase

could be detected independently using cantilevers functionalized with the corresponding antibodies, in unspecific protein background.

Enantioselective antibodies modified cantilevers have been investigated for its stereoselective detection of trace amounts of an important class of chiral analytes [26]. The  $\alpha$ -amino acids represent one of the most important classes of substances in nature that incorporate a stereogenic center and, therefore, exemplify an excellent model system to demonstrate chiral discrimination. This system is the first demonstration of chiral discrimination using highly scalable microelectromechanical systems. The antibodies used were raised in such a way that they selectively bind to either D- or L-R-amino acids. The temporal response of the cantilever ( $\Delta\text{deflection}/\Delta\text{time}$ ) is linearly proportional to the analyte concentration and allows the quantitative determination of enantiomeric purity up to an enantiomeric excess of 99.8%.

Virus detection is important for medical diagnostics. Efforts on virus measurements using cantilevers focused on antibody functionalization of microcantilevers. In an example, Escherichia Coli (E.coli) was successfully detected using an anti E. Coli O157:H7 antibody-immobilized silicon microcantilever [27]. The antibody immobilization on silicon was completed through a well-established four step process of surface conjugate chemistries [28]. When the aquaria E. coli O157:H7 positive sample is injected into the fluid cell where the microcantilever is held, the microcantilever bends upon the recognition of the E. coli O157:H7 antigen by the antibody on the surface of the silicon side of microcantilever. A negative control sample that does not contain E. coli O157:H7 antigen did not cause any bending of the microcantilever. The detection limit of the sensor was  $1 \times 10^6$  cfu/ml when the assay time was less than two hours. This

time is much shorter than traditional *E. coli* strain identification technique that normally takes two to three days for selective and confirmative enrichments and up to four days for a final biochemical and serological characterization.

Because of the relatively large size and mass of the virus or bacteria compared to small biomolecules, the resonance of microcantilevers can also be used to detect those pathogens. Microcantilevers are sensitive enough to measure the absorbed mass of individual vaccine virus particles with an average mass of 9.5 fg [29] (Figure 1-6 B). Based on this model, microcantilevers modified with specific antibodies were developed for detecting a single cell, such as *E. coli* cell [30-31] (Figure 1-6 A), and a single virus, such as baculovirus [32].

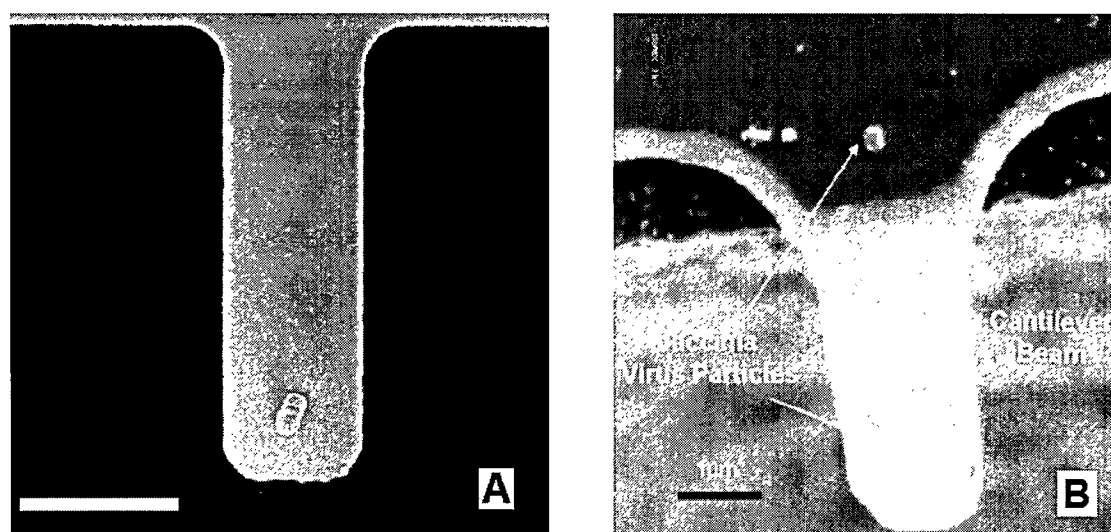


Figure 1-6 The microcantilever resonator for detection of a single cell and a single virus. **A**, a single *E. coli* cell on a microcantilever, **B**, a single vaccine virus particle on a microcantilever.

It is of clinical interest to detect and differentiate between low-density lipoproteins (LDL) from their oxidised form (oxLDL). Their uptake from plasma, principally favored to the oxidised form, is believed to be responsible of the accumulation



of cholesterol in the aortic intima and is associated with the first stage of coronary heart disease. A LDL and oxLDL differentiation by antibody modified microcantilevers was significant.

Biowarfare agents such as anthrax and other category A-C agents pose a severe threat to the health of the general population and the military. In-field, rapid diagnosis of category A-C agents is essential to implement effective therapies to treat the infection because these agents can be released or dispersed in a given area days or weeks before the appearance of symptoms. Tularemia, the most infectious pathogenic bacteria and ricin, was detected by using a microcantilever functionalized by antibodies to *F. Tularensis* [33]. When antibody modified microcantilevers were exposed to a tularemia solution of concentration from  $10^8$  to  $10^4$  organism/ml, the microcantilever had a downward bending of 20 – 1100 nm in 6 hours. Another experiment showed that ricin antibody modified cantilevers responded to as low as 40 ppt level of ricin [33].

Another independent work focused on the detection of *Salmonella enterica* [34]. With the help of a field emission scanning electron microscope, they found that when a microcantilever was exposed to Salmonella solution, the antibody functionalized side produced clear evidence of bacteria as shown in Figure 1-7, while the unfunctionalized side of the cantilever showed no binding of bacteria. It was also found that the smallest number of the bacteria that yielded a discernable deflection was about 25, which was corresponding to the bacteria concentration in solution around  $1 \times 10^6$  cfu/ml.

Many other antibodies-based microcantilever sensors have recently been developed. The stability, lifetime and reusability of monoclonal antibodies to myoglobin attached on microcantilever surface were investigated by Grogan, et al [35]; the antibody-

peptide interaction was studied by Kim, et al [36]; the detection of pesticide dichlorodiphenyltrichloroethane (DDT) using a synthetic hapten of the pesticide was reported by Tamayo's group [37]. Similar to DNA detection, the piezoresistive approach could also be used to investigate antibody-antigen interaction [38].

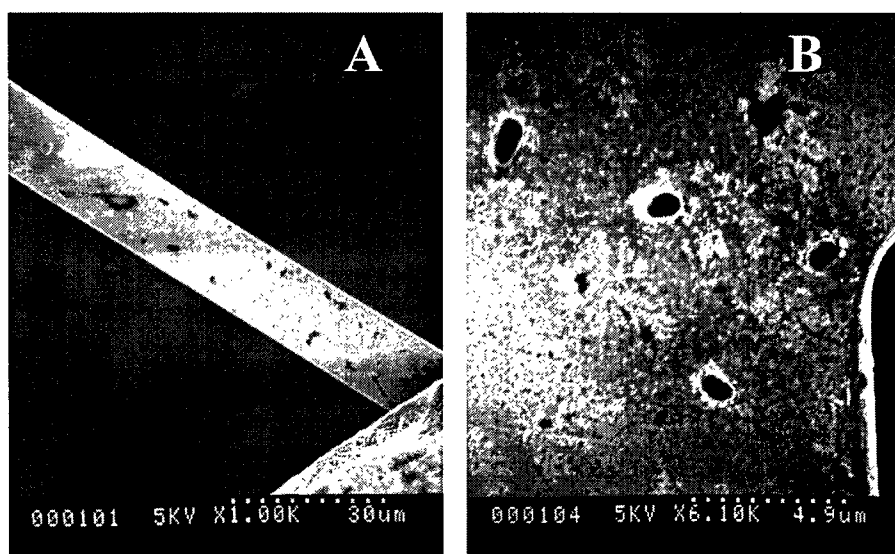


Figure 1-7. **A**, SEM micrograph showing *Salmonella* attached to the cantilever surface functionalized with the antibody. No *Salmonella* was observed in the unfunctionalized areas. **B**, Close up of *Salmonella* on cantilever.

Since the surface modification is critical in microcantilever sensing, adsorption of IgG (one type of immunoglobulins produced by plasma cells) and bovine serum albumin (BSA) on the microcantilever surface were carefully studied [39]. A very slow microcantilever bending response upon antibody injection occurs over more than over 10 h for both antibodies. This slow process was found not to be associated with adsorption of additional protein. Two explanations were proposed including the expansion of the protein after being adsorbed on the gold surface and the protein's rearrangement caused by attractive (hydrophobic) protein-protein interactions.

### 1.2.3 Enzyme Immobilized Microcantilever Biosensors

Enzyme-based biosensors have been widely used for specific chemical detection. However, enzyme modified cantilever sensors are still in their infant stage, although several sensors have been developed recently. These works are focused on glucose measurement using glucose oxidase (GOx) for proof-of-concept study.

Several approaches have applied to modified cantilever surfaces and the results are different in the deflection amplitude and response time, etc. Subramanian, et al. [40] immobilized the GOx on the microcantilever surface using typical surface conjugation chemistry, such as cross-linking the GOx enzyme with the poly-L-Lysine on the cantilever surface by glutaraldehyde. Larger deflections of cantilevers were observed when the microcantilevers were modified by adding bovine serum albumin (BSA) to block the unmodified side of the microcantilever and dropping a thicker layer of glucose oxidase on one side of the cantilever [41].

### 1.3 Objective of This Dissertation

The research of this dissertation is aimed at exploring different microcantilever modification methods for chemical and biological sensing applications. Basically, two types of modification method of microcantilevers are studied. They are self-assembly monolayer (SAM) technique and layer-by-layer (LbL) technique. For the first time, layer-by-layer technology was used in modification of a microcantilever for biosensing applications. For each technique, the study covers the methodology of the technology followed by specific examples of applications.

### 1.4 Organization of This Dissertation

Chapter One provides an introduction of microcantilever sensors, which includes their history, basic concept, and sensing mechanism. It also gives a throughout review of the latest development of microcantilever-based biosensors. Chapter Two is about the first modification method of microcantilevers, self-assembly monolayer (SAM). After an introduction to the methodology of this method, the application of using this method for immobilization acetylcholinesterase (AChE) on microcantilevers for detection of organophosphates was presented. Chapter Three is another example for using self-assembly monolayer method to immobilize antibodies on microcantilever for biowarfare agent detection. In Chapter Four, a novel method of microcantilever modification was developed – layer-by-layer method. The fundamental study of this method is presented. Chapter Five is about using layer-by-layer technique to immobilize glucose oxidase in nano assembly on the microcantilever surface for glucose detection. Chapter Six is another example of using layer-by-layer method for hydrogen peroxide detection. Chapter Seven presents conclusions and future work.

## CHAPTER TWO

### DETECTION OF ORGANOPHOSPHATES USING AN ACETYL CHOLINESTERASE (ACHE) COATED MICROCANTILEVER

#### 2.1 Introduction

The majority of nerve agents belong to a class of compounds known as the organophosphates, which are among the most toxic chemical substances. The nerve agents interfere with the action of the nervous system. Their primary mode of action is inhibition of acetylcholinesterase (AChE), which results in acetylcholine (ACh) accumulation in synaptic junctions, and produces an initial stimulation followed by prevention of cholinergic neurotransmission [42]. Early detection of organophosphates neurotoxins is critical for national security against terrorism activity, including warning of the chemical warfare attacks, protecting of our water resources and food supplies, and monitoring of detoxification processes, etc. Accordingly, there are considerable interests in the development of reliable devices for the sensitive detection of organophosphates.

## 2.2. Self-Assembly Monolayer (SAM)

### 2.2.1. Introduction

Self-assembled monolayers (SAMs) can be prepared using different types of molecules and different substrates. Widespread examples are alkylsiloxane monolayers, fatty acids on oxidic materials, and alkanethiolate monolayers. All these systems have been reviewed in great detail [44]. This introduction will concentrate exclusively on SAMs of functionalized alkanethiols on gold surfaces. This type of SAMs holds great promise for applications in several different areas. Some examples of suggested and implemented applications are molecular recognition, SAMs as model substrates, and biomembrane mimetics in studies of biomolecules at surfaces, selective binding of enzymes to surfaces, chemical force microscopy, metallization of organic materials, corrosion protection, molecular crystal growth, alignment of liquid crystals, pH-sensing devices, patterned surfaces on the  $\mu\text{m}$  scale, electrically conducting molecular wires, and photoresists. Research in this area began in 1980's [44-45]. The principle is simple: a molecule which is essentially an alkane chain, typically with 10-20 methylene units, is given a head group with a strong preferential adsorption to the substrate used. Thiol (S-H) head groups and Au(111) substrates have been shown to work excellently. The thiol molecules adsorb readily from solution onto the gold, creating a dense monolayer with the tail group pointing outwards from the surface. By using thiol molecules with different tail groups, the resulting chemical surface functionality can be varied within wide limits. Alternatively, it is also possible to chemically functionalize the tail groups by performing reactions after assembly of the SAM.

### 2.2.2. Preparation

The preferred crystal face for alkanethiolate SAM preparation on gold substrates is the (111) direction, which can be obtained either by using single crystal substrates or by evaporation of thin Au films on flat supports, typically glass or silicon. A schematic outline of the SAM preparation procedure on such gold substrates is given in Figure 2-1, together with a schematic of a mixed SAM (see below). Several different solvents are usable at the low thiol concentrations (typically 1-2 mM) that are used in preparation of SAMs, but care must be taken when using mixed thiol solutions, since the final composition of the monolayer depends upon the relative solubilities of the different thiols. The most commonly used solvent is ethanol. It is advisable to minimize the water content in the solvent if the SAMs are to be used in UHV; this minimizing will limit incorporation of water into the SAM structure, which reduces outgassing and increases repeatability in the UHV experiments. Even though a self-assembled monolayer forms very rapidly on the substrate, it is necessary to use adsorption times of 15 h or more to obtain well-ordered, defect-free SAMs. Multilayers do not form, and adsorption times of two to three days are optimal in forming highest-quality monolayers. In preparing SAMs for UHV use, meticulous rinsing and drying are, of course, highly important. As mentioned above, the tail group that provides the functionality of the SAM can be widely varied. CH<sub>3</sub>-terminated SAMs are commercially available; other functional groups can be synthesized by any well-equipped chemical laboratory, providing almost infinite possibilities of variation. In addition, chemical modification of the tail group is entirely possible after formation of the SAM, expanding the available range of functionalities

even further. Examples of functionalities used at our laboratory are:  $-\text{CH}_3$ ,  $-\text{OH}$ ,  $-(\text{C}=\text{O})\text{OCH}_3$ ,  $-\text{O}(\text{C}=\text{O})\text{CH}_3$ ,  $-\text{O}(\text{C}=\text{O})\text{CF}_3$ ,  $-\text{O}(\text{C}=\text{O})\text{C}_6\text{H}_5$ ,  $-\text{COOH}$ ,  $-\text{OSO}_3\text{H}$

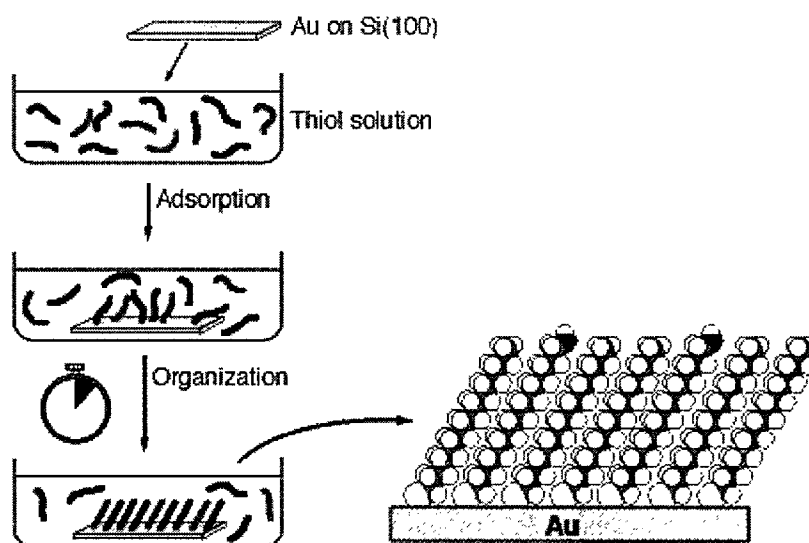


Figure 2-1 Preparation of SAMs. The substrate, Au on Si, is immersed into an ethanol solution of the desired thiol(s). Initial adsorption is fast (seconds); then an organization phase follows which should be allowed to continue for >15 h for best results. A schematic of a fully assembled SAM is shown to the right.

### 2.2.3. Mixed SAMs

By mixing two differently terminated thiols in the preparation solution, we can prepare mixed SAMs. The relative proportion of the two functionalities in the assembled SAM will then depend upon several parameters, like the mixing ratio in solution, the alkane chain lengths, the solubilities of the thiols in the solvent used, and the properties of the chain-terminating groups. In general, the composition will not be the same in the SAM as in the preparation solution. Measurements with a surface-sensitive probe like, e.g., X-ray photoelectron spectroscopy, are necessary to calibrate the mixing ratio. In cases where



the two thiol molecules are of equal alkyl chain length and no special circumstances (like bulky tail groups) are at hand, the SAM composition will be almost identical to the composition of the solution, though. One example of this is the case for mixtures of  $\text{HS}(\text{CH}_2)_{15}\text{CH}_3$  and  $\text{HS}(\text{CH}_2)_{16}\text{OH}$ .

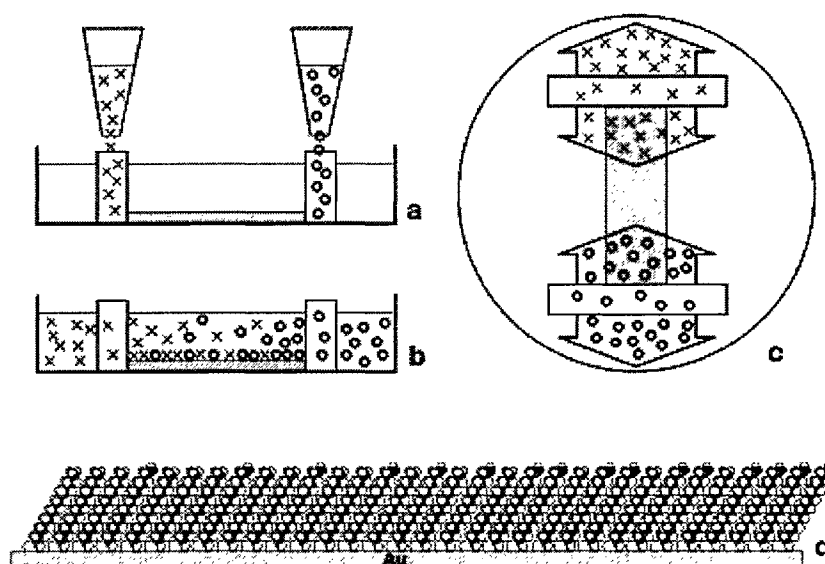


Figure 2-2. Schematic illustration of the preparation of two-component alkanethiolate gradients. (a) The two different thiols, represented by X and O, are injected into glass filters. (b) They diffuse slowly through the polysaccharide gel and attach to the gold substrate. (c) Top view showing the placement of the gold substrate between the filters. (d) Schematic illustration of a fully assembled gradient.

Another useful SAM preparation method is the formation of two-component molecular gradients, as first described by Liedberg and Tengvall [46]. By cross-diffusion of two differently terminated thiols through an ethanol-soaked polysaccharide gel (Sephadex LH-20, a chromatography material) that is covering the gold substrate, a continuous gradient of 10-20 mm length may be formed. The principle of preparation is outlined in Figure 2-2. Ethanol solutions of each of the two thiols are simultaneously

injected into two glass filters at opposite ends of the gold substrate. The presence of the polysaccharide gel makes the diffusion and the thiol attachment to the surface slow enough for a gradient of macroscopic dimension (several mm) to form.

#### 2.2.4. Characteristic

SAMs have been thoroughly characterized using a large number of surface analytical tools. Among the most frequently used techniques are infrared spectroscopy, ellipsometry, studies of wetting by different liquids, x-ray photoelectron spectroscopy, electrochemistry, and scanning probe measurements. It has been clearly shown that SAMs with an alkane chain length of 12 or more methylene units form well-ordered and dense monolayers on Au(111) surfaces. The thiols are believed to attach primarily to the threefold hollow sites of the gold surface, losing the proton in the process and forming a  $(\sqrt{3} \times \sqrt{3})R30^\circ$  overlayer structure (shown in Figure 2-3).

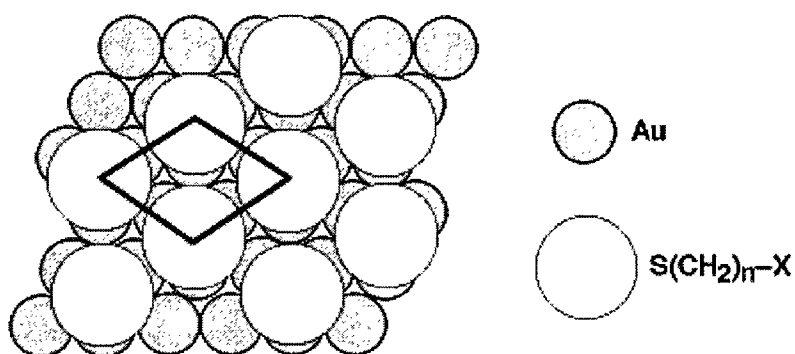


Figure 2-3. A schematic model of the  $(\sqrt{3} \times \sqrt{3})R30^\circ$  overlayer structure formed by alkanethiolate SAMs on Au(111).

The distance between pinning sites in this geometry is 5.0 Å, resulting in an available area for each molecule of 21.4 Å<sup>2</sup>. Since the van der Waals diameter of the alkane chain is somewhat too small (4.6 Å) for the chain to completely occupy that area, the chains

will tilt, forming an angle of approximately  $30^\circ$  with the surface normal. Depending on chain length and chain-terminating group, various superlattice structures are superimposed on the  $(\sqrt{3}) \times (\sqrt{3}) R30^\circ$  overlayer structure. The most commonly seen superlattice is the  $c(4 \times 2)$  reconstruction, where the four alkanethiolate molecules of a unit cell display slightly different orientations when compared with each other.

The Au-thiolate bond is strong - homolytic bond strength 44 kcal/mol - and contributes to the stability of the SAMs together with the van der Waals forces between adjacent methylene groups, which amount to 1.4-1.8 kcal/mol. The latter forces add up to significant strength for alkyl chains of 10-20 methylenes and play an important role in aligning the alkyl chains parallel to each other in a nearly all-trans configuration. At low temperatures, typically 100 K, the order is nearly perfect, but even at room temperature there are only few gauche defects, concentrated to the outermost alkyl units.

One convenient method of checking a SAM for well-ordered and dense structure is infrared reflection-absorption spectroscopy (IRAS). The CH stretching vibrations of the alkyl chain are very sensitive to packing density and to the presence of gauche defects, which makes them ideally suited as probes to determine SAM quality. In particular, the antisymmetric  $\text{CH}_2$  stretching vibration (d-) at  $\sim 2918 \text{ cm}^{-1}$  is a useful indicator; its position varies from 2916 or 2917  $\text{cm}^{-1}$  for SAMs of exceptional quality or cooled below room temperature, via 2918  $\text{cm}^{-1}$  which is the normal value for a high-quality SAM, to  $\sim 2926 \text{ cm}^{-1}$  which is indicative of a heavily disordered, "spaghetti-like" SAM. A typical IRAS spectrum of the CH stretching region of a hexadecanethiolate ( $\text{HS}(\text{CH}_2)_{15}\text{CH}_3$ ) SAM is shown in Figure 2-4.

Thickness measurements using ellipsometry yield SAM thicknesses that are in good agreement with the  $30^\circ$  chain tilt mentioned above. For example, reported ellipsometric thicknesses of hexadecanethiolate SAMs lie in the  $21 \pm 1$  Å range, to compare with the 21.2 Å that result if a fully extended hexadecanethiol molecule of 24.5 Å length is tilted  $30^\circ$ . Contact angle measurements further confirm that alkanethiolate SAMs are very dense and that the contacting liquid only interacts with the topmost chemical groups.

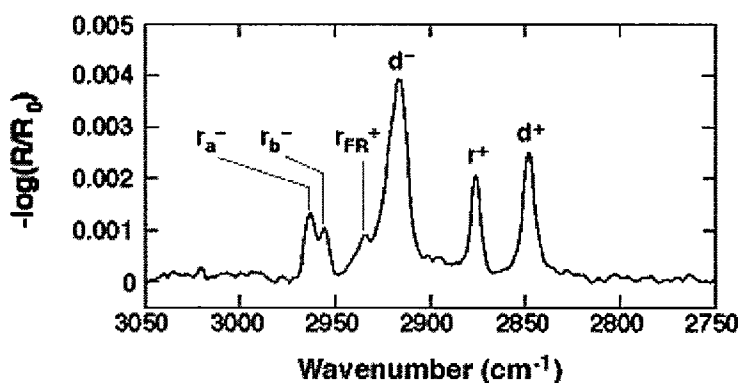


Figure 2-4. IRAS spectrum of a hexadecanethiolate SAM in the CH stretching region.

The most prominent vibrations are indicated.  $d^+$  and  $d^-$  are the symmetric and antisymmetric  $\text{CH}_2$  stretches;  $r^+$  and  $r^-$  are the symmetric and antisymmetric  $\text{CH}_3$  stretches, respectively. At the measurement temperature used (82 K), the  $r_a^-$  and  $r_b^-$  components of the  $r^-$  peak are resolved.

Reported advancing contact angles with water range from  $111^\circ$  to  $115^\circ$  for hexadecanethiolate SAMs. At the other end of the wettability scale, there are hydrophilic monolayers, e.g., SAMs of 16-mercaptohexadecanol ( $\text{HS}(\text{CH}_2)_{16}\text{OH}$ ), that display water contact angles of  $<10^\circ$ . These two extremes are only possible to achieve if the SAM surfaces are uniform and expose only the chain-terminating group at the interface. Mixed

SAMs of CH<sub>3</sub>- and OH-terminated thiols can be tailor-made with any wettability (in terms of contact angle) between these limiting values. The characteristics of mixed two-component SAMs depend strongly upon the precise chemical identity of the components and upon their proportion in the preparation solution, as already stated above. Apart from the composition of the SAMs, the issue of island formation is very important for mixed monolayers. In mixed CH<sub>3</sub>/CO<sub>2</sub>CH<sub>3</sub> SAMs, scanning tunnelling microscopy has revealed island formation on the 20-50 Å scale. For mixed SAMs of hexadecanethiol and 16-mercaptohexadecanol, which is a commonly used model system at our lab, IRAS, wetting, laser desorption spectroscopy, and TOF-SIMS data support a picture of randomly pinned, well-mixed monolayers, although mixing at a true molecular level has neither been contradicted nor confirmed at the present stage. Undoubtedly though, macroscopic phase segregation into single component domains does not occur.

### 2.3 Experiment Material

The commercially available silicon microcantilevers (Veeco Instruments, CA) were used in this experiment (Figure 2-5).



Figure 2-5 A SEM picture of a silicon microcantilever

The dimensions of the V-shaped silicon microcantilevers were 180  $\mu\text{m}$  in length, 25  $\mu\text{m}$  in leg width, and 1  $\mu\text{m}$  in thickness. One side of these cantilevers was covered with a thin layer of chromium (3 nm) followed by a 20-nm layer of gold, both deposited by e-beam evaporation. In these experiments, all the solutions were prepared with a 0.01 M sodium phosphate buffer solution at pH = 7.2. The pH of the phosphate buffer solution was adjusted by changing the ratio of 0.01M of  $\text{NaH}_2\text{PO}_3$  and  $\text{Na}_2\text{HPO}_3$  stock solutions.

#### 2.4. Microcantilever Modification

Microcantilever modification was completed in three steps (Figure 2-6) according to known surface conjugation chemistry [47].

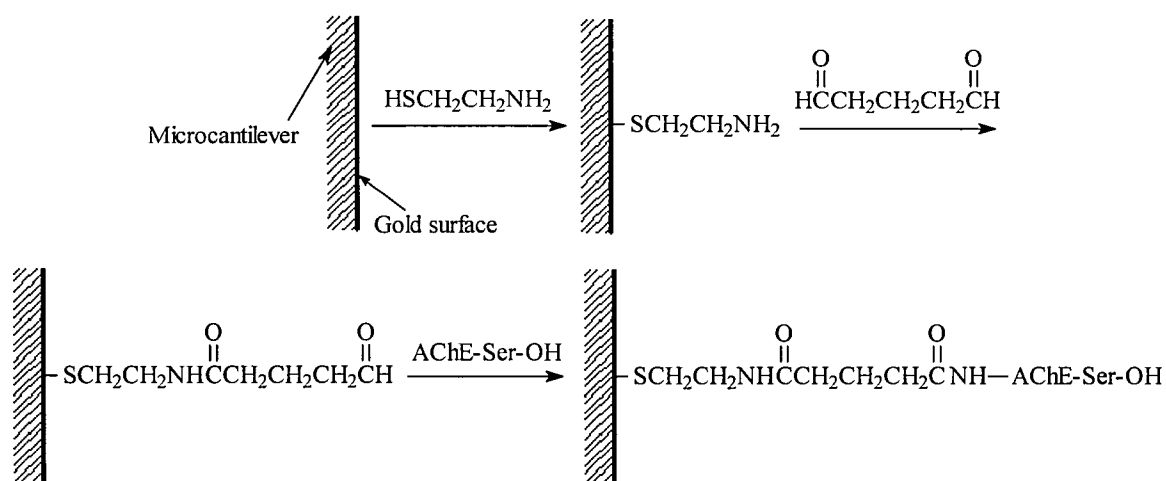


Figure 2-6 The modification procedure of an AChE covered microcantilever.

First, a self-assembled monolayer (SAM) of 2-aminoethanethiol was formed on the gold film by immersing the cantilever into a  $5 \times 10^{-3}$  M solution in a 0.01 M phosphate buffer for 12 hours, followed by rinsing the microcantilever in  $\text{H}_2\text{O}$ . Secondly, the cross-linker,

glutaraldehyde, was linked to the amino groups of 2- aminoethanethiol SAM by immersing the microcantilever into a glutaraldehyde solution (2.5% wt) for 12 hours. At last, the enzyme, AChE, was immobilized on a microcantilever by cross-linking its amino groups with the glutaraldehyde-activated surface. This cross-linking was realized by incubating the microcantilever in an AChE solution (1mg/ml) for 24 hours.

### 2.5 Experiment Setup

The deflection experiments were performed in a quartz flow glass cell (Digital Instruments, CA) such as that used in atomic force microscopy.

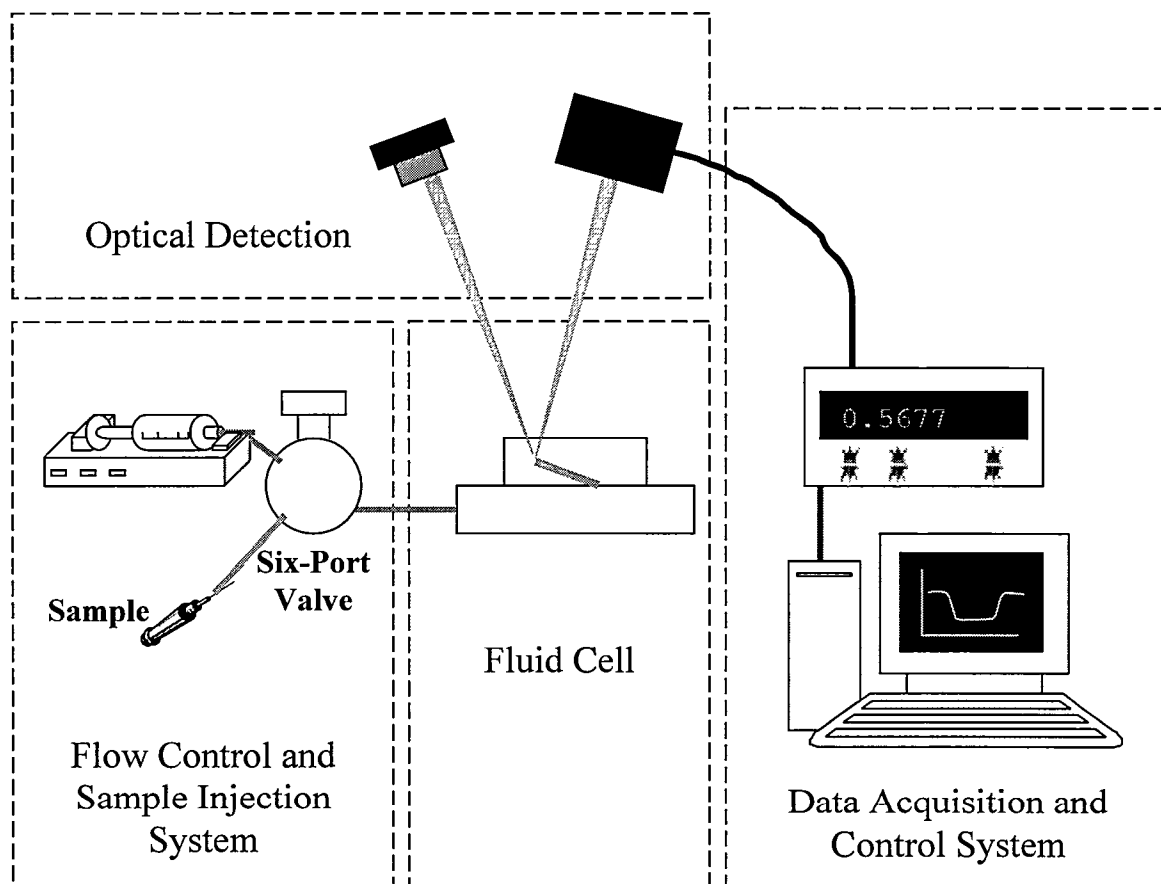


Figure 2-7 A schematic of the experimental setup used in this work.

The V-shaped microcantilever was placed in the flow cell and equilibrated with phosphate buffer solution (0.01M with pH = 7.2), which was circulated through the cell using a syringe pump.

A schematic diagram of the apparatus used in this study is shown in Figure 2-7. Since a change in the flow rate induces noise in the cantilever bending signal due to turbulence, a constant flow rate of 4 mL/h was maintained during the entire experiment.

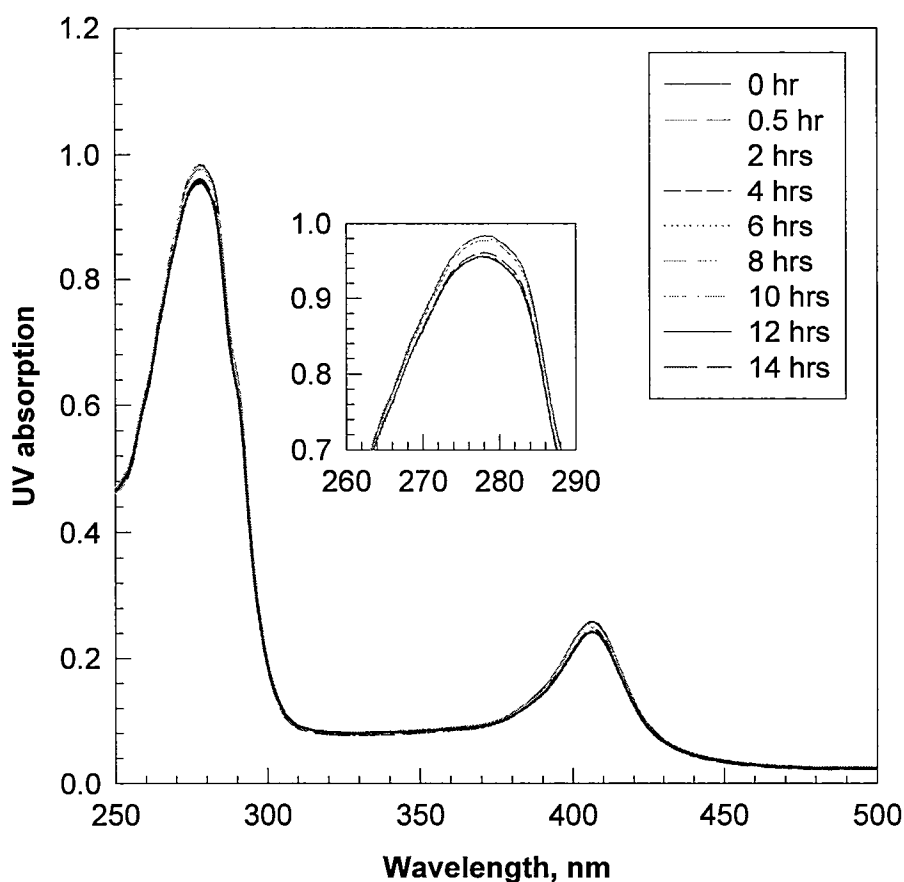


Figure 2-8 The change of UV absorption of a 1mg/ml AChE solution in 0.01M phosphate buffer solution in a UV-transparent cuvet before and after exposure to a glutaraldehyde activated microcantilever at certain hours. The cuvet (BrandTech Scientific Inc.) is transparent between 220 nm and 900 nm. No UV absorption change was observed to an AChE solution in the cuvet in the presence of a bare gold coated microcantilever (figure not shown). This control experiment suggests that AChE does not adsorb onto the wall of cuvet and the gold surface of a microcantilever.



Experimental solutions containing different concentrations of paraoxon were injected directly into the slowly flowing fluid stream via a low-pressure injection port/sample loop arrangement with a loop volume of 2.0 ml. This arrangement allowed for continuous exposure of the cantilever to the desired solution without disturbing the flow cell or changing the flow rate. Since the volume of the glass cell, including the tubing, was only 0.3ml, a relatively fast replacement of the liquid in contact with the cantilever was achieved. Microcantilever deflection measurements were determined using the optical beam deflection method.

Briefly, the bending of the cantilever was measured by monitoring the position of a laser beam reflected from the cantilever onto a four-quadrant photodiode. In our experiment, the laser beam was reflected off the gold surface. We define “bending down” as cantilever bending toward the silicon side while “bending up” refers to bending toward the gold side. For each measurement, a new cantilever was used.

## 2.6 Results and Discussions

### 2.6.1. Enzyme Immobilization

Surface modification is critical in developing a microcantilever chem/biosensor. It has been determined that full surface coverage of molecular recognition agents on a microcantilever was required for maximum microcantilever deflection response. UV absorption was used to monitor the conjugation of AChE on the microcantilever surface as shown in Figure 2-8 and Figure 2-9.

It was observed that the conjugation of AChE by the cantilever was complete after 10 hours, suggesting that the gold surface of the microcantilever was fully covered

by the conjugated AChE enzyme. In our experiments, the cantilevers were incubated in an AChE solution 24 hours.

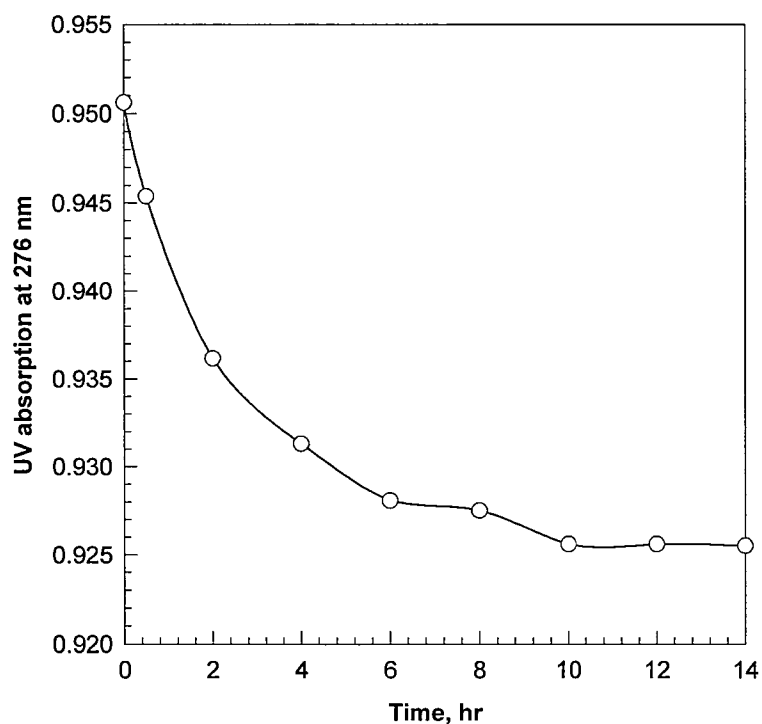


Figure 2-9 Changes in the UV absorption intensity at 278 nm of a 1mg/ml AChE solution in 0.01M phosphate buffer solution to a glutaraldehyde activated microcantilever versus the exposure time.

When a  $10^{-4}$ M solution of paraoxon in phosphate buffer (pH = 7.2) was introduced into the liquid cell to replace the buffer solution at a 4 ml/hr flow rate, the microcantilever bent up and reached a maximum amplitude in about 30 minutes as shown in Figure 2-10. The maximum amplitude of the microcantilever deflection was approximately 6 nm. It took about 30 minutes for the injected paraoxon solution to flow through the fluid cell, and at this time the phosphate buffer was circulated back into the fluid cell. When a phosphate buffer solution entered into the liquid cell to replace the paraoxon solution, the

microcantilever stopped bending, but the microcantilever did not return to the initial position.

### 2.6.2. Microcantilever Deflection Due to AChE Inhibition by Paraoxon

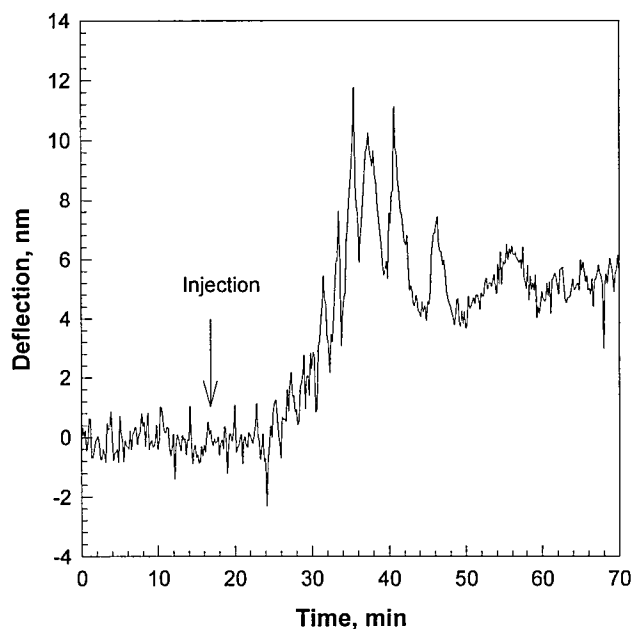


Figure 2-10 Bending response as a function of time,  $t$ , for a silicon microcantilever with AChE enzyme coated on its gold side after injection of  $10^{-4}$  M paraoxon in 0.01 M phosphate buffer solution at  $\text{pH} = 7.2$ . The microcantilever was preequilibrated in a 0.01 M phosphate buffer solution before injection of the paraoxon solution.

Figure 2-11 shows the maximum deflection amplitudes of AChE coated microcantilevers versus the concentration of paraoxon in the 0.01 M phosphate buffer solutions. The concentrations of paraoxon in the solutions were varied from a low concentration of  $1 \times 10^{-8}$  M to a high concentration of  $1 \times 10^{-3}$  M, and the cantilever deflection changed from 0 nm to 7 nm. The microcantilever deflection increased as the concentration of paraoxon increased. The detect limit was  $10^{-8}$  M. For each measurement,

a 2.0-ml aliquot of paraoxon solution was switched into the fluid cell where the microcantilever was held. As the detection limit of the AChE-based biosensor is directly related to the capacity of the target chemical to inhibit AChE, the detection limit might be different for other organophosphorus compounds or other inhibitors.

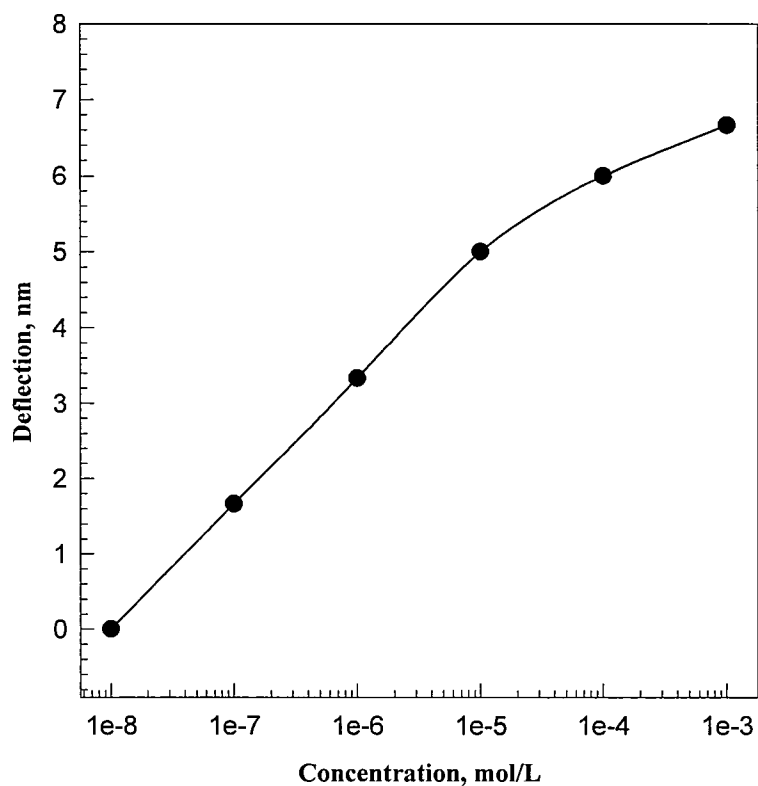
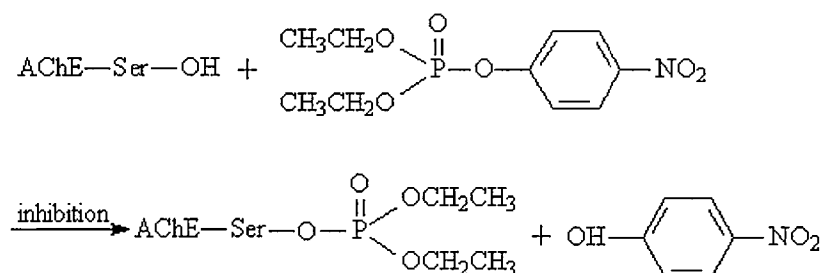


Figure 2-11 Maximum deflection of a silicon microcantilever coated with AChE enzyme on its gold side as a function of the concentration of paraoxon in 0.01M phosphate buffer solution at pH = 7.2.

### 2.6.3 Sensing Mechanism

Many organophosphorus compounds inhibit the activity of AChE through phosphorylation of the serin group of an AChE, according to the following reaction [48].

The inhibition of AChE by many organophosphorus compounds, including paraoxon, is irreversible. Bending of the microcantilever may result from a change in the conformation of AChE due to exposure to paraoxon.



Change in conformation can result in the surface stress variation of the microcantilever. Since the AChE only slightly changes its conformation upon complexation with organophosphates [49], the surface stress change on the microcantilever caused by possible AChE conformational change was very small. For a 6 nm deflection, the surface stress change was only 0.014 N/m according to the following equation [50].

$$\Delta Z = \left( \frac{3(1-\nu)L^2}{Et^2} \right) \delta s \quad (2.1)$$

Where  $\Delta Z$  is the observed deflection at the end of the cantilever,  $\nu$  and  $E$  are Poisson's ratio (0.2152) and Young's modulus (155.8 GPa) for the silicon substrate, respectively,  $t$  is the thickness of the cantilever (1  $\mu\text{m}$ ),  $L$  is the length of the cantilever (180  $\mu\text{m}$ ), and  $\delta s$  is the differential stress on the cantilever.

## 2.7 Summary

The results of this research have demonstrated that the slightly conformational change of AChE caused by inhibition of organophosphates can be used to detect

organophosphates by confining AChE on a microcantilever. The same concept can be used to develop other microcantilever biosensors by varying the enzyme. Because the bending amplitude of the microcantilever generated by the inhibition of AChE was relatively small, this microcantilever sensor will by no means be a real time sensor for field detection of organophosphates. However, significant microcantilever deflection can be achieved by changing the structure or materials of the cantilever. For instance, the predicted deflection of a 0.3- $\mu\text{m}$ -thick silicon microcantilever under the same surface stress change can be 10 fold of that of the commercially available 1- $\mu\text{m}$ -thick microcantilever used in this work according to equation 2.1.

## **CHARTER THREE**

### **MOLECULAR RECOGNITION OF BIOWARFARE AGENTS USING MICROCANTILEVER SENSORS**

#### 3.1. Introduction

Early detection of terrorist threats is an absolute must in the fight against terrorism. Terrorist threats involve chemical, biologic, radiological and explosive substances. Terrorist acts involving explosives are the most common. The use of biologic agents as a warfare or terrorist weapon has been reported recently, although it is less prevalent than the use of explosives. Very small amounts of biologic agents (e.g., micrograms of anthrax) can potentially inflict large-scale damage to people, much more than an equivalent amount of an explosive substance. Also, biologic agents can be widely distributed in both air and water. Biowarfare agent detection is one of the primary areas where the war on terrorism urgently requires new developments in sensor technology. At present, a considerable threat exists for bioterrorist attacks on drinking water, food processing industries, public transportation systems, and other infrastructure. Unlike explosives and chemicals, biowarfare agents can be slow in affecting a large number of people.

Currently available sensors are inadequate to address the complexity and enormity of the threat involving biowarfare agents. As a practical consequence, there is an urgent need for rugged, low-cost sensing systems that are highly sensitive and selective and thus well suited for real-time detection of biowarfare agents. A number of agents can be used for bioterrorism. Recent attacks using anthrax have claimed many lives. Use of biotoxins such as ricin as terrorist weapons has been reported. As a number of organisms and biotoxins exist that can be used as biowarfare agents, it is essential to have a technology that is capable of simultaneous detection of multiple agents. In addition, the biowarfare agents can be dispersed in a number of scenarios, and, therefore, a sensor platform that can operate in air as well as in solution is required for large-scale deployment. Currently fielded-sensing technologies fail to show the potential for broad deployment due to their high volume, weight, power requirements and expense. Furthermore, presently employed technologies are based on bulky and complex equipment and are not amenable to miniaturization. Therefore, no currently available technology offers a clear path to the development of a device with the required attributes: an extremely sensitive and selective handheld, battery-operated biologic sensor that can be mass-produced.

### 3.1.1 Antibody-Antigen

An antibody is an immunoglobulin, a specialized immune protein produced because of the introduction of an antigen into the body, and which possesses the remarkable ability to combine with the very antigen that triggered its production. This reaction could happen not only in vivo but also in vitro. See Figure 3-1 [51] for the basic structure of an antibody.



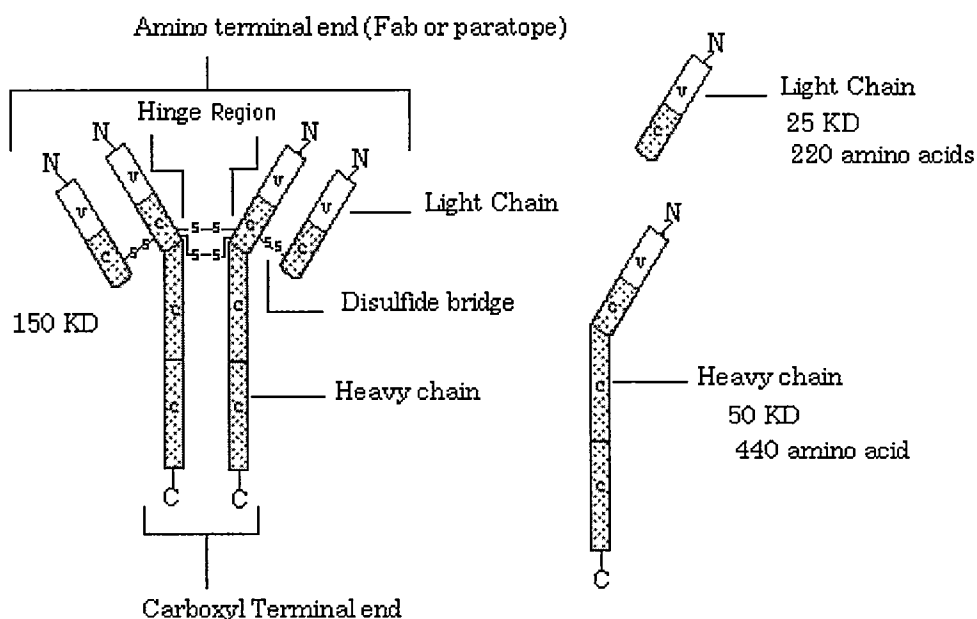


Figure 3-1 Structure of a typical immunoglobulin (antibody) protein. Two identical heavy chains are connected by disulfide linkages. The antigen-combining site is composed of the variable regions of the heavy and light chains, whereas the effector site of the antibody (which controls whether it agglutinates antigens) is determined by the amino acid sequence of the heavy chain constant region.

The forces that act to hold the antibody and antigen together are partly physical and partly chemical. Physical forces include complementary shape, i.e., a "key in lock" fitting together, as shown in Figure 3-2 [52].

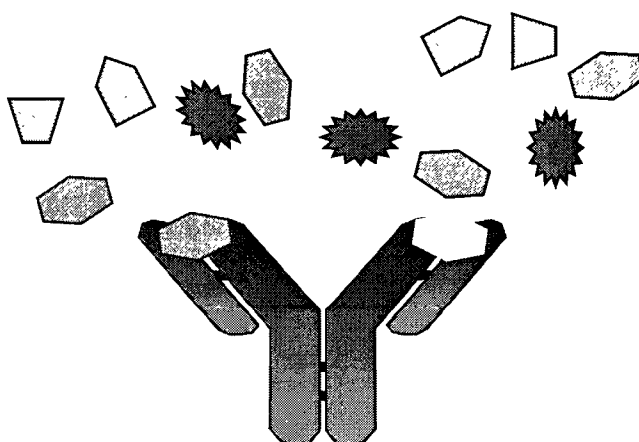
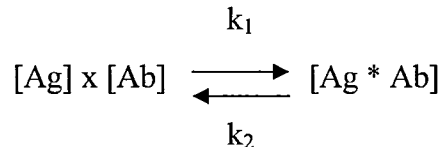


Figure 3-2 Illustration of antigen-antibody recognition by complementary shape

The law of mass action can be represented as follows:



where [ ] = concentration,  $k_1$  = association constant, and  $k_2$  = disassociation constant.

Because we want a large  $[Ag * Ab]$ , we want  $k_1$  to be larger than  $k_2$ . Put another way,

$$k = \frac{k_1 [Ag * Ab]}{k_2 [Ag] \times [Ab]}$$

The chemical forces are not well understood. They are believed to be relatively weak forces that act to hold the antigen and antibody together chemically. In order for these forces to work, the antigen and antibody must be very close together. We will now look at factors that affect reactions. Some factors can be manipulated to enhance the reaction so that we can detect them.

1. **Ionic Bonds:** This bond results from the electrostatic attractive forces between charged sites on antigens (e.g.  $COO^-$ ) and oppositely charged sites on antibodies (e.g.  $NH^{3+}$ ).
2. **Hydrogen Bonds:** These relatively weak bonds occur when proton donors (OH, NH) and acceptors ( $COO^-$ ) on antigens and antibodies share hydrogen atoms.
3. **Van der Waals Forces:** These are very short-range bonds which result from the interaction of electron clouds of two atoms. When electrons swing to one side of an atom, a slight positive charge occurs at the other side which can attract the negatively charged electrons of a nearby atom.

4. Hydrophobic Bonds: The two hydrophobic surfaces on an antigen and antibody are brought close together, and the water molecules between the surfaces are excluded. The two hydrophobic surfaces then come together to decrease the total surface area exposed. Hydrophobic bonds result from the tendency of all molecules to exist in the lowest free energy state and are entropy driven (energy required to maintain structural order).

Other environmental factors also affect the recognition between Ab and Ag. Ultimately, we want a large number of antibody molecules to be bound to each antigen. To achieve this goal, reactions require a large Ag to Ab ratio. Most antibodies can react within a large pH range of 5.5 to 8.5, and many appear to react best between 6.5-7.5. To maintain a physiologic pH, the isotonic saline used in our experiment may be buffered to a pH of about 7.0. Some antibodies react best at 37°C (warm antibodies), and some react best at 4°C (cold antibodies). Cold antibodies may only react at 4°C, or they may have a higher thermal range and react at 15°C, 22°C, or even 37°C. For warm antibodies, temperature affects the speed of the reaction, e.g., a warm antibody may take four hours to react at 4°C, but only 30 minutes to react at 37°C. As a general rule, antigen-antibody reactions occur at a faster rate in low-ionic-strength solutions (LISS). In saline phases most antibodies will react optimally between 30-60 minutes, thus, this incubation period is the one usually used. If too short an incubation period is used, false negatives can result as enough Ag\*Ab complex will not have formed. Likewise, too long an incubation period can cause false negatives as  $k_2$  may overtake  $k_1$  (from the law of mass action) [52].

### 3.2. Experimental Material

Tularemia (*Francisella tularensis*) is a small ( $0.2 \mu\text{m} \times 0.2\text{--}0.7 \mu\text{m}$ ), pleomorphic, poorly staining, nonmotile, gramnegative aerobic coccobacillus. It is one of the most infectious pathogenic bacteria known. It has a thin lipopolysaccharide-containing envelope and is a hardy nonspore-forming organism that survives for weeks at low temperatures in water, moist soil, hay, straw and decaying animal carcasses [53]. It has been divided into two major subspecies (biovars) by virulence testing, biochemical reactions, and epidemiologic features [54]. *F. tularensis* biovar tularensis (type A) may be highly virulent in humans and animals, produces acid from glycerol, demonstrates citrulline ureidase activity, and is the most common biovar isolated in North America [55]. Biovar palaeartica (type B) is relatively avirulent, does not produce acid from glycerol, and does not demonstrate citrulline ureidase activity. Transformed plasmids have been engineered to express chloramphenicol and tetracycline resistance in *F. tularensis* [56]. Virulent, streptomycin-resistant *F. tularensis* strains have been examined in biowarfare agent studies [57]. Although its virulence factors are poorly understood and characterized [58], it is possible that strain virulence could be enhanced through laboratory manipulation.

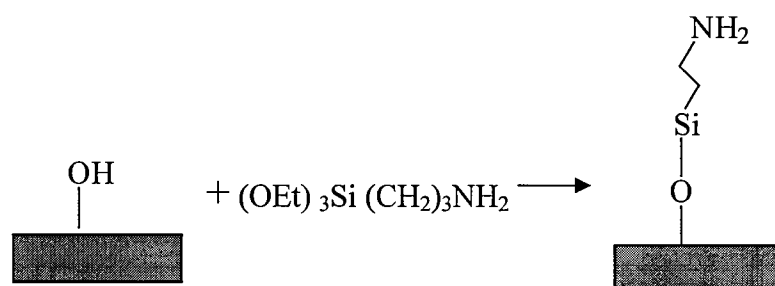
*F. tularensis* has been identified by using gram stain, direct fluorescent antibody, or immunohistochemical stains. Microscopic demonstration by fluorescent-labeled antibodies is a rapid diagnostic procedure [59]. The affinity-purified antibody to *F. tularensis* that was used in the authors' experiments was obtained from Voigt Global Distribution LLC. The *F. tularensis* sample was purchased from Biodesign International. The virus used in this work was killed by heat. A 0.1 M phosphate-buffered saline (PBS)

(pH = 7.3) buffer solution was used in all the experiments. The buffer solution was composed of 137 mM NaCl, 2.7 mM KCl, 4.3 mM Na<sub>2</sub>HPO<sub>4</sub>, and 1.4 mM KH<sub>2</sub>PO<sub>4</sub>.

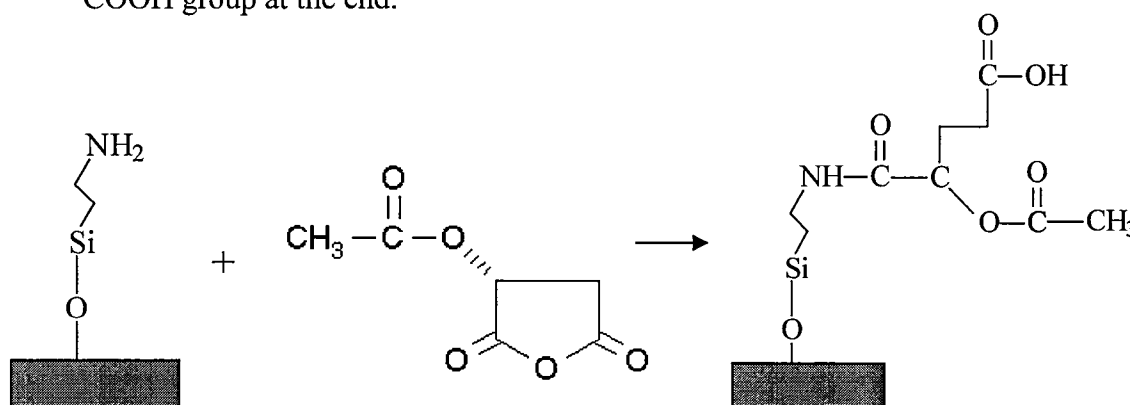
### 3.3. Microcantilever Modification

Microcantilever modification was completed in four steps according to known surface conjugation chemistry as following [28].

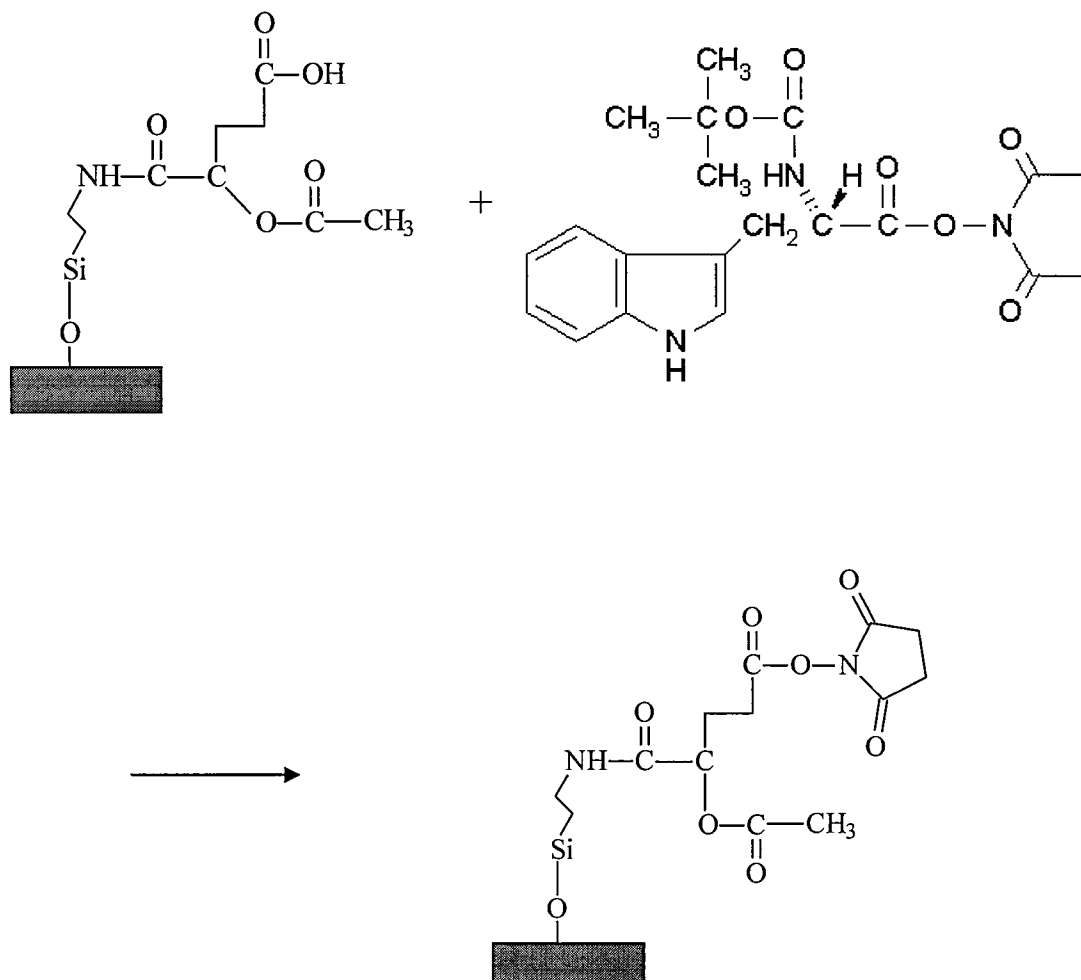
Step 1: Aminopropyl triethoxysilane (ATS) grows on silicon with NH<sub>2</sub> as the ending function group.



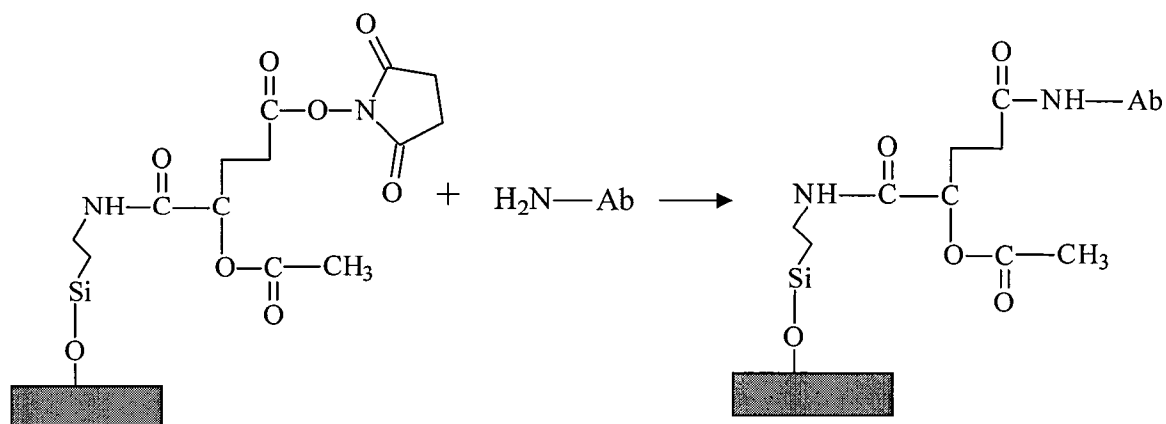
Step 2: Succinic anhydride (SA) reacts with the amino group and forms amide and a COOH group at the end.



Step3: N-hydroxysuccinimide (NHS) has an exchange reaction with H in COOH on surface as there are many NHS available, and the following structure formed.



Step 4: Antibodies covalently links the SAMs via amines on protein. Amines attack the C in C-O and form a new C-N bond.



First, a thin film of aminopropyl triethoxysilane (ATS) was formed on the silicon surface by immersing the cantilever for 24 h at room temperature in a 1% solution of ATS in EtOH:H<sub>2</sub>O = 95:5 (no piranha cleaning was used).

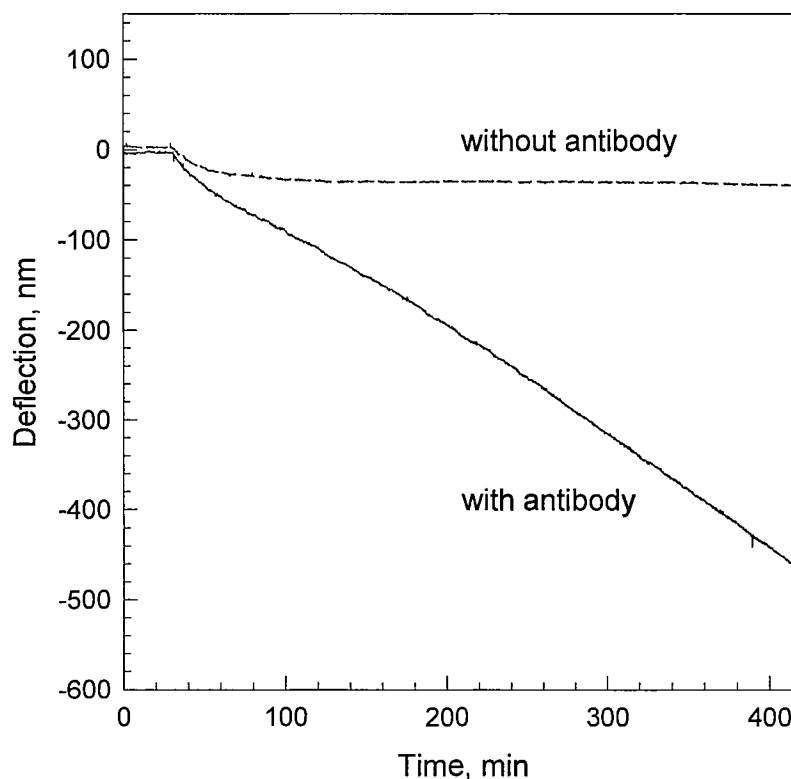


Figure 3-3 Bending response as a function of time for an antibody immobilized microcantilever and a microcantilever modified by the same procedure except the final antibody attaching step upon injection of a  $1 \times 10^6$  organisms/mL solution of *F. Tularensis* in 0.1M phosphate-buffered saline buffer (pH=7.3)

Immersion was followed by rinsing in H<sub>2</sub>O. The cantilever was then immersed into a 10% succinic anhydride solution in N<sub>2</sub>-saturated N,N-dimethylformamide (DMF) for 6 h, followed by a thorough H<sub>2</sub>O rinsing. The microcantilever was then activated by immersion for 30 minutes at room temperature in a buffer solution of 0.05 mM 4-morpholinepropanesulfonic acid (MES) containing 100 mg/ml of 1-ethyl-3-(3-

dimethylaminopropyl)carbodiimide hydrochloride (EDC) and 100 mg/ml of N-hydroxy-succinimide (NHS) (pH= 6.8). In the final preparation step, the antibodies were covalently immobilized on the microcantilever surface by incubating the microcantilever in a 5  $\mu$ g/ml antibody solution in 0.1 M PBS (pH = 7.3) for 3 hours.

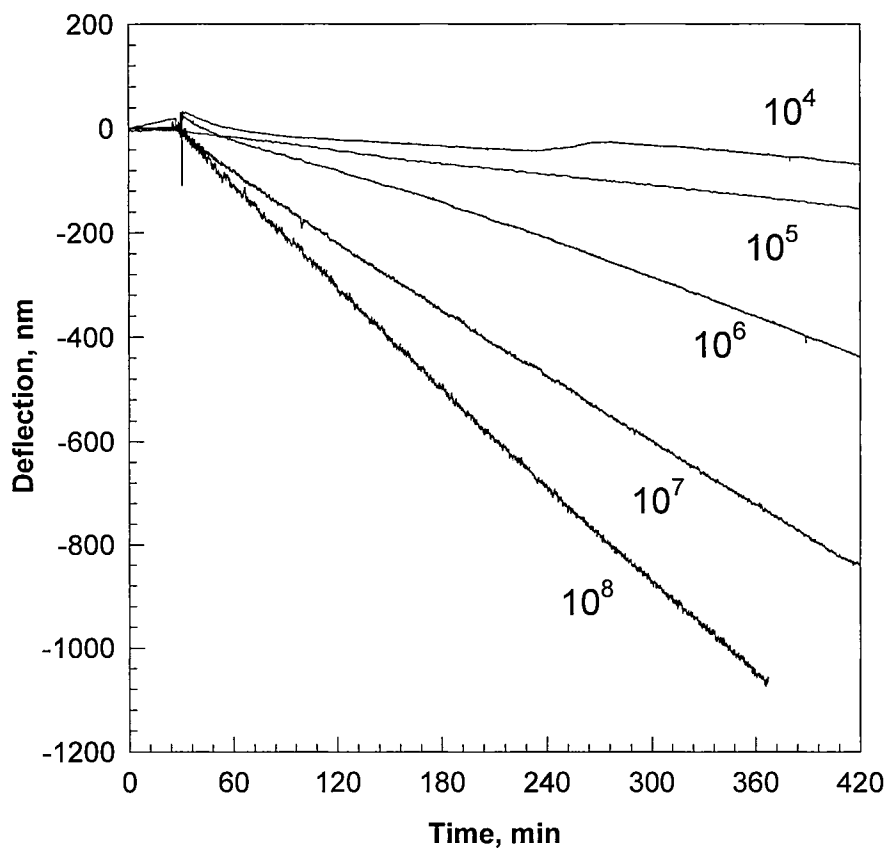


Figure 3-4 Bending response as a function of time for antibody immobilized microcantilevers upon injection of different concentration (organisms/mL) solutions of *F. Tularensis* in 0.1M phosphate-buffered saline buffer (pH=7.3)

### 3.4. Experiment Setup

The same experiment setup as described in Section 2.5. was used for this experiment. For this experiment, the static experiment mode was chosen considering that normally a longer reaction time is needed for antigen-antibody interaction. This means



that there is no flow rate. The system was first balanced until a stable base line was reached. The different concentration of the antigen solution was then injected.

### 3.5. Results and Discussions

The deflection of an antibody-coated cantilever as a function of time for a  $1 \times 10^6$  organisms/ml concentration of *F. tularensis* in a 0.1 M PBS buffer solution (pH = 7.3) is displayed in Figure 3-3.

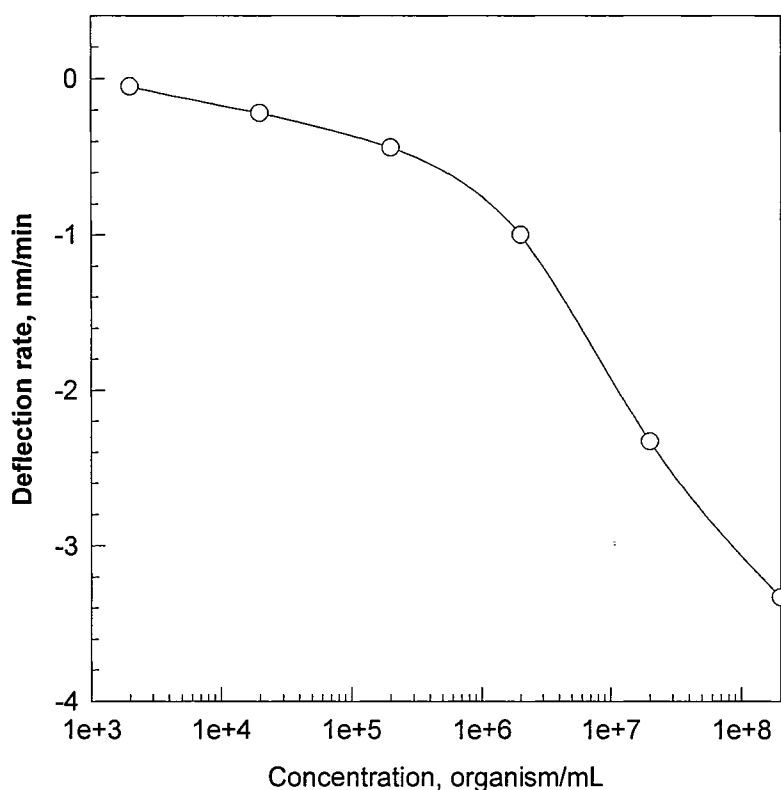


Figure 3-5 Deflection rate for antibody modified microcantilevers after exposure to *F. Tularensis* vs. the concentration of *F. Tularensis*.

The microcantilever bent down after exposure to the *F. tularensis* solution, but the bending did not reach its maximum, even five hours after the injection, suggesting that the capture of *F. tularensis* by the antibodies on the microcantilever surface was not

complete. This result may be due to the steric effect caused by the size of the cells or fragments. The deflection versus time curve is almost linear in the observed time scale. Furthermore, when the *F. tularensis* solution was replaced by the buffer solution, the cantilever did not bend back to its original position; it remained at the same level, ruling out the possibility of physical adsorption of antibodies on the cantilever surface. Due to experimental constraints, this group did not carry out the experiments longer than 5 hours.

A control experiment was performed with a modified microcantilever. The same procedure was used as described previously with the exception that the final antibody-attaching step was not done. When the cantilever was exposed to a  $1 \times 10^6$  organisms/ml concentration of *F. tularensis*, the cantilever bent slightly and saturated after 10 minutes. This result was attributed to nonspecific binding of organisms with organic functional groups on the microcantilever.

The deflection of antibody-coated cantilevers as a function of time for different concentrations of *F. tularensis* in a 0.1 M PBS buffer solution (pH = 7.3) is illustrated in Figure 3-4. The rate of bending is a function of the *F. tularensis* concentration. The cantilever bent more quickly at high concentrations. The increase in deflection rate at high concentrations may be due to the irreversible nature of adsorption. The deflection rate of an antibody-modified microcantilever after exposure to *F. tularensis* versus the concentration of *F. tularensis* is shown in Figure 3-5. The figure demonstrates that microcantilevers can be used for the detection of *F. tularensis* with a detection limit of  $10^3$  organisms/ml. Since some nonspecific binding is contributing to the signal, a differential measurement using two cantilevers is required for improving sensitivity.

### 3.6 Summary

An anti *F. Tularensis* antibody-immobilized microcantilever has been demonstrated as a novel biosensor for the detection of *F. Tularensis* with a detection limit of less than  $1 \times 10^3$  organisms/mL after exposure to *F. Tularensis* at room temperature. These results suggested that many other pathogens can be sensitively detected by using microcantilever sensor technology.

## CHAPTER FOUR

### MICROCANTILEVER MODIFICATION WITH LAYER-BY-LAYER TECHNIQUES

#### 4.1. Introduction to Layer-by-Layer Technique

Layer-by-Layer (LbL) assembly can construct an ultra thin film via alternate adsorption of oppositely charged polyions, nanoparticles, biomolecules, etc [60-65]. The obtained films have thicknesses in the nanometer range and tunable properties to their surroundings, such as permeability, solubility, and morphology [60-65]. The development of polyelectrolyte microcapsules is based on LbL assembly on nano- or micro-scale cores, for instance, cells, inorganic or organic particles, dyes, and drugs, which have recently gained intensive attention [66-67]. Cores, with diameters ranging from nanometers to microns, are coated with alternating layers of polycations, polyanions, and other materials. After dissolving the cores, hollow microcapsules were gained with ordered walls of needed composition, and thickness in the range of 20-100 nm. The capsules have tunable permeability for molecules of different sizes on the basis of open-and-close mechanisms by adjusting the environmental stimuli [68-70]. These capsules offer broad perspectives in encapsulation, transport, and controllable delivery of drugs,

minerals, and proteins. Furthermore, they are promising reaction containers useful in chemical and biomedical field, like microreactors, or biosensors.

#### 4.1.1. Polyanion / Polycation Alternate Assembly

The LbL method for film self-assembly makes use of the alternate adsorption of oppositely charged macromolecules (polymers, nanoparticles, and proteins) [71-76]. The assembly of alternating layers of oppositely charged linear or branched polyions and nanoparticles is simple and provides the means to form 5–500 nm thick films with monolayers of various substances growing in a pre-set sequence on any substrates at a growth step of about 1 nm. These films have a lower molecular order than LB or free-standing films, but they have the advantage of high strength and the easy preparation. T. Mallouk [73] has called this technique “molecular beaker epitaxy,” meaning with simple instruments (exploiting the materials self-assembly tendency), one can produce molecularly organized films similar to the ones obtained with highly sophisticated and expensive molecular beam epitaxy technology used for metals and semiconductors.

#### 4.1.2. Standard Assembly Procedure

The general procedure of LbL assembly is as follows: a cleaned substrate of any shape and dimension is immersed into a dilute solution of a cationic polyelectrolyte, for a time optimized for the adsorption of a single monolayer (ca 1 nm thick), and then it is rinsed and dried. The next step is the immersion of the polycation-covered substrate into a dilute dispersion of polyanions or negatively charged nanoparticles (or any other nanosize charged species) also for a time optimized for the adsorption of a monolayer, and then it is rinsed and dried. These operations complete the self-assembly of a polyelectrolyte monolayer and monoparticulate layer sandwich unit onto the substrate

(Figure 4-1). Subsequent sandwich units are self-assembled analogously. Linear polycation/polyanion multilayers can be assembled by similar methods. Different nanoparticles, enzymes and polyions may be assembled in a pre-planned order in a single film.

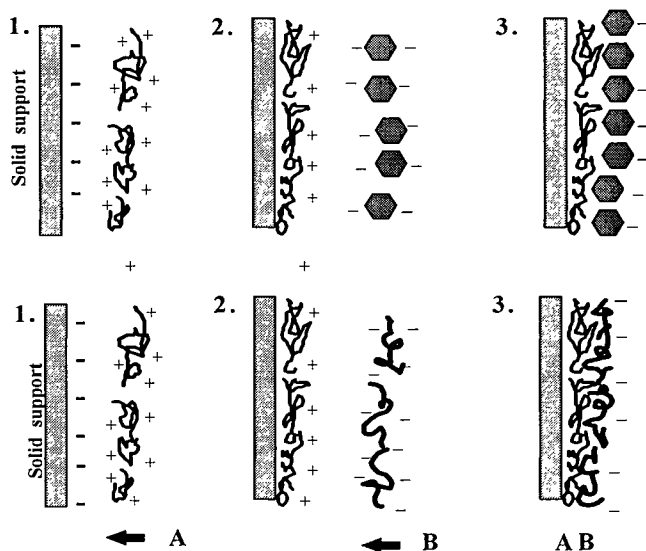


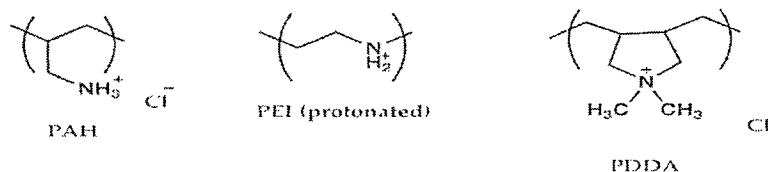
Figure 4-1 Schematic picture of polycation/polyanion multilayer, neighbor layers interpenetrate on about 30%, so that only first and third layers are well separated.

The forces between polyion layers govern the spontaneous layer-by-layer self-assembly of ultrathin films. These forces are primarily electrostatic and covalent in nature, but they can also involve hydrogen bonding, hydrophobic, and other types of interactions. The properties of the self-assembled multilayers depend on the choice of building blocks used and their rational organization and integration along the axis perpendicular to the substrate.

The sequential adsorption of oppositely charged colloids was reported in a seminar paper in 1966 by Iler [71]. The electrostatic self-assembly was subsequently “rediscovered” in the nineties and extended to the preparation of multilayers of

polycations and phosphonate ions, as well as to the layering of linear polyions, proteins and nanoparticles by Mallouk, Decher, Möhwald, Lvov, Rubner, Fendler, Hammond, Kunitake, Tsukruk, Schlenoff, Caruso, and others. This self-assembly is now employed in the fabrication of ultrathin films from charged polymers (polyions) [74-77], dyes [78-80], nanoparticles (metallic, semiconducting, magnetic, insulating) and clay nanoplates [81-82], proteins [83], and other supramolecular species [84]. That any of these species in any order can be adsorbed layer-by-layer is the greatest advantage of this self-assembly. The oppositely charged species are held together by strong ionic bonds, and they form long-lasting, uniform, and stable films. Self-assembly is economical and readily amenable to scaling-up for the fabrication of large-area defect-free devices on any kind and shape of surfaces.

#### Polycations (MW 50 000-70 000)



#### Polyanions (MW 50 000-70 000)

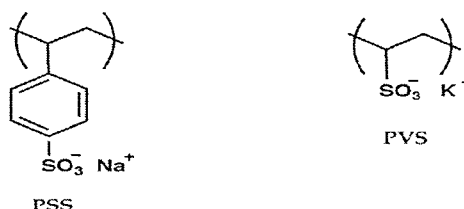


Figure 4-2. Common polyions used in LbL assembly

Polyions predominately used in the assembly are as follows (Figure 4-2): polycations: poly(ethylenimine) (PEI), poly(dimethyldiallylammonium chloride) (PDDA), poly(allylamine) (PAH), polylysine, chitosan; polyanions: poly(styrenesulfonate) (PSS), poly(vinylsulfate), poly(acrylic acid), dextran sulfate, sodium alginate, heparin, DNA. One can grow polymer nanocomposite films by means of the sequential adsorption of different material monolayers that employ hundreds of commercially available polyions. The only requirement is that there should be a proper (positive / negative) alternation of the component charges.

#### 4.1.3. Kinetics of Polyion Adsorption

For the time-dependent control of adsorption and monitoring of the assembly in situ, the quartz crystal microbalance method is quite suitable. The kinetics of the adsorption process could be delineated by the QCM-technique, which is indispensable for establishing proper assembly conditions (e.g., a saturation adsorption time).

The multilayer assemblies are characterized by means of quartz crystal microbalance technique in two ways: 1) drying a sample in a nitrogen stream we measured the resonance frequency shift and calculated an adsorbed mass by the Sauerbrey equation; or 2) monitoring the resonator frequency during the adsorption process onto one side of the resonator which was in permanent contact with polyion solutions. While performing experiments in permanent contact with the polyion solution, we touched the surface of solutions with one side of the resonator, while the upper electrode was kept open to air and the upper contact wire was insulated from the solution by a silicone paint covering.



The fitting of adsorption to an exponential law yields a first-order rate of adsorption for poly(styrenesulfonate) (PSS)  $\tau = 2.5 \pm 0.2$  minutes and for polyallylamine (PAH)  $\tau = 2.1 \pm 0.2$  minutes. This rate means that during the first five minutes about 87% of the material is adsorbed onto the charged support and  $t = 8$  minutes ( $t = 3\tau$ ) gives 95% full coverage. Typically, in most publications on polyion assembly, adsorption times of 5 to 20 minutes are used. One does not need to maintain an adsorption time with great precision: a minute more or less does not influence the layer thickness if we are at the saturation region. For other species, poly(dimethyldiallylammonium chloride) (PDDA), polyethyleneimine (PEI), montmorillonite clay, myoglobin, lysozyme, and glucose oxidase, the first-order rate of adsorption onto an oppositely charged surface was found to be 2, 3, 1.8, 3, 4 and 5 minutes respectively. Interestingly, 5 - 20 minutes is essentially greater than the diffusion-limited time (mass transport limitation), which is necessary for complete surface covering (for the used linear polyion concentrations it is a few seconds). Only for 45-nm silica/PDDA assembly do we have an example when two seconds time corresponds to the diffusion limited time for the SiO<sub>2</sub> monolayer adsorption.

One could suppose that linear polyion adsorption occurs in two stages: quick anchoring to a surface and slow relaxation. To reach a surface charge reversion during linear polyion adsorption one needs a concentration greater than  $10^{-5}$  M. The dependence of polyion layer thickness on concentration is not great: thus, in the concentration range of 0.1 - 5 mg/ml poly(styrenesulfonate)/poly(allylamine) (PSS/ PAH) pair yielded a similar bilayer thickness. A further decrease in polyion concentration (using 0.01 mg/ml) decreases the layer thickness of the adsorbed polyion. An increase in the component concentrations to 20-30 mg/ml may result in the non-linear (exponential) enlargement of

the growth rate with adsorption steps, especially if an intermediate sample rinsing is not long enough.

#### 4.1.4. First Layers and Precursor Film

At the very beginning of the alternate assembly process one often sees non-linear film growth. At the first 2 - 3 layers, smaller amounts of polyion are adsorbed as compared with further assembly, when the film mass and thickness increase linearly with the number of adsorption cycles. Tsukruk et al explained this as an island-type adsorption of the first polyion layer on a weakly charged solid support. In the following two-three adsorption cycles these islands spread and cover the entire surface, and further multilayer growth occurs linearly. If a substrate is well charged, then a linear growth with repeatable steps begins earlier.

In studying the possibility of using new compounds in the assembly, a precursor film approach was used. On a substrate (silver electrode of QCM resonator or quartz slide) we deposited 2 - 3 layers of polyions, and on this "polyion blanket," with a well defined charge of the outermost layer, an assembly of proteins, nanoparticles, or other compounds was produced. In a typical procedure, precursor films were assembled by repeating two or three alternate adsorptions of PEI and PSS. The outermost layer became "negative" or "positive," respectively.

QCM monitoring of multilayer growth was often the first stage of the assembly procedure elaboration. Initially, we estimated the time needed for a component's saturated adsorption in a kinetic experiment. Then, we performed the assembly typically with 10 minutes alternate adsorption. After every other adsorption step, a layer was dried by a nitrogen stream, and the QCM resonator frequency was registered. The frequency

shift with adsorption cycles gave us the adsorbed mass at every assembly step. A linear film mass increase with the number of assembly steps indicated a successful procedure.

#### 4.1.5 Multilayer Structure

The polycation/polyanion bilayer thickness depends on the charge density of the polyions. It was shown that more than 10% of polyion side groups have to be ionized for a stable reproducible multilayer assembly via alternate electrostatic adsorption. High ionization of polyions results in a smaller step of film growth (1 - 2 nm) and lower ionization gives a larger growth step (3 - 6 nm). Ionization can be reached either by adding salt to a polyion solution (as discussed above for strong polyelectrolytes, such as PDDA and PSS), or by varying the pH for weak polyelectrolytes (e.g., polyacrylic acid (PAA) and poly(allylamine) (PAH), as was analyzed by Rubner et al). Direct zeta-potential measurements confirmed a symmetric positive/negative alternation of the polycation/polyanion multilayer's outermost charge with adsorption cycles.

#### 4.2. Objective of This Research

This research is about a general and convenient microcantilever surface modification method by layer-by-layer technology for biochemical recognition. Since microcantilever bending is generated from absorption-induced surface stress by one side of the microcantilever, the key surface modification technology is to control the formation of multilayers on one surface of the microcantilever but not the other by choosing appropriate surface materials.

### 4.3. Experiment Material and Procedure

The experiments were focused on surface modification of the commercially available silicon microcantilevers (Park Instrument, CA) for such purpose. The dimensions of the V-shaped microcantilever are 200  $\mu\text{m}$  length, 20  $\mu\text{m}$  width, and 1  $\mu\text{m}$  thickness. One side of the cantilever had a thin film of chromium (3 $\mu\text{m}$ ) followed by a 20  $\mu\text{m}$  layer of gold deposited by e-beam evaporation. Another side of the microcantilever is made of silicon with a thin naturally grown oxide layer. Poly(diallyldimethylammonium chloride) (PDDA) and poly(sulfonate styrene) (PSS) were used for layer-by-layer modification of the cantilever surface. The step-by-step modification procedure was illustrated in Figure 4-3. As in fact, the formation of polymeric layer-by-layer multilayer films in virtue appears on almost any metal or non-metal surfaces [60] [83]; therefore, it is difficult to perform LbL assembly only on one side of the cantilever.

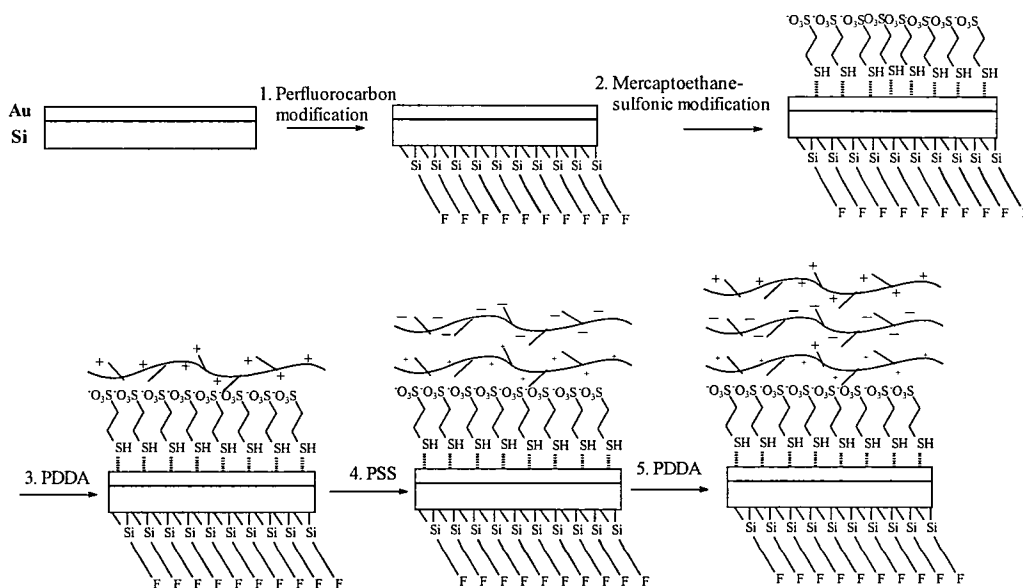


Figure 4-3 Schematics of the microcantilever modification procedure

It was well known that perfluorocarbons are both hydrophobic and lipophobic. Fluorocarbon and hydrocarbons exhibit pronounced mutual phobicity. By immobilizing perfluorocarbon materials on one surface of a microcantilever, we expect that the formation of multilayer film will occur solely on the other surface of the microcantilever due to the unique property of perfluorocarbons. (Tridecafluoro-1,1,2,2-tetrahydrooctyl)triethoxysilane (TTS) was used to develop a thin perfluorocarbon film on a silicon surface using a typical silicon surface modification procedure.<sup>17</sup>

A TTS treated microcantilever was dipped into a  $10^{-2}$  M solution of PDDA 20 minutes. After rinsing with water, the cantilever was dipped into a  $10^{-2}$  M solution of PSS 20 min and rinsed with water. This procedure was repeated several times until a desired multilayer film was formed. During the procedure, after rinsing with water, the cantilever was dried in air, and the contact angle of water on the cantilever surface was measured.

#### 4.4. Results and Discussions

##### 4.4.1. Contact Angle Measurement

After a typical multilayer formation procedure, i.e. alternate dipping the cantilever into a PDDA and PSS solution [60], contact angle data show that the formation of PDDA/PSS multilayer films due to electrostatic attraction occurs on both sides of a cantilever (Figure 4-4).

As expected, the contact angles of water on this TTS treated silicon surface remained at approximately  $90^{\circ}$  after a couple of cycles of PDDA/PSS layer-by-layer formation procedure, indicating that no multilayer forms on this surface (Figure 4-5). On the other hand, a monolayer of mercaptoethane sulfonate (MES) was self-assembled on

the gold surface in order to increase the adhesion of multilayer film on gold surface, the contact angles of water on the gold surface upon multilayer formation are also shown in Figure 4-5.

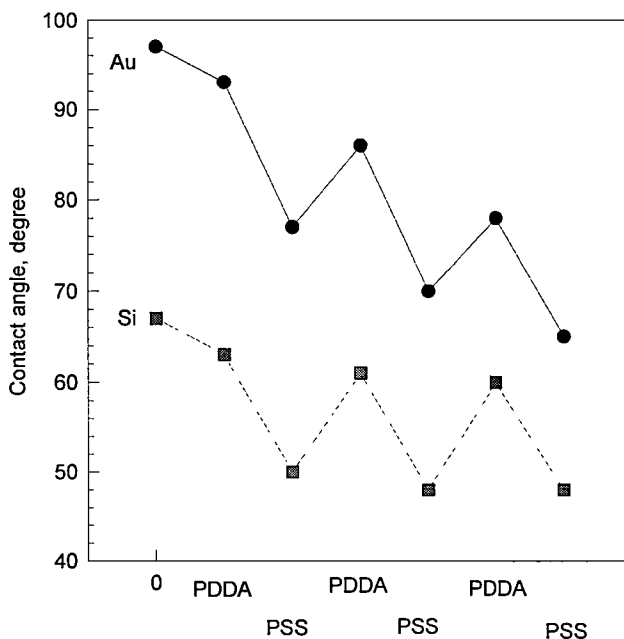


Figure 4-4 Contact angles of water on the gold and silicon surface of a microcantilever during the procedure of layer-by-layer formation

#### 4.4.2 Microcantilever Deflection

Figure 4-6 shows an *in situ* bending deflection of a TTS treated microcantilever when the PDDA and PSS were alternately switched into a fluid cell that holds the cantilever at a constant 4 ml/h flow rate. The microcantilever was pre-equilibrated in a 0.01 M PBS buffer solution before injection of the polymer solution. Immediately after the injection of the polymers, the cantilever bends vigorously down and up as shown in Figure 4-6, this movement is due to the electrostatic interaction of the ionic polymer film and its counter-ionic polymer in the solution.

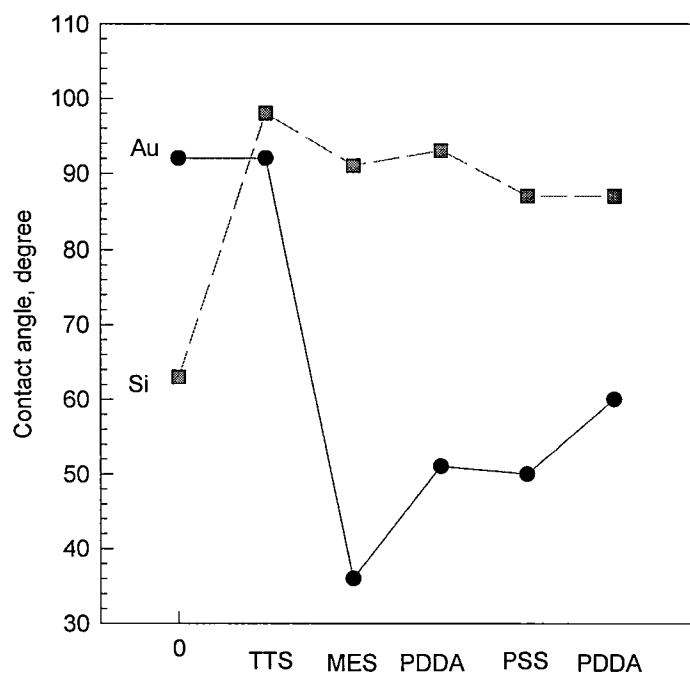


Figure 4-5 Contact angles of water on the TTS treated silicon surface and MES coated gold surface of a microcantilever during the procedure of layer-by-layer formation.

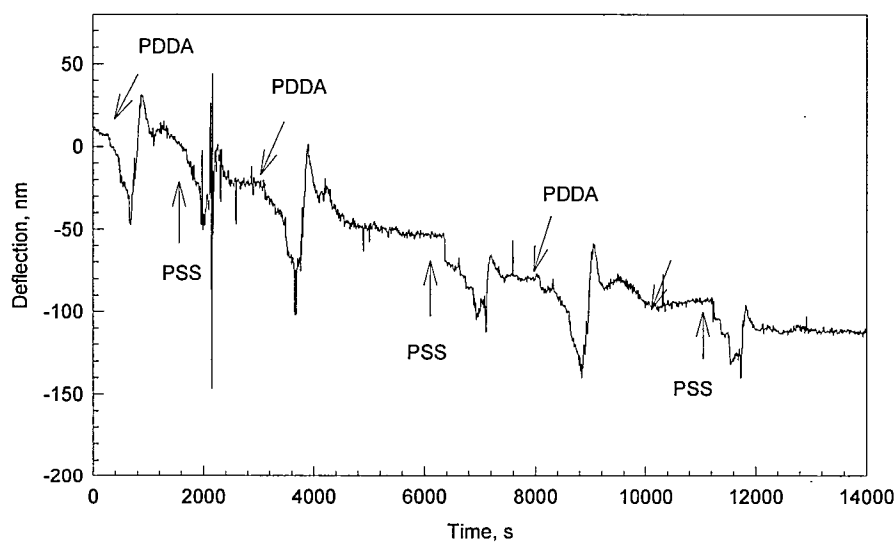


Figure 4-6 Bending response as a function of time for a TTS and MES treated silicon microcantilever upon alternate injection of a  $10^{-2}$  M solution of PDDA and PSS in  $10^{-2}$  M PBS buffer (pH=6.5) at a constant 4ml/h flow rate.

After 15 minutes interaction time, a buffer solution was switched into to cell to flush away the remaining polymers in the solution. At equilibrium, the microcantilever bends down approximately 20 nm after each polymer injection. After three PDDA/PSS cycles, the cantilever bends down approximately 120 nm due to the formation of multilayer on the gold surface of the cantilever. As a comparison, a cantilever without TTS modification does not bend since the formation of layer-by-layer film occurs on both surfaces of the microcantilever. As shown in Figure 4-7, after four PDDA/PSS layers, the neat deflection of the microcantilever is close to 0, suggesting the offset of the surface tensions caused on both sides of the microcantilever.

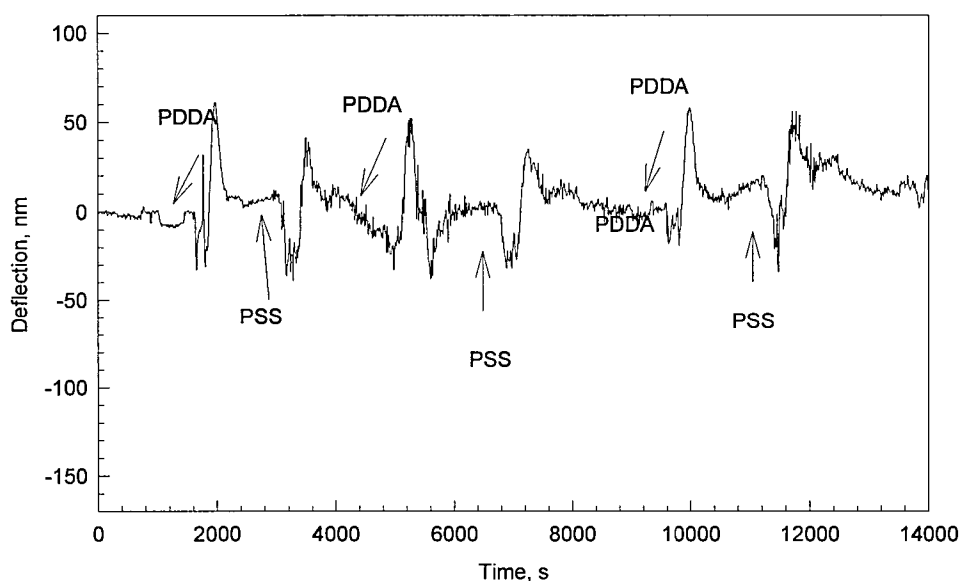


Figure 4-7 Bending response as a function of time for a unmodified coated silicon microcantilever upon alternate injection of a  $10^{-2}$  M solution of PDDA and PSS in PBS buffer (pH=6.5) at a constant 4ml/h flow rate.



#### 4.5 Summary

A general method for the microcantilever modification with multilayer film was developed. Such controllable multilayer modification method could be potentially used to detect chemical and biological species when a molecular recognition receptor is embedded in or onto the multilayer. This method provides an easy, practical approach for immobilization of those enzymes or other biomolecules that may be difficult to be immobilized on microcantilevers through conjugate chemistries.

## CHAPTER FIVE

### **MODIFICATION OF MICROCANTILEVER WITH LAYER-BY-LAYER NANO-ASSEMBLY FOR GLUCOSE MEASUREMENT**

#### 5.1. Introduction

More than 18 million Americans have diabetes, a group of serious diseases characterized by high blood glucose levels that result from defects in the body's ability to produce and/or use insulin. Diabetes can lead to severely debilitating or fatal complications, such as heart disease, blindness, kidney disease and amputations. It is the fifth leading cause of death by disease in the U.S. Unfortunately, there is no drug available for a complete treatment of diabetes yet. Accurate and in-time measurement of blood glucose concentration is essential for good diabetes control. Up to now, the way to test blood sugar requires sticking the patient's finger with a lancet to draw a drop of blood that is then tested using a test strip and a meter. It is painful for the patients, who have to do it one to several times a day. So a method of painless, continuous blood monitoring is highly desirable by diabetes patients. One attractive solution to this problem is an implantable micro sensor for blood glucose monitoring. This research investigates using microcantilever-based sensor with the possibility to be used for in vivo blood sugar measurement.

## 5.2 Experiment Material

In the experiments, commercially available silicon microcantilevers (Veeco Instruments) were used. The dimensions of the V-shaped silicon microcantilevers were 180  $\mu\text{m}$  in length, 25  $\mu\text{m}$  in leg width, and 1  $\mu\text{m}$  in thickness. One side of these cantilevers was covered with a thin film of chromium (3 nm) followed by a 20 nm layer of gold, both deposited by e-beam evaporation. On the uncoated side of the commercial microcantilever was silicon with a 2 nm thick naturally grown  $\text{SiO}_2$  layer, which is called “native oxide”.

Glucose Oxidase (GOx) (EC 1.1.3.4, Type VII-S, from *Aspergillus niger*, 166,500 units/g solid),  $\beta$ -D-glucose, D-fructose, D-galactose, D-mannose, sodium salt of 2-mercaptoethane sulfonic acid (MES), and Poly (sodium 4-styrenesulfonate) (PSS,  $M_w=70,000$ , powder) were used as received from Sigma-Aldrich. Polyethyleneimine (PEI, 14%,  $MW=25,000$ ,  $\rho = 1.043$ ) was a gift from Max Planck Institute, Germany. A  $10^{-2}$  M MES solution was prepared in ethanol. All other solutions were prepared in a 0.01M NaCl electrolyte solution (pH=6.5).

## 5.3. Experiment Setup

The deflection experiments were performed in a flow-through glass cell (Digital Instruments, CA) similar to those used in atomic force microscopy (AFM). The microcantilever was immersed in the 0.01 M NaCl electrolyte solution.

For continuous flow-through experiments, initially, the electrolyte solution was circulated through the cell using a syringe pump. A schematic diagram of the apparatus used in this study was the same as described in Section 2.5. A constant flow rate was

maintained during each experiment. Experimental solutions containing different concentrations of glucose were injected directly into the flowing fluid stream via a low-pressure injection port sample loop arrangement with a loop volume of 2.0 ml. This arrangement allowed for continuous exposure of the cantilever to the desired solution without disturbing the flow cell or changing the flow rate. Since the volume of the glass cell, including the tubing, was only 0.3ml, a relatively fast replacement of the liquid in contact with the cantilever was achieved. Microcantilever deflection measurements were determined using the optical beam deflection method. The bending of the cantilever was measured by monitoring the position of a laser beam reflected from the gold-coated side of the cantilever onto a four-quadrant AFM photodiode. We define bending toward the gold side as “bending up”; “bending down” refers to bending toward the silicon side. The cantilever was immersed in the electrolyte solution until a baseline was obtained and the voltage of the position-sensitive detector was set as background corresponding to 0 nm.

#### 5.4 Microcantilever Layer-by-Layer GOx Surface Immobilization Process

The electric charge of a polyelectrolyte solution depends on the difference between the isoelectric point (pI) of the polyelectrolyte and the solvent. Isoelectric point is an index for measuring the electric charge for a polyelectrolyte or protein. It is a pH value where solution has a zero net charge. A polyelectrolyte is positively charged in a solvent with pH is less than its pI; otherwise, it is negatively charged. pIs of PEI and PSS are 11 and 2, respectively, so they are positively and negatively charged, respectively, in the pH = 6.5 buffer solution. The glucose oxidase's pI is 4.2. It is used as a negatively charged polyelectrolyte in the LbL assembly process.

The key to microcantilever surface modification technology is to selectively modify one side of a microcantilever surface with molecular recognition layers. In a typical multilayer formation procedure, the substrate was alternately dipped into a PDDA and PSS solution and the process was repeated several times for multilayer formation. It is difficult to perform LBL assembly only on one side of the cantilever because the formation of polymeric layer-by-layer multilayer films in virtue appears on almost any metal or non-metal surfaces [60]. In the previous chapter, a microcantilever multilayer modification method taking advantage of hydrophobic/lipophobic properties of the perfluorocarbon materials was presented. In this method, (Tridecafluoro-1,1,2,2-tetrahydrooctyl)triethoxysilane (TTS) was used to develop a thin perfluorocarbon monolayer on silicon surface using a typical silicon surface modification procedure, and the polymeric multilayers were found grown only on the gold surface of the cantilever. However, after a couple of polycation/polyanion cycles, the polymeric multilayer eventually built on the perfluorocarbon surface, especially when there were defects in the perfluorocarbon film.

In this work, it was found that the polymeric electrolyte does not stick on a nonmodified gold or silicon surface if the cantilever was rinsed in a high flow running water (>100ml/min). Furthermore, the multilayer can built up on a charged (e.g. a MES layer) surface in such severe condition. The strong running water on one hand washes away the absorbed layer on the silicon side, and on the other hand enhances the absorption between the layers on the gold side of the microcantilever.

The modified LbL procedure specific for MCL surface modification used in this experiment is the following: A) A monolayer of MES was self-assembled on the gold

surface of a MCL by immersing in a 5mM MES solution for 12 hours and the MCL was then rinsed with EtOH three times followed with deionized (DI) water three times. B) MCLs were immersed in a PEI for 10 minutes; it was rinsed with 100mL/minutes running water for 1 min, and then immersed in the opposite polyelectrolyte for 10 mins followed with another rinsing of running water. C) This cycle has been repeated several times until a desired number of layers were reached. Figure 5-1 is a schematic of the LbL assembly.

The method is so efficient that the pretreatment with perfluorocarbon film is not necessary. In these experiments, we used a running water method that is a better control than the static multilayer approach. In this LbL assembly, first 3 bilayers of PEI / PSS were formed, which provides a solid base for further enzyme immobilization. After that three bilayers of PEI /GOx were formed on the top of MCL surface with three layers of GOx immobilized in this nano assembly. Each layer of PEI or PSS was about 1~ 2nm thick, and GOx was approximately 8nm thick. The whole assembly was approximately 40nm thick.

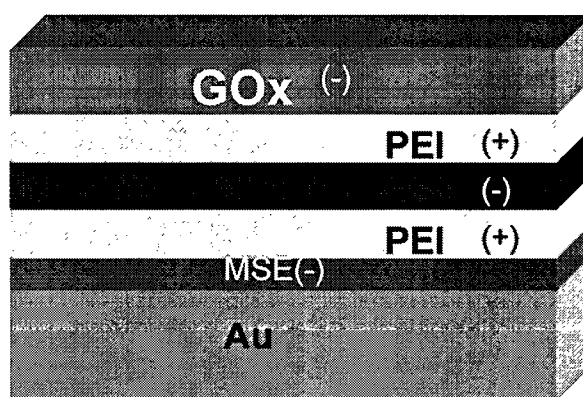


Figure 5-1 LbL nano assembly with immobilized enzyme on MCL surface.

## 5.5. Results and Discussions

### 5.5.1. Selective Modification of Microcantilever

Experiments were performed to check the possibility of selective modification of the microcantilever on either the silicon side or the gold side. The plan was to block one side of microcantilever before starting layer-by-layer modification. (Tridecafluoro-1,1,2,2-tetrahydrooctyl) triethoxysilane (TTS) and 1H,1H,2H,2H-perfluorodecanethiol (PFDT) were used to develop a thin perfluorocarbon film on the silicon surface or the gold surface using typical surface modification procedures, respectively. The multilayer modified TTS or PFDT treated cantilevers were named microcantilever-A and microcantilever-B (Figure 5-2).

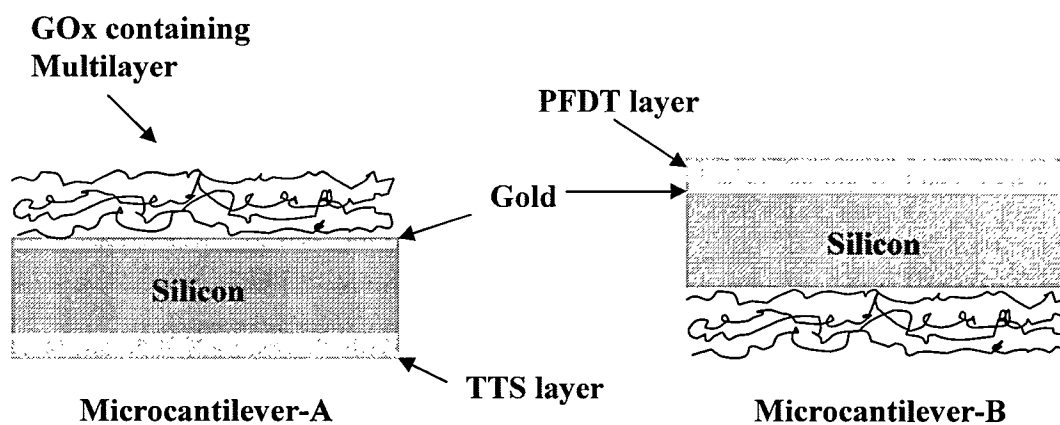


Figure 5-2 Selective modification of microcantilever.

When exposed to a solution containing  $8 \times 10^{-3}$  M glucose in the 0.01M NaCl solution, the microcantilever-A bent down, but the microcantilever-B bent up, respectively, as shown in Figure 5-3. This reaction was in accordance with our expectation that the bending direction of microcantilever-A and microcantilever-B should

be opposite since the multilayer films were assembled on the opposite sides of the two types of microcantilevers.

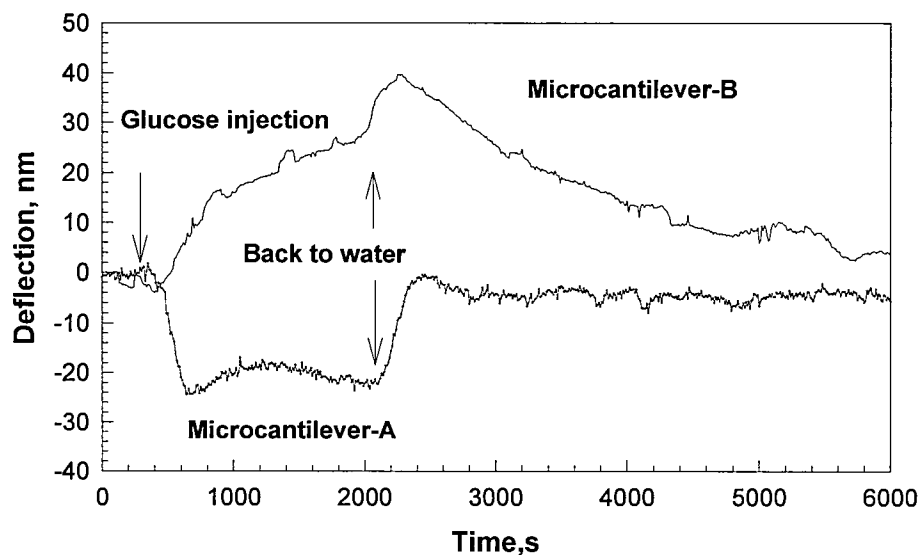


Figure 5-3. The bending response for a microcantilever-A and a microcantilever-B to a  $8 \times 10^{-3}$  M glucose solution in 0.01M NaCl, respectively.

However, microcantilever-A reached its equilibrium in five minutes after exposure to glucose, but microcantilever-B did not reach its equilibrium even  $\sim 30$  minutes after the injection of the glucose solution. For the rest of experiment of this research, the microcantilevers were modified with the same method as that for microcantilever-A.

#### 5.5.2. Flow Rate and Measurement Accuracy

Figure 5-4a shows a typical MCL deflection profile when the MCL was exposed to a glucose solution at relative fast flow rate (60mL/h), and Figure 5-4b shows the calculated corresponding glucose concentration change in the fluid cell at the same time frame. These two curves show that there was a positive proportional relationship between the deflection of MCL and the glucose concentration in the fluid cell.



At the point of  $A_1$ , a 2.0 mL aliquote of 10 mM glucose solution was switched into the fluid cell. It took 120 s for the injected glucose solution to flow through the fluid cell. After that the NaCl electrolyte solution was circulated back into it. MCL first underwent a downwards bending and reached a maximum point at  $A_2$  in about 20s, at which the bending was 20nm. There was a small upward adjustment for MCL after that (from point  $A_2$  to  $A_3$ ). Then the bending of MCL reached a balanced state. Point  $A_4$  is where the NaCl solution started to switch back in. In this stage, the glucose concentration in the cell was kept at the concentration at which it was injected. The MCL then bent backward and reached the highest point  $A_5$ , which was a point higher than the original position. In this stage, the NaCl solution moves into the cell and replaces the glucose solution. There a small downward adjustment for MCL before it finally balanced at the original baseline position (from point  $A_6$  to  $A_7$ ).

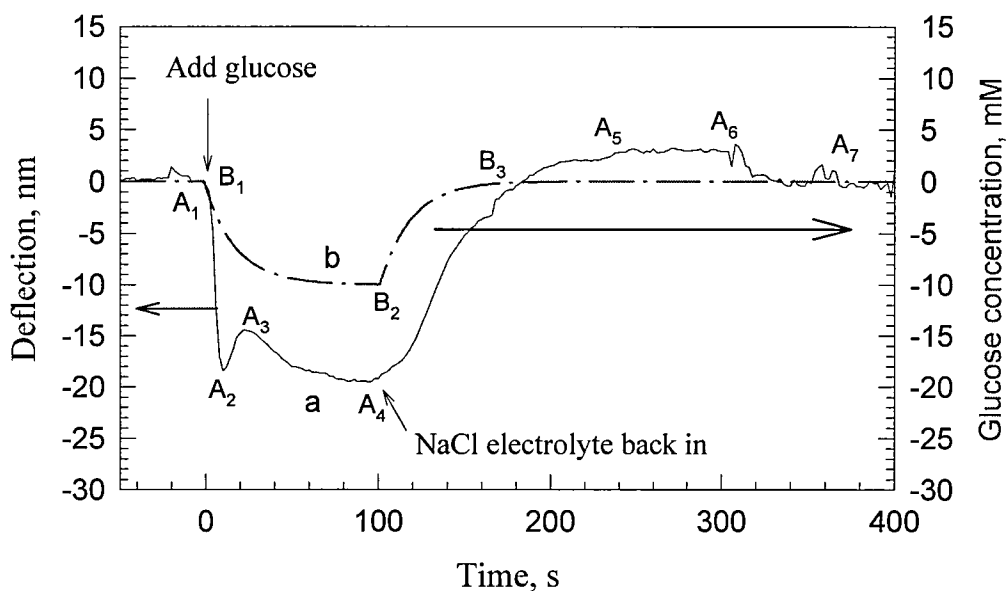


Figure 5-4 a) Deflection of MC when exposure to 10mM glucose. b) Calculated glucose concentration in the reaction cell after injection of 10mM glucose solution.

In our and many other's systems, the fluid cell where the MCL was holds up to approximately 0.3 mL solution that will retain the solution for a while when a sample or NaCl solution was injected. The calculated glucose concentration change for the solution in the cell based on the following equation was compared to the microcantilever deflection as shown in Figure 5-4b.

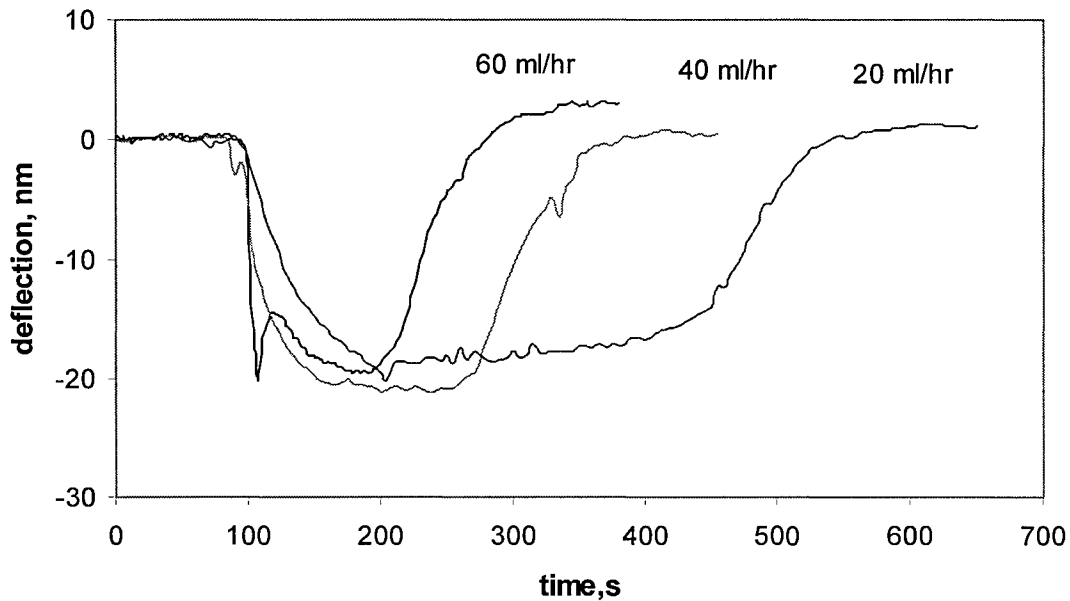


Figure 5-5 Microcantilever deflection at different flow rate when exposed to 10mM glucose solution.

In every  $dt$  time interval, the molar glucose change in the fluid cell equals the amount of glucose ( $C_{Gr}$ ) flowed in minute the amount of glucose flowed out ( $C_{lr}$ ) and the amount of glucose oxidized by GOx ( $vdt$ ). The amount of glucose oxidized GOx is very small compared to the amount of input and output glucose, so it is negligible. When the glucose was injected, the concentration,  $dc$ , was the assumed concentration of glucose that can flow into the whole cell in  $dt$  time.

thus

$$\frac{\partial C_t}{\partial t} = \frac{(C_G - C_t)r}{V} \quad (5.1)$$

where  $C_G$  is the concentration of glucose injected,  $C_t$  is the concentration of glucose in the cell at time  $t$ ,  $r$  is the flow rate,  $V$  is the volume of the flow cell.

Integration of the Equation 5.1 gives

$$C_t = C_G - C_G e^{-\frac{r}{V}t} \quad (5.2)$$

When the NaCl solution was switched back into to fluid cell to replace the glucose, then in every  $dt$  time interval, the mole glucose change in the fluid cell equals the amount of glucose diffusing out ( $C_t r$ ).

$$\frac{\partial C_t}{\partial t} = -\frac{C_t r}{V} \quad (5.3)$$

Integration of the Equation 5.1 gives

$$C_t = C_G e^{-\frac{r}{V}t} \quad (5.4)$$

So by combination of Equation 5.2 and 5.4, the curve of the glucose concentration change in the fluid cell can be plot as it was shown in Figure 5-4b. From B1 to B2, it follows Equation 5.2, and from B2 to B3 it follows Equation 5.3.

At different flow rates, MCL deflection profiles were similar, and the cantilever bending magnitudes at equilibrium were the same at 20 nm (Figure 5-5). However, it's obvious that faster flow rate gives faster response because the MCL deflection reaches equilibrium in a shorter time.

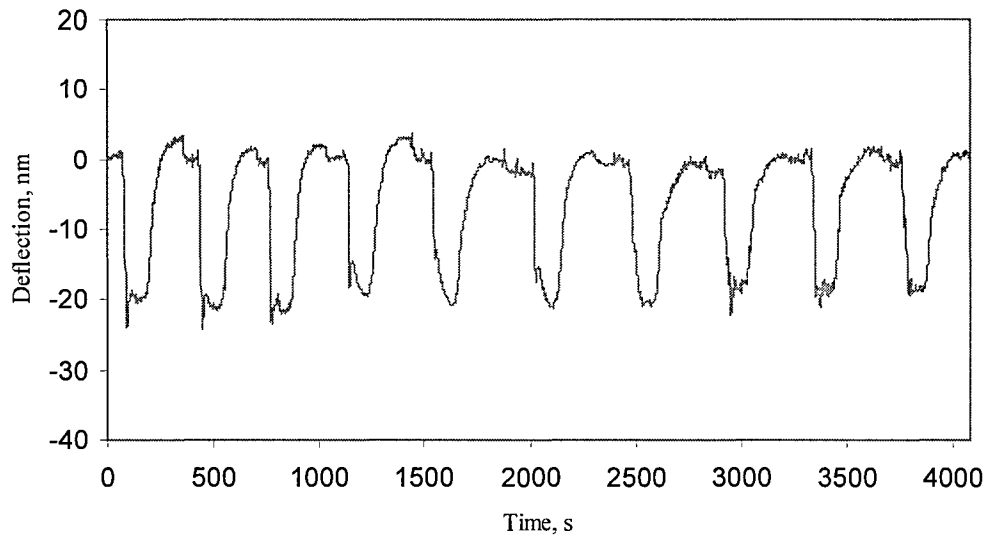


Figure 5-6 Reproducibility experiment with one microcantilever exposed to 10mM glucose solution for 10 times.

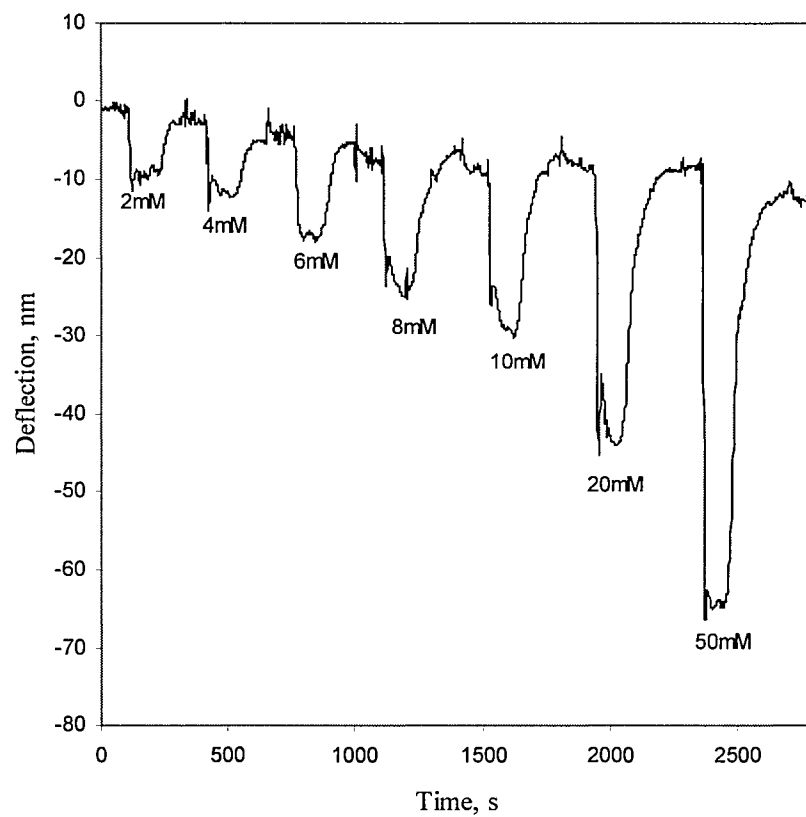


Figure 5-7 Microcantilever deflection upon exposure to glucose solution from 2 to 50mM.

On the contrary, the faster flow rate will be better used for glucose measurement based on two reasons: first, it will provide shorter response time since the concentration reaches its maximum and the same as the cantilever deflection in a shorter time. Second, the noise was significantly lowered. This lowering occurred because the response time is short, so the MCL pre-equilibrium is not necessary. In our previous studies, the MCL has to remain in the flow cell for a certain amount of time until a perfect baseline was obtained. This process may take minutes, hours, or days.

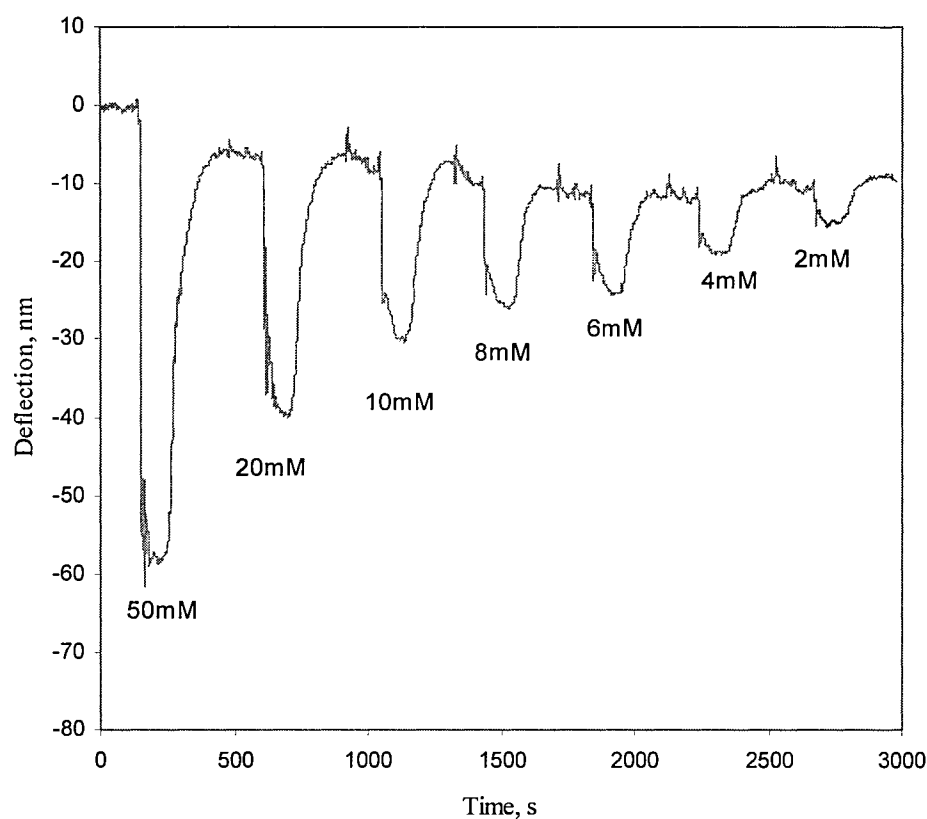


Figure 5-8 Microcantilever deflection upon exposure to glucose solution from 50 to 2mM.

Some uncertain factors can still cause deflection of the MCL during the measurement, such as bubbles, slight temperature changes, laser intensity variations,

MCL internal stress changes, etc. They are all going to cause noise of the MCL during the experiment that will risk the accuracy of MCL measurement, especially when the MCL deflection is not significant enough. Drifting is also a concern when the measurement is long. At a higher flow rate, such as 60 mL/h, the whole process takes less than 200s. In general, no significant noise or drifting was experienced during the experimental process. No pretreatment is necessary and the sample injection can be done once the flow liquid started to circulate throughout the flow cell.

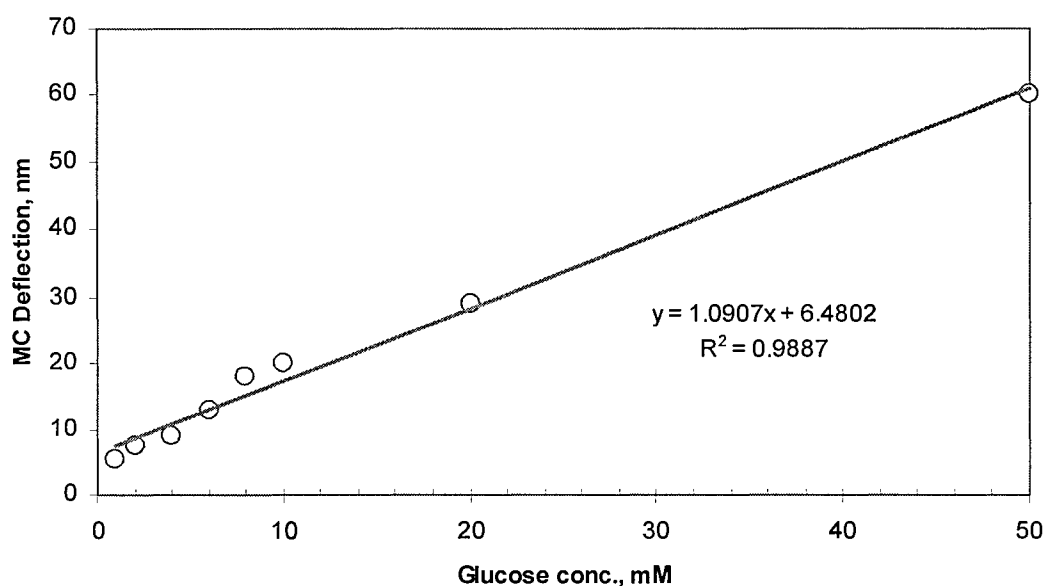


Figure 5-9 Linear relationship between the magnitude of microcantilever deflection and the concentration of tested glucose solution.

The reproducibility experiments were conducted sample by sample and MCL by MCL measurement. Exposure of the 10 mM solution of glucose caused the same deflection rate as shown in Figure 5-6. The standard error was within 3%. Exposure of the 10 mM solution of glucose to five different MCL prepared under the same conditions

caused similar deflection amplitudes, and bending rates with the standard error were within 5%, indicating good cantilever-to-cantilever reproducibility.

### 5.5.3. Deflection Amplitude vs the Concentration of Glucose

At different glucose concentrations of in the range of 1~50 mM, the magnitude of MCL deflections at equilibrium was proportional to the concentration of glucose injected.

The normal human blood glucose concentration is in the range of 4~6 mM (70-110 mg/dL). If blood glucose concentration is above 10 mM (160 mg/dL), it is considered diabetes. In serious cases of diabetes, the blood glucose concentration can be as high as 50mM. The microcantilever was exposed to different glucose solutions in the order from low concentration to high concentration and reverse. Figure 5-7 and Figure 5-8 show the deflection of the microcantilever when it was exposed to from 2-50mM and reverse, respectively.

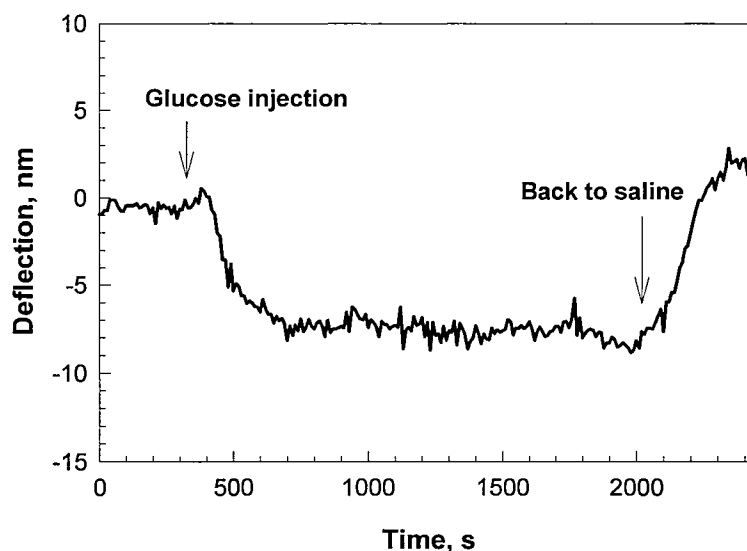


Figure 5-10. Bending response of a microcantilever-A to a  $10^{-2}$  M glucose solution from a  $4 \times 10^{-3}$  M glucose solution in a 0.01M NaCl solution.

The results show that this is a very robust sensor. It has excellent reproductivity no matter if it is used in the order of low to high concentration or in the reverse. There is a linear relationship between the magnitude of microcantilever deflection and the concentration of tested glucose solution as it shown in Figure 5-9.

#### 5.5.4. Microcantilever Deflection in a Saline Solution

Figure 5-10 shows the bending response of a microcantilever to a  $10^{-2}$  M glucose solution from a  $4 \times 10^{-3}$  M glucose solution, which further suggested that such a cantilever may be used for continuous monitoring of the glucose level in a saline solution.

#### 5.5.5. Selectivity and Lifetime

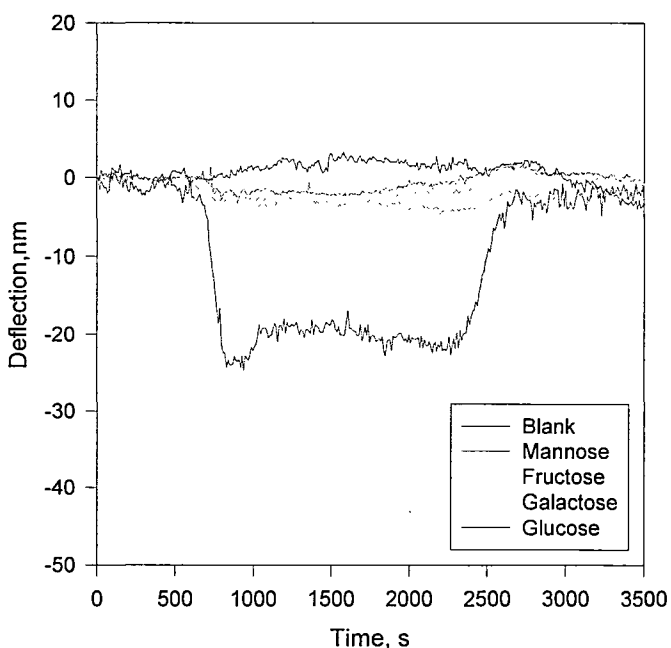


Figure 5-11 MCL deflection with exposure to glucose, mannose, fructose, and galactose at concentration of 4mM.



Experiments were carried out on the selectivity of the GOx immobilized MCLs to  $\beta$ -glucose over some other monosaccharoses, namely mannose, fructose, and galactose at same concentration of 4mM. The results are shown in Figure 5-11.

When exposed to mannose, fructose, and galactose, MCL experienced small nonspecific bending. Only when exposed to glucose was MCL bending clearly specific, and at a much larger scale because GOx has a very high specificity for glucose. If the oxidation of  $\beta$ -glucose is set as 100, that of mannose = 0.98, and of galactose = 0.14, whereas the other isomers are not oxidized [20].

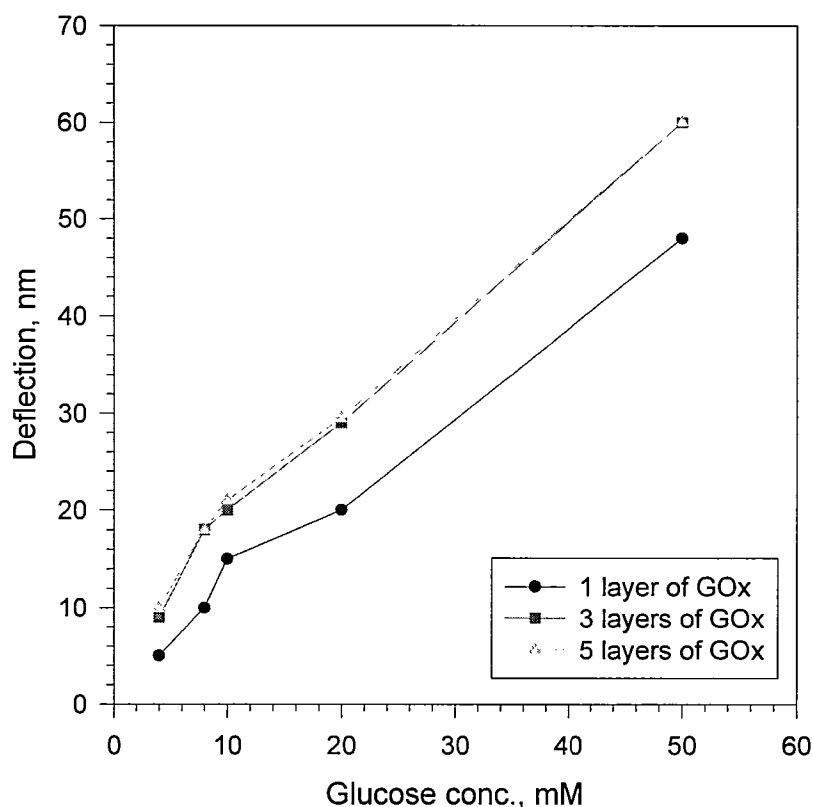


Figure 5-12 Deflection of microcantilever modified with different layers of GOx.

In addition, stability experiments were conducted on microcantilevers after three months of storage in air. The deflection of the stored cantilevers showed a similar profile and bending amplitude as those in Figure 5-2.

#### 5.5.6. Number of GOx Layers in the Multilayer Assembly

The available amount of enzyme could effect the enzyme catalyzed reaction. Theoretically speaking, the more the enzyme, the faster the reaction. For this layer-by-layer enzyme immobilized system, the amount of enzyme is decided by the number of layer of GOx in side. Microcantilevers had been modified with 1, 3, and 5 layers of GOx, respectively, with the same procedure as described in Section 5.4. They were exposed to the same solution of glucose of 10mM.

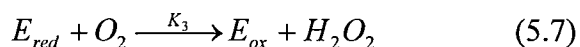
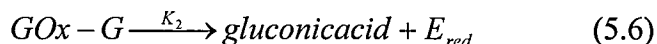
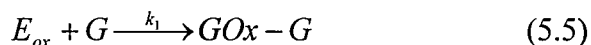
Their deflection results (Figure 5-12) show that there is an observable increase of the magnitude of microcantilever deflection when GOx layer is increased from 1 layer to 3 layers. But for the change of GOx from 3 to 5 layers, there is just a very small difference. According to layer-by-layer theory, in the layer-by-layer assembly, the function layers are normally only the top several layers. So by increasing of layers after certain number of layers will not make much difference for the function of the assembly. That is why for most of this research, the pattern of (PEI/PSS)<sub>3</sub>/(PEI/GOx)<sub>3</sub> was chosen for the modification of microcantilevers.

#### 5.5.7. Deflection Mechanism

Enzyme immobilization method and immobilized enzyme concentration could affect substrate diffusion speed inside the enzyme matrix. A high concentration of enzyme loading in the immobilization matrix requires rapid transfer of substrate into the matrix to maintain the enzyme-catalyzed reaction rate. Thus, a high enzyme loading often

results in operation with internal mass transfer as the rate-limiting step. In the present study the enzyme loadings were rather low ( $4.2 \times 10^{-14}$  mol / mm<sup>2</sup>), thus it was reaction kinetic control.

One simple GOx enzymatic reaction mechanism can be expressed as [85].



In this mechanism, the  $GOx-G \rightarrow E_{ox}$  reverse binding was neglected due to the much smaller dissociation constant ( $k-1$ ) compared to  $k_1$ . Another approximation was made for the second stage of the enzymatic reaction ( $E_{red}$  to convert back to  $E_{ox}$ ).

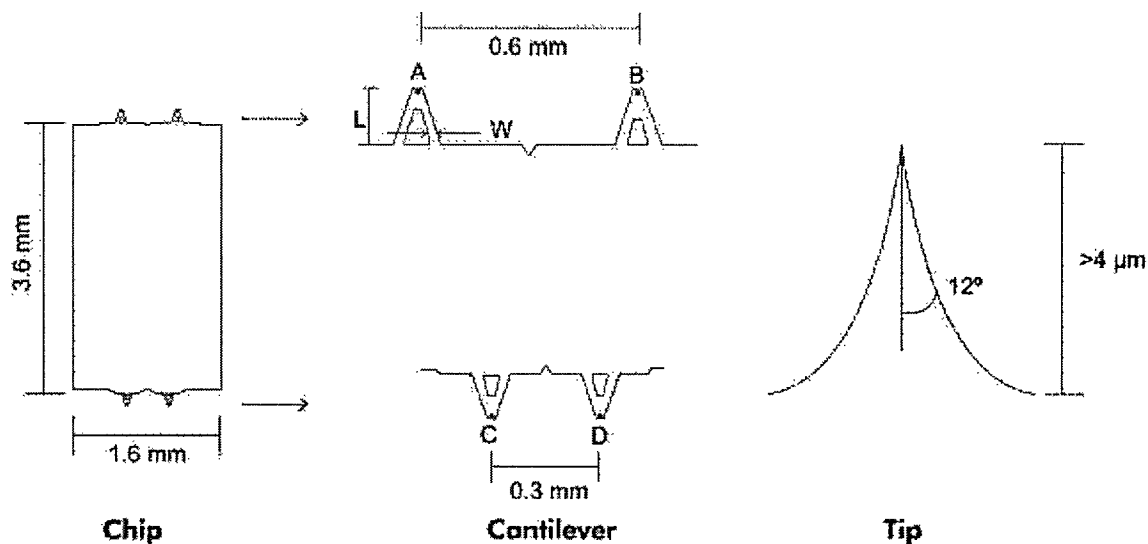


Figure 5-13 Dimension of the commercial microcantilever used in the research.

This stage may involve the formation of  $E_{red} \cdot O_2$  complex, decomposition of the complex to  $E_{ox}$  and  $H_2O_2$ , and enzymatic formation change. However, since there has

been no direct evidence for the formation of the  $E_{\text{red}} \cdot O_2$  complex [86], a one step reaction (Equation 5.7) was used in this work for simplicity. This glucose oxidation reaction is an exothermic reaction with a heat release at  $-80\text{kJ/mol}$ .

The MCLs used in these experiments were triangle silicon MCL, which have a dimension of  $180 \times 38 \times 1\ \mu\text{m}$  and a layer of  $20\text{nm}$  gold on one surface. (See figure 5-13, where  $L = 18\ \mu\text{m}$ ,  $W = 38\ \mu\text{m}$ ). The MCL surface area is  $1.12 \times 10^{-2}\ \text{mm}^2$ . Assuming the thickness of the three GOx/PEI multilayer film is approximately  $25\ \text{nm}$  (based on the known structure), the volume of the three GOx/PEI film is approximately  $2.8 \times 10^{-13}\ \text{L}$ . Klitzing, R. et al [87] reported the thickness of the first three GOx/PEI layer is  $1.65\ \mu\text{g}/\text{cm}^2$ , which is corresponding to  $8.85 \times 10^{-12}\ \text{mol}/\text{cm}^2$ , i.e.  $9.91 \times 10^{-16}\ \text{mol}$  on the MCL surface. Thus, the concentration of the GOx in the multilayer film is calculated to be  $3.54 \times 10^{-3}\ \text{M}$ . It is assumed that the glucose concentration inside multilayer film is constant and equals to the concentration of glucose injected. This assumption is feasible because the film is thin and the sample flow is fast ( $3\ \text{mm/s}$  over the MCL surface).

At equilibrium, the reaction rate in the film can be determined by the Michaelis-Menton equation [86].

$$V = \frac{\partial P}{\partial t} = k_2[E_{\text{ox}} - G] = \frac{C_E k_2}{1 + \frac{k_2}{k_1[G]} + \frac{k_2}{k_3[O_2]}}, \quad (5.8)$$

where  $P$  is the product gluconic acid,  $C_E$  is the total GOx concentration on the MCL surface,  $[G]$  is the glucose concentration ( $10\ \text{mM}$  in Figure 5.4), and  $[O_2]$  is the concentration of  $O_2$  in water ( $1.2\ \text{mM}$ ).

The kinetic constants vary in different conditions as reported from different groups. The literature survey revealed that the following data were widely accepted for

GOx catalyzed glucose oxidation in solution,  $k_1 = 1.2 \times 10^4 \text{ M}^{-1} \text{ s}^{-1}$ ,  $K_2 = 800 \text{ s}^{-1}$ ,  $K_3 = 3 \times 10^6 \text{ M}^{-1} \text{ s}^{-1}$  [85] [86]. Among this,  $k_2/k_1$  is the so called Michaelis constant ( $K_M$ ). Recently, Calvo and McShane's work showed that these kinetic parameters in multilayers are the same as those in solutions. Based on these data the reaction rate is  $V = 0.36 \text{ M/s}$ . This reaction rate is extremely high, which is due to the high concentration of GOx on the surface. It is expected that this high reaction rate is possible only when the flow rate is high, otherwise, the  $[G]$  will drop significantly due to the reaction where mass transfer must be taken into consideration.

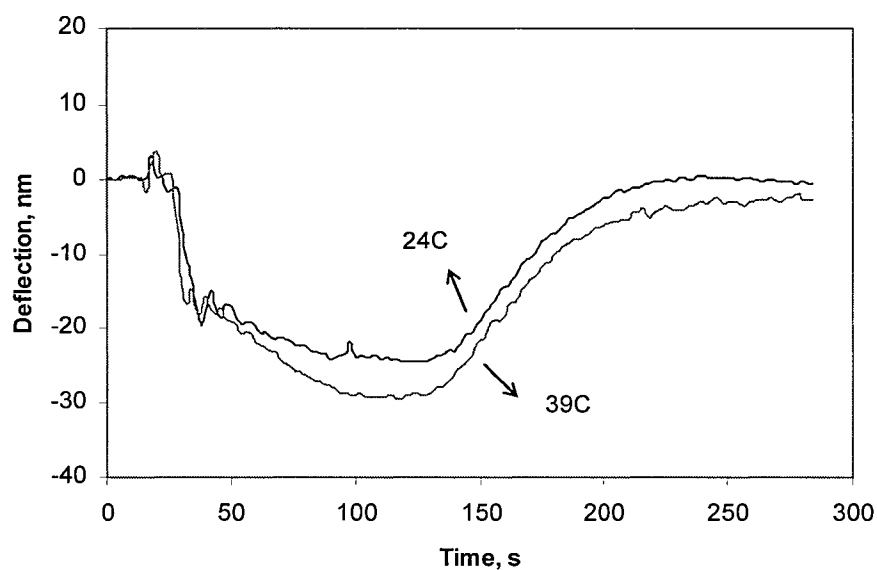


Figure 5-14 Deflection of microcantilever upon exposure to 10mM at different temperature.

Recently, MCLs modified by GOx for glucose detection were reported by using typical surface conjugation chemistry and drop coating technique [40] [41]. However, the bending origins were unknown. In order to understand the bending mechanism of MCL, it is a necessity to analyze all the possible contributions to the MCL bending based on the

glucose oxidation mechanism discussed above. The possible contributions include thermal output, pH change, H<sub>2</sub>O<sub>2</sub> produced, and the conformational change of the enzymes.

5.5.7.1 Thermal Effect In a monolayer approach, Subramanian, A. et al [40] concluded that the deflection of MCL was not likely due to thermal energy. Since solution flow was not counted into consideration in their work, the effect of thermal energy will be further discussed here.

An experiment was done first for a concept-proof of the effect of temperature change to the deflection of this modified microcantilever. A microcantilever modified in the same way as described in Section 5.4 was exposed to 10mM glucose solution at the temperature of 24<sup>0</sup>C and 39<sup>0</sup>C. The results (Figure 5-14) show that the increasing of temperature causes a net downward deflection of microcantilever.

But the real situation is more complicated; many other factors must be included, such as the thermal diffusion in the solution. It is hard to run an isolated experiment to verify the contribution of the temperature changes to the deflection of microcantilever. The following part is an analysis on this point from a theoretical point of view.

The conversion rate of glucose in the thin multilayer film calculated above is corresponding to  $8.85 \times 10^{-12}$  mol / min, and it would produce thermal output (dQ/dt) on the order of  $7.2 \times 10^{-9}$  J/s.

At equilibrium or steady state, the temperature difference between the GOx/PEI multilayer covered surface and the surroundings is constant, i.e. the  $dT/dt = 0$ . From one-dimensional heat flow equation, the heat flow can be given by:

$$\frac{dQ}{dt} = kA\left(\frac{dT}{dx}\right)_{x \rightarrow 0^-} + hA\left(\frac{dT}{dx}\right)_{x \rightarrow 0^+}, \quad (5.9)$$

where  $k$  is the thermal conductivity of silicon ( $83.5 \text{ W/m K}$ ),  $A$  is the MCL surface area ( $8.51 \times 10^{-3} \text{ mm}^2$ ),  $h$  is the convection coefficient of water in these experimental conditions ( $1020 \text{ W/m}^2 \cdot \text{K}$ ) that can be calculated from  $Nu_x$ , assuming the water is laminar flow and assuming the temperature on the other side (silicon) of the MCL equals to the surrounding liquid. Again, this assumption is feasible especially because the flow is fast. Thus, solving the Equation 5.9 revealed that the temperature difference between the GOx/gold surface and surrounding solutions ( $\Delta T$ ) was  $7.7 \times 10^{-4} \text{ K}$ .

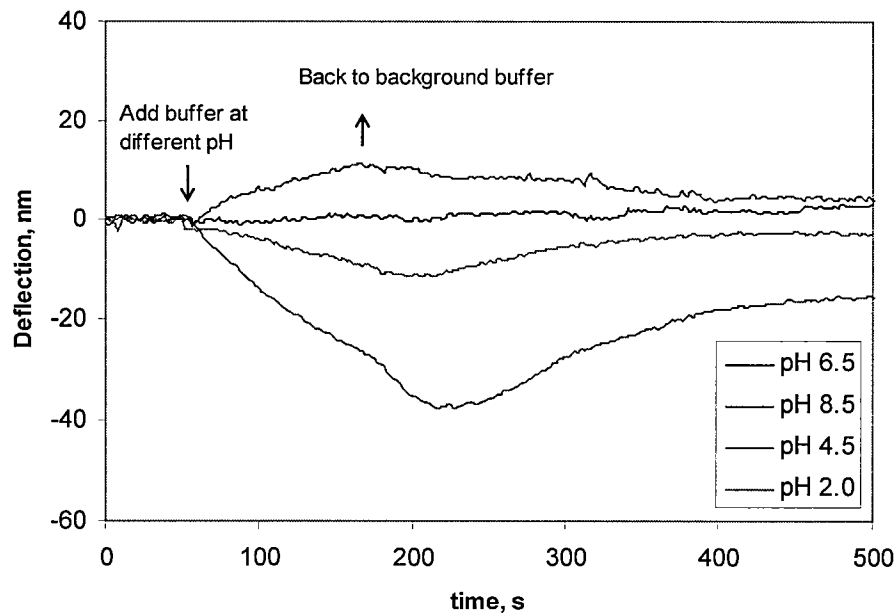


Figure 5-15 pH effect on microcantilever.

According to bimetallic theory of cantilever [88],

$$\Delta T = \frac{h[3(1+m)^2 + (1+mn)(m^2 + \frac{1}{mn})]}{6(\alpha_1 - \alpha_2)(1+m)^2} \frac{2D}{L^2 + D^2} \quad (5.10)$$

where  $\Delta T$  is the temperature difference before and after the bimetallic strip was heated, i.e., the temperature difference between the GOx/gold surface and surrounding solutions in our experiments,  $h$  is the thickness of the MCL,  $m$  and  $n$  are the ratio of the thickness and ratio of the modulus of elasticity, respectively, of the gold layer (thickness of 3 nm, modulus of elasticity  $0.8 \times 10^{11}$  Pa) to that of the bottom layer (silicon 1.0  $\mu\text{m}$  thick,  $1.79 \times 10^{11}$  Pa), and  $\alpha_1$  and  $\alpha_2$  are the coefficients of expansion for the two materials (gold,  $14.2 \times 10^{-6} \text{ } ^\circ\text{C}^{-1}$ , silicon  $2.5 \times 10^{-6} \text{ } ^\circ\text{C}^{-1}$ ),  $D$  is the deflection amplitude, and  $L$  is the length of the MCL (180  $\mu\text{m}$ ).

For the  $7.7 \times 10^{-4}$  K  $\Delta T$  in the presence of 10 mM of glucose (Figure 5-4), this change would correspond to a  $7.45 \times 10^{-3}$  nm MCL deflection. Obviously, this deflection is far less than the 20 nm deflection observed in the presence of 10 mM of glucose. So the contribution from enthalpy change is negligible.

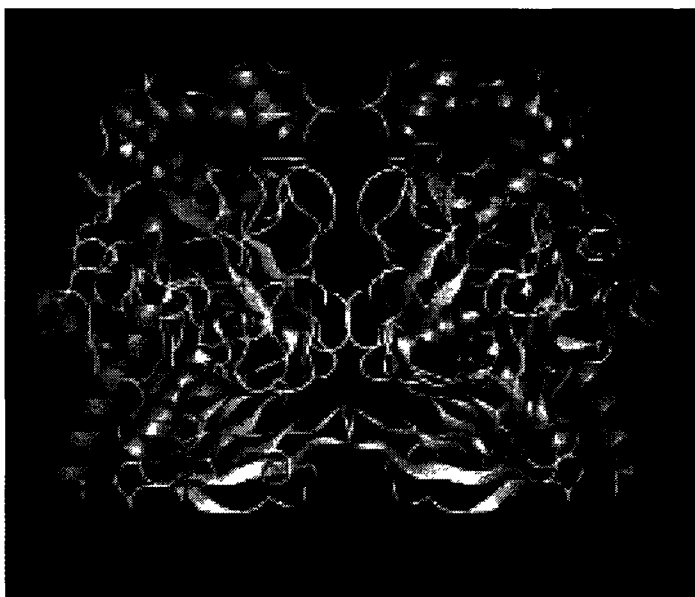


Figure 5-16 Overall topology of glucose oxidase holoenzyme [89]



5.5.7.2. pH Change in the Film One product of the oxidation reaction is gluconic acid, which might protonate the amino groups in PEI and results in repulsive multilayer swelling and consequent bending down of the MCL. It is known that pH change can affect the surface stresses on the silicon side. Experiments were performed under different pH levels for the microcantilever of the same modification as described above, i.e. (PEI/PSS)<sub>3</sub>/(PEI/GOx)<sub>3</sub> (Figure 5-15).

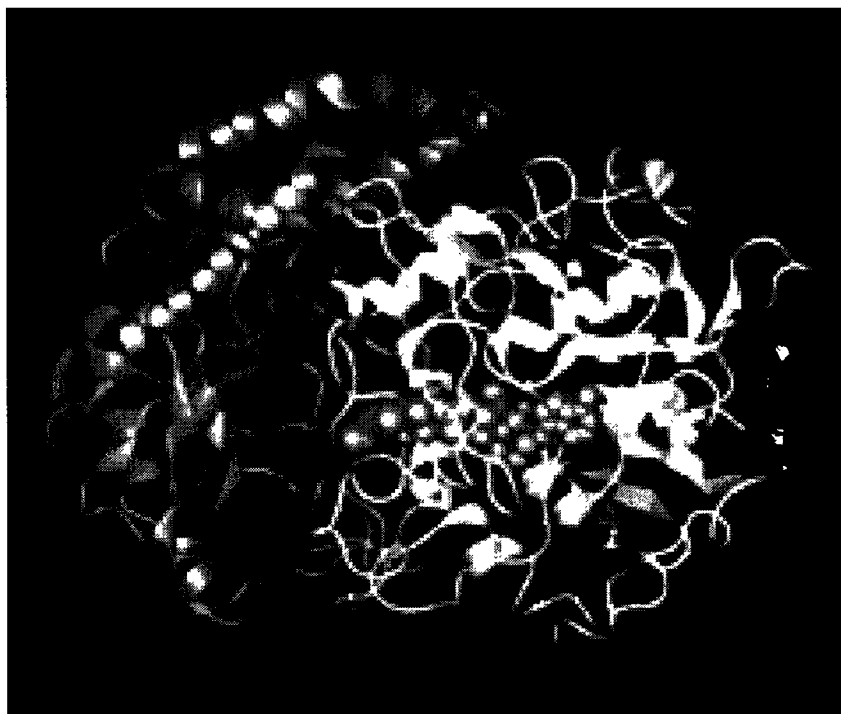


Figure 5-17 Subunit structure of GOX showing FAD (red spacefill) [89]

The results show that when the system pH decreases, it will cause a downwards bending of microcantilever. That result confirmed the contribution of pH to the microcantilever bending, although the magnitude is still not clear. To calculate the exact contribution of pH change to microcantilever deflection, one need know the diffusion

constant of gluconic acid in the (PEI/GOx) multilayer system. After a thorough literature search, there is no direct research work has been done about this issue. This question will be an important part of future work.

5.5.7.3. Conformation Change of Glucose Oxidase Glucose oxidase is a dimeric protein (Figure 5-16) with a molecular weight of 160 kDa, containing one tightly bound ( $K_a = 1 \times 10^{-10}$ ) flavin adenine dinucleotide (FAD) per monomer as cofactor (actually two FAD-sites per the enzyme). The two identical monomers of MW circa 80,000 D are connected non-covalently via a long but narrow contact area.

There are 120 contact points between the dimers centered on 11 residues that form either salt linkages or hydrogen bonds. The monomeric molecule is a compact spheroid with approximate dimensions 60 Å x 52 Å x 37 Å. The monomer folds into two structural domains (Figure 5-17). One of the domains binds FAD, and the other is involved with substrate binding. The corresponding dimensions of the dimer are 70 Å x 55 Å x 80 Å. So, one molecule of GOx has two binding sites for substrate. Before the enzyme catalyzed reaction happens, the substrate would bind to the enzyme. According to induced-fit theory [90], the binding process of substrate to enzyme will induce a change in the shape of one or both so that they can fit each other. When they are bound together, neither has the shape it had when free in solution. In this reaction, glucose first bound to GOx. This binding would cause two results: one is the reaction of Equation 5.5 and 5.6 and the other is GOx adjusting its conformation for the second substrate, dioxygen. Dioxygen then bound to GOx, and reaction of Equation 5.7 happened. So the conformation of GOx changed both during the induced-fit binding process and after that. These two will cause a change of the architecture of GOx layers on MCL, so surface

stress of MCL will be changed. That change would make contribution to the bending of MCL. It is not very clear that how much bigger exactly is the conformation change of GOx during the reaction.

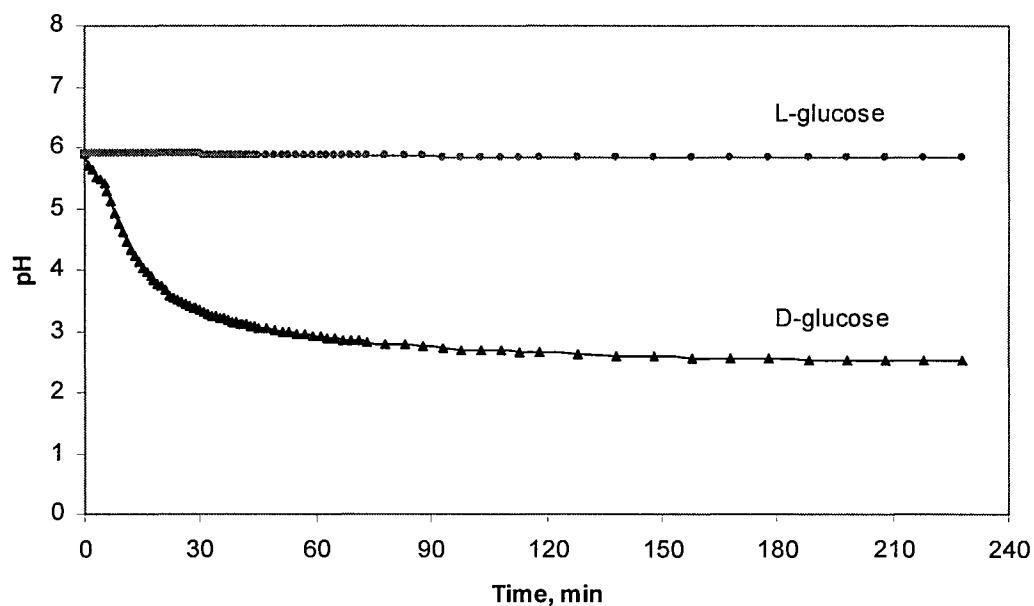


Figure 5-18 pH variation of L-glucose and D-glucose solution upon exposure to glucose oxidase.

Experiments for verification of the contribution of the conformation change of glucose oxidase to the deflection of microcantilever were done using L-glucose. Although the conformation changes of the two combinations are different, a complex of L-glucose with glucose oxidase can provide valuable information on the cantilever deflection mechanism. It was studied that L-glucose can complex with GOx, but no catalyzed reaction occurs [91]. The same concentration of L-glucose and D-glucose, 10mM, were exposed to same glucose oxides, and the pH of the system was measured every minute at the beginning and every five minutes later on. The results were shown in Figure 5-18. For L-glucose, no catalyzed reaction happened after the exposure to glucose

oxides, because no pH change was observed. While for D-glucose, there was a big change in pH, which verified that the glucose oxidase catalyzed reaction was happened.

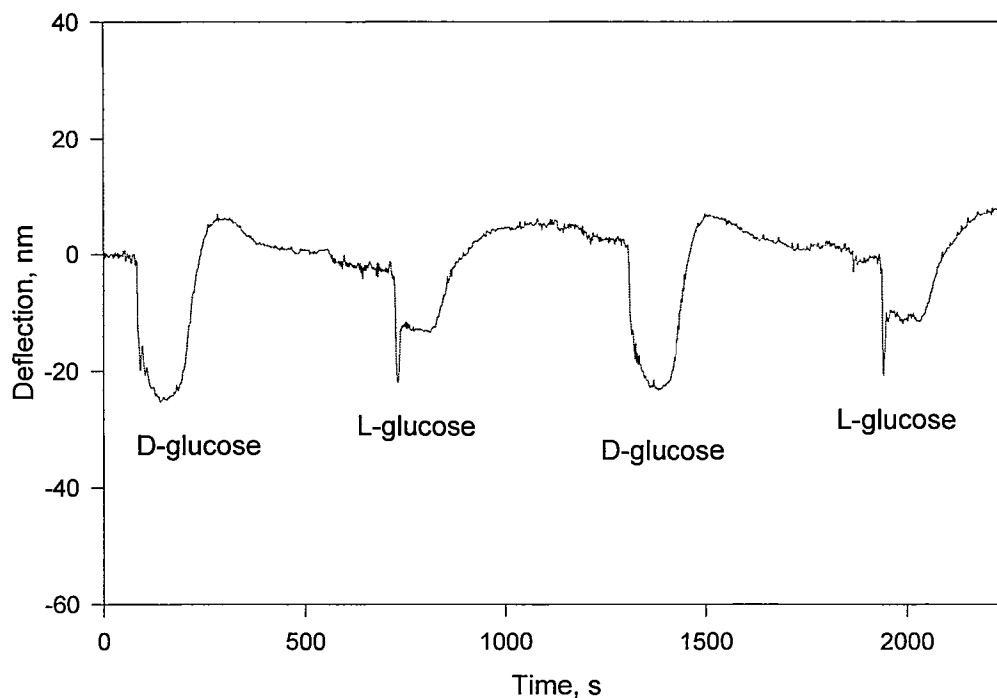


Figure 5-19 Microcantilever deflection upon exposure to 10mM D-glucose and L-glucose.

GOx modified microcantilevers were exposed to 10mM D-glucose and L-glucose solutions, respectively. A different deflection pattern was found (Figure 5-19). For D-glucose the deflection of microcantilever was the same as it was shown in Figure 5-4. But for L-glucose, the microcantilever first reached a downwards peak deflection, and then quickly bent backward and balance at the place different than that of D-glucose. Since the difference between these two sugars is that one catalyzes the reaction while the other does not, the difference in the deflection pattern could be concluded to be the results of the reaction, such as thermal output and products. The common parts of these

two deflection curves can be considered as the contribution from the binding of sugar and the enzyme.

5.5.7.4. Hydrogen Peroxide The last factor that might contribute to the deflection of microcantilever is hydrogen peroxide. Experiments were run by exposure to microcantilevers modified by the same procedure as described in Section 5.4 to  $10^{-2}$ M  $H_2O_2$ , but no bending was observed. Experiments were also run under non-oxygen conditions for the  $10^{-2}$ M glucose solution. The corresponding bending of MCL is similar to that of a normal condition (data not shown).

According to Equation 5.6 -5.7, in the non-oxygen condition, there would be no product of hydrogen peroxides. At this case, if the pattern and the magnitude of deflection of microcantilevers are the same as those of under normal conditions, it confirmed that the presence or absence of hydrogen peroxide has no or a very limited effect on the deflection of the microcantilever.

## 5.6. Summary

This research has shown that a glucose sensor was developed by combination of layer-by-layer enzyme immobilization technology with microcantilever technology. The magnitude of bending is proportional to the concentration of glucose in the range of normal to diabetes blood glucose concentration, and responding time could be down to 10s. It shows specific bending towards glucose, but not with other sugar like mannose, fructose, or galactose. The bending of microcantilever is caused by the surface stress change of its enzyme functionized side. Three factors that might contribute to the bending of microcantilever are the thermal output of the GOx catalyzed reaction, the

conformation change of GOx during the reaction, and the products of the reaction, i.e. gluconic acid and hydrogen peroxide. Among them, gluconic acid appears to be the major contributor. This technique provides an easy, nanoscale control of the sensing part of the sensor with high sensitivity and selectivity. It has great potential to be used as implantable glucose sensor for continuous blood glucose monitoring. It is a platform for enzyme functionized cantilever biosensors.

## CHAPER SIX

### **MICROCANTILEVER MODIFICATION BY HORSERADISH PEROXIDASE (HRP) INTERCALATED NANO-ASSEMBLY FOR HYDROGEN PEROXIDE DETECTION**

#### 6.1. Introduction

The relatively low toxicity and vapor pressure of hydrogen peroxide compared to hydrazine makes it a very attractive substance for propellant for satellites. However, there have been a few reports of hydrogen peroxide leakage from the thrusters during tests. High concentrations of hydrogen peroxide can cause skin and eye irritation. Although the effects are usually benign, direct contact is very painful. Long term accumulation of low concentrations of hydrogen peroxide is also very detrimental to the eyes and lung tissue. In addition to these propellant hazards, highly concentrated hydrogen peroxide exposure has been known to cause tremendous material degradation. Furthermore, since hydrogen peroxide is a byproduct of many enzyme catalyzed reactions, detection of  $H_2O_2$  is of biological importance as well [92-94]. Also, evidence showed that uncontrolled formation of hydrogen peroxide could be a sign of human diseases, such as Parkinson's disease [92].

Current methods for hydrogen peroxide measurements include UV-vis spectrophotometry (UV) [95], chromatography (GC) [96], and high-performance liquid

chromatography (HPLC) [97]. These methods are either not sensitive enough or require instrumentation that is practically non-portable, quite expensive, and very complex. Electrochemical technique [98] has been considered as most promising because of its simplicity and low-cost [99]. However, the sensitivity of this technique is not sufficiently high for early hydrogen peroxide leak detection; the detection limit falls in between the nM and  $\mu$ M range [100-103].

## 6.2. Experimental Material

Silicon microcantilevers used in these experiments were commercially available from Park Instrument, CA. The dimensions of the V-shaped microcantilever were 180  $\mu$ m in length, 20  $\mu$ m in width, and 1  $\mu$ m in thickness. One side of the microcantilever had a thin film of chromium (3nm), followed by a 20 nm layer of gold deposited by e-beam evaporation. Another side of the microcantilever was made of silicon with a thin, naturally grown oxide layer.

(Tridecafluoro-1, 1, 2, 2-tetrahydrooctyl)triethoxysilane (TTS) was used to develop a thin perfluorocarbon film on the silicon surface using a typical surface modification procedure. This non-sticky perfluorocarbon coating was used to control the formation of multilayers only on the gold surface of the microcantilever because the differentiation between the two sides of a microcantilever is essential for cantilever deflection.

Cationic polyethyleneimine (PEI), anionic poly(sulfonate styrene) (PSS), and horseradish peroxidase (HRP, Sigma, EC 1.11.7, type VI, 263,000unit/g, isoelectric point (pI) = 9.0, it is positive charged at pH = 6.5) were used for microcantilever surface



modification by using a layer-by-layer self-assembly technique. All solution were prepared in a 0.01M NaCl solution with pH = 6.5.

### 6.3. Microcantilever Modification

The formation of a multilayer on the microcantilever was conducted at pH = 6.5 using the following multilayer formation procedure: a TTS treated microcantilever was immersed in a  $10^{-2}$  M mercaptoethanesulfonate (MES) solution for 12 hours to form a negatively charged film on the gold surface. This negatively charged film could strengthen the stability of the multilayer film on the gold surface of the microcantilever. The microcantilever was then immersed into a 1.5 mg/mL solution of PEI (or HRP 1mg/ml) for 20 minutes, and rinsed with a stream (~100 ml/min) of water for 30s.

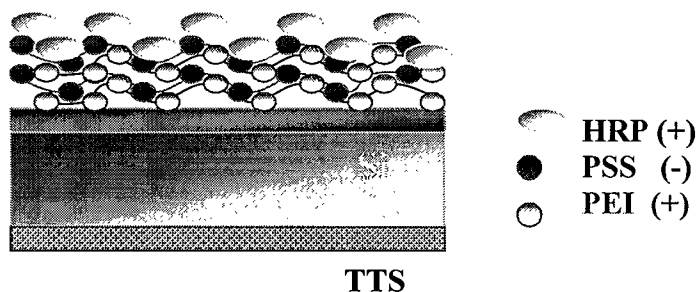


Figure 6-1 Schematic of microcantilever modification. The final nano-assembly on the gold side of silicon microcantilevers were  $MES/(PEI/PSS)_3/(HRP/PSS)_3$

The cantilever was then immersed into a 3 mg/mL solution of PSS also for duration of 20 minutes and again rinsed with the water stream. This procedure was repeated several times until a desired multilayer film was formed. In this experiment, the final structure of the multilayer on the gold side of microcantilevers (Figure 6-1) were  $MES/(PEI/PSS)_3$ , followed by  $(HRP/PSS)_3$ .

#### 6.4. Experiment Setup and Procedure

The experiment setup was the same as described in Section 2.5. The microcantilevers were initially exposed to a constant flow (4mL/h) of a 0.01M NaCl solution in a fluid cell. The NaCl solution was circulated through the cell using a syringe pump. For each measurement of the deflection of microcantilever, a 2.0-mL aliquot of the hydrogen peroxide solution at certain concentration was switched into the fluid cell where the microcantilever was held. It took 30 minutes for the injected hydrogen peroxide solution to flow through the fluid cell, and at this time, the original 0.01M NaCl solution was circulated back into the fluid cell. Since HRP lost certain level of activity after exposure to hydrogen peroxide,<sup>33</sup> a freshly modified microcantilever was used for each experiment.

#### 6.5. Results and Discussion

##### 6.5.1. Typical Deflection of Microcantilever Upon Exposure to Hydrogen Peroxide Solution

When a solution of 1mM hydrogen peroxide was injected into the fluid cell, the microcantilever bent downwards immediately after injection (Figure 6-2).

The bending amplitude increased quickly and reached its maximum in approximately 10 minutes. The deflection amplitude maintained at this level before the H<sub>2</sub>O<sub>2</sub> solution was replaced by the 0.01M NaCl solution 30 minutes after H<sub>2</sub>O<sub>2</sub> rejection. When the H<sub>2</sub>O<sub>2</sub> solution was flush out of the fluid cell, the microcantilever gradually bent back to its original position. It took approximately 100 minutes for the cantilever to return to its original deflection position, suggesting a slow enzyme restoring process. The

slow restoring process is consistent with the observation that third step of the reaction is the rate-limiting step in peroxidase catalysis [104].

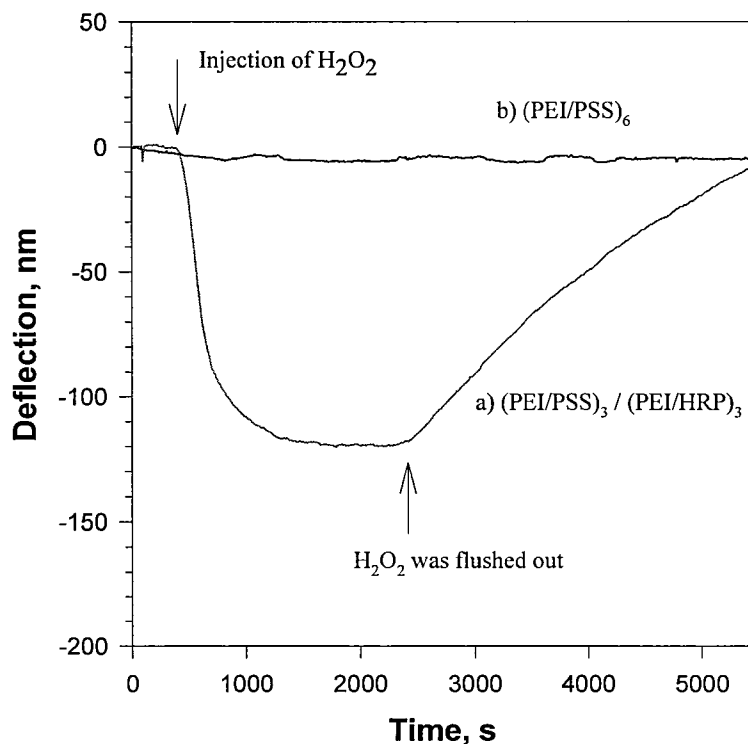


Figure 6-2 Deflection of microcantilevers upon exposure to a 1mM hydrogen peroxide solution. The microcantilevers were modified with a)  $(\text{PEI/PSS})_3 / (\text{PSS/HRP})_3$  and b)  $(\text{PEI/PSS})_6$ .

The control experiment was carried out with a microcantilever modified with a multilayer composite of  $(\text{PSS/PEI})_6$ , which is also shown in Figure 6-2. In the absence of HRP, this cantilever did not deflect when it was exposed to a 1 mM hydrogen peroxide solution. This result clearly indicated that the deflection of a microcantilever was generated from reduction of hydrogen peroxide to  $\text{H}_2\text{O}$  by the immobilized HRP enzyme.

### 6.5.2. Deflection of Microcantilever Upon Exposure to Different Concentrations of Hydrogen Peroxide

The deflection amplitude of HRP immobilized microcantilever was proportional to the concentration of hydrogen peroxide (Figure 4). In this work, the cantilever deflected 5 nm at  $1 \times 10^{-9}$  M concentration of  $\text{H}_2\text{O}_2$ . Since the noise level can be controlled within 1 nm when the experimental conditions, such as temperature, are well controlled, the detection limit for HRP multilayer modified cantilever can be claimed as low as  $1 \times 10^{-9}$  M.

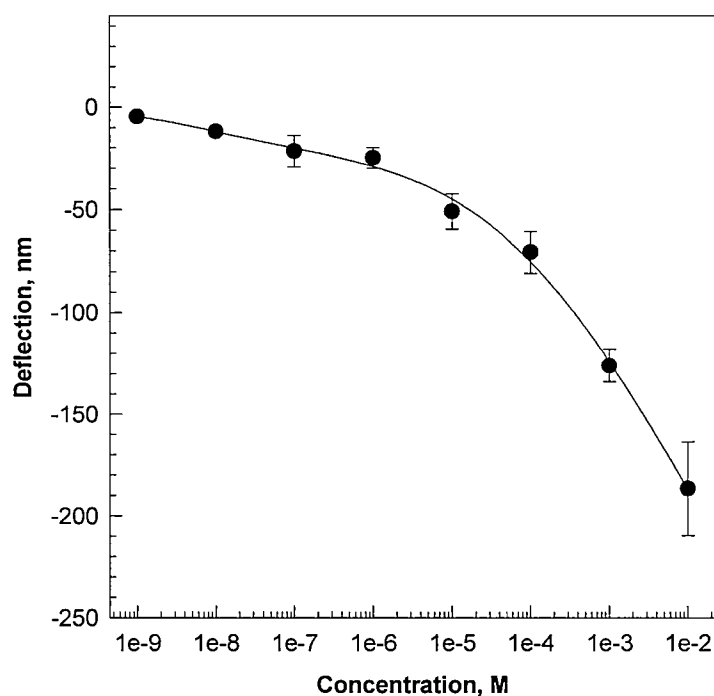


Figure 6-3 The average maximum deflection of  $(\text{PEI}/\text{PSS})_3/(\text{HRP}/\text{PSS})_3$  modified microcantilevers at different hydrogen peroxide concentrations.

### 6.5.3. Selectivity

Possible interfering gases in air for  $\text{H}_2\text{O}_2$  detection include  $\text{CO}_2$ ,  $\text{SO}_2$ ,  $\text{H}_2\text{S}$ ,  $\text{NO}_2$ ,  $\text{NO}$ , etc. These gases form acids when they come into contact with water. Figure 6-3 is bending responses of the  $(\text{PEI}/\text{PSS})_3/(\text{PSS}/\text{HRP})_3$  modified microcantilevers to  $1 \times 10^{-5}$  M solutions of these acids compared with bending response to a  $1 \times 10^{-6}$  M solution of hydrogen peroxide. None of these chemicals caused as much deflection of the cantilever as  $\text{H}_2\text{O}_2$  does, suggesting that such HRP-modified cantilevers could be a  $\text{H}_2\text{O}_2$  sensors with high selectivity.

### 6.5.4. Sensing Mechanism

Horseshoe peroxidase is a heme-containing peroxidase (EC 1.11.1.7.), and it reduces hydrogen peroxide through a three-step reaction [105-107]. The optimum catalytic reaction occurs in the pH range of 6.0 to 6.5.

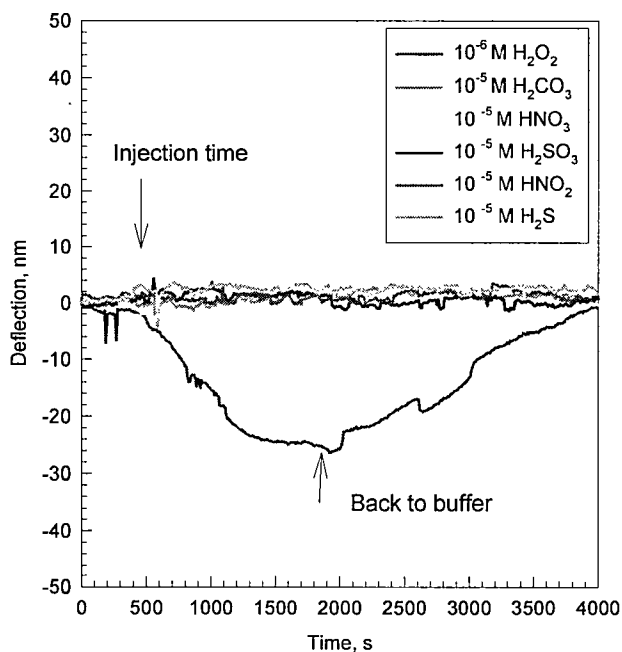
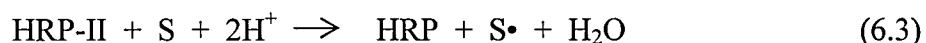
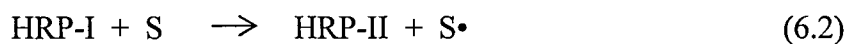


Figure 6-4 Deflection of  $(\text{PEI}/\text{PSS})_3/(\text{HRP}/\text{PSS})_3$  modified microcantilevers to a  $1 \times 10^{-6}$  M solution of hydrogen peroxide and  $1 \times 10^{-5}$  M concentration of different acids solutions.



where HRP-I and HRP-II are oxidized intermediates of HRP that were often referred to as compounds I and II, respectively, and S and S• are an electron donor substrate and the radical product of the oxidation reaction. In the absence of donor substrates, protein amino acid residues in HRP itself can provide electrons [108]. The reaction is an exothermic reaction, and in the reaction there are structural or conformation changes of the enzyme, hydrogen peroxides. Both the structural or conformation change of HRP and the thermal output produced from the reaction could contribute to the cantilever deflection. The ratio of contribution from each part is not clear yet and needed to be investigated in future work.

### 6.6. Summary

This research has shown that microcantilevers modified by HRP containing multilayer nano-assembly responded quantitatively to horseradish peroxide, which could be potentially used for the detection of hydrogen peroxide. By changing microcantilever materials and optimizing the structures, the detection limit can be further improved. Layer-by-layer technique provides a supreme approach for cantilever sensor development. A controllable multilayer modification method could be used to detect many other chemical and biological species when different enzymes or receptors are embedded in the multilayer. In the experiments, the measurements will be conducted by bench-top optical instruments to demonstrate the feasibility of multilayer methods for cantilever

modifications. However, it is noteworthy that piezoresistive microcantilever-based devices are better applied for on site chemical detections. Without the loss of sensitivity, the piezoresistive method eliminates the complexity inherent to optical instruments, which require laser system adjustment.

## CHAPTER SEVEN

### CONCLUSIONS AND FUTURE WORK

#### 7.1 Conclusions

In this research work, self-assembly monolayer(SAM) and layer-by-layer(LbL) were successfully used in the modification of microcantilevers for biosensing applications. This result constitutes the first time that the layer-by-layer technique was used for forming nano assembly with recognition molecules inside on one side of the microcantilever surface. The following results have been achieved in this research.

1. Developed a procedure for modification of microcantilever using layer-by-layer technique.
2. Developed a glucose sensor using microcantilever with layer-by-layer nano assembly containing glucose oxidase. The sensor has a responding time in the range of seconds.
3. Developed a hydrogen peroxide sensor using microcantilever with layer-by-layer nano assembly containing hydrogen peroxide. The detection limit for this sensor is  $10^{-9}$ M.
4. Developed a sensor for detection of biowarfare agents. For the measurement of Tularemia, this sensor reached the detection limit of  $10^3$  organism/ml.



5. Developed a sensor for detection of chemical warfare agents with sensitivity of  $10^{-7}$ M for organophosphates.

The results obtained from this research have demonstrated that the microcantilever-based biosensors can be developed for detection of various biomolecules or monitoring different processes. The glucose sensor developed in this research has great potential to be used as implantable glucose sensor for continuous blood glucose monitoring, which is critical in diabetes care. And the sensor for detection of biowarfare agents could be used for homeland security, which is one of the most important issues of the nation.

### 7.2 Future Work For This Research

This research work can go further on following research works.

1. Develop new modification methods for microcantilevers, such as using hydrogel, so-gel, nanoparticle, etc.
2. For layer-by-layer method, the diffusion constant of some related chemicals in the multilayer system could be measured. That would provide a better understanding of the reasons that caused the bending of microcantilever.

### 7.3 Future Work for Microcantilever-Based Biosensor Development

Microcantilevers provide an ideal platform for biosensors. The micron-sized transducer brings several advantages, such as high sensitivity, small quantity of sample for analysis, the possibility to be portable, implantable sensor devices, ability to be mass produced and integrated into standard microelectronic processing technologies like

complementary metal oxide semiconductors (CMOS). The above summarized examples demonstrate that microcantilever-based biosensors can be developed for detection of various biomolecules or monitoring different bioprocesses. We can foresee the upcoming of more microcantilever biosensors for different biosensing purposes. However, there is a long way to go to convert these results to robust commercially available products. Efforts in following areas are critical.

1) Development of robust microcantilever modification procedures. This step is critical in making commercially available cantilever sensor devices. Modification methods are different from case to case, so adjustment is necessary for each case. The modified coating should be uniform and normally applied only on one side of microcantilever; the modification procedure should be easy to use.

2) Optimizations of cantilever materials, dimensions, and shapes for best performance. Microcantilevers in most case are made of silicon, or silicon nitride. Silicon dioxide microcantilevers demonstrated a larger deflection under the same surface stress because of its low spring constant [109]. Microcantilevers made from other materials, such as SU-8 [110], Polystyrene [110], or alloys [111] [112] were developed for biosensing applications. Simulation and modeling are useful tools for the optimization [114-117].

3) Deflection detection system. For implantable biosensing applications or for the operation of tens to hundreds of cantilever arrays which are a few microns apart from the neighbor ones, the deflection detection based on the piezoresistive approach seems to be most suitable. The performance of these piezoresistive cantilevers needs to be further

improved although many piezoresistive microcantilever sensors have been developed (Gunter, R. L., et al, 2004; Kooser, A., et al, 2003).

Microcantilever-based biosensor is very promising, and the limitation on microcantilever-based biosensors will be reduced or eliminated through the above optimizations.

## REFERENCES

1. Chen, G. Y.; Warmack, R. J.; Thundat, T.; Allison, D. P. and Huang, A., *Rev. Sci. Instrum.* **1994**, *65*, 2532.
2. Thundat, T.; Warmack, R. J.; Chen, G. Y. and Allison, D. P., *Appl. Phys. Lett.* **1994**, *64*, 2894.
3. Gimzewski, J. K.; Gerber, C.; Meyer, E. and Schlittler, R. R., *Chem. Phys. Lett.*, **1994**, *217*, 589.
4. Stoney, G. G. *Proc. Roy. Soc. (London)*, **1909**, *82*, 172.
5. Fritz, J.; Baller, M. K.; Lang, H. P.; Rothuizen, H.; Vettiger, P.; Meyer, E.; Guntherodt, H.-J.; Gerber, Ch.; Gimzewski, J. K., *Science*, **2000**, *288*, 316.
6. McKendry, R.; Zhang, J.; Arntz, Y.; Strunz, T.; Hegner, M.; Lang, H. P.; Baller, M. K.; Certa, U.; Meyer, E.; Guntherodt, H.; and Gerber, C, *P Natl. Acad. Sci. USA*, **2002**, *99*, 9783.
7. Wu, G.; Ji, H.-F.; Hansen, K.; Thundat, T.; Datar, R.; Cote, R.; Hagan, M. F.; Chakraborty, A. K. and Majumdar, A., *P Natl. Acad. Sci. USA*, **2001**, *98*, 1560.
8. Hansen, K. M.; Ji, H-F; Wu, G.; Datar, R.; Cote, R.; Majumdar, A.; Thundat, T., *Anal. Chem.*, **2001**, *73*, 1567.
9. Holmberg, M.; Kuhle, A.; Garnæs J.; Boisen, A., *Ultramicroscopy*, **2003**, *97*, 257.
10. Bietsch, A.; Zhang, J.; Hegner, M.; Lang, H. P.; and Gerber, C., *Nanotechnology*, **2004**, *15*, 873.
11. Bietsch, A.; Hegner, M.; Lang, H. P.; and Gerber, C., *Langmuir*, **2004**, *20*, 5119.
12. Stevenson, K. A.; Mehta, A.; Sachenko, P.; Hansen, K. M.; Thundat, T, *Langmuir*, **2002**, *18*, 8732.
13. Alvarez, M.; Carrascosa, L. G.; Moreno, M.; Calle, A.; Zaballos, A; Lechuga, L. M.; Martinez-A, C; and Tamayo, J.; *Langmuir*, **2004**, *20*, 9663.

14. Hagan, M. F.; Majumdar, A.; Chakraborty, A. K., *J. Phys. Chem. B*, **2002**, 106, 10163.
15. Liu, F.; Zhang, Y.; Ou-Yang, Z., *Biosens. Bioelectron.*, **2003**, 18, 655.
16. Savran, C. A.; Knudsen, S. M.; Ellington, A. D.; and Manalis, S. R., *Anal. Chem.*, **2004**, 76, 3194.
17. Savran, C. A.; Sparks, A. W.; Sihler, J.; Li, J.; Wu, W. C.; Berlin, D. E., *J Microelectromech. S.*, **2002**, 11, 703
18. Marie, R.; Jensenius, H.; Thaysen, J.; Christensen, C. B.; Boisen, A., *Ultramicroscopy*, **2002**, 91, 29.
19. Gunter, R. L.; Zhine, R.; Delinger, W. G.; Manyoats, K.; Kooser, A. and Porter, T. L. *IEEE Sensors J.*, **2004**, 4, 430.
20. Tortonese, M.; Barret, R.C.; Quate, C. F.; *Appl. Phys. Lett.*, **1993**, 62, 834.
21. Linnemann, R.; Gotszalk, T.; Hadjiiski, L.; Rangelow, I.W., *Thin Solid Film*, **1995**, 264, 195.
22. Weizmann, Y.; Patolsky, F.; Lioubashevski, O.; and Willner, I., *J. Am. Chem. Soc.*, **2004**, 9, 1073.
23. Raiteri, R.; Nelles, G.; Butt, H.; Knoll, W.; Skladal, P.; *Sens. Actuat. B-Chem.*, **1999**, 61, 213.
24. Wu, G.; Datar, R. H.; Hansen, K. M.; Thundat, T.; Cote, R. J.; Majumdar, A., *Nat. Biotechnol.*, **2001**, 19, 856.
25. Arntz, Y; J D Seelig, H P Lang, J Zhang, PHunziker, J P Ramseyer, E Meyer, M Hegner and Ch Gerber, *Nanotechnology*, **2003**, 14, 86.
26. Dutta, P.; Tipple, C. A.; Lavrik, N. V.; Datskos, P. G.; Hofstetter, H.; Hofstetter, O.; Sepaniak, M. J., *Anal. Chem.*, **2003**, 75, 2342.
27. Zhang, J. and Ji, H-F., *Anal. Sci.*, **2004**, 20, 585.
28. Patel, N.; Davies, M. C.; Hartshorne, M., *Langmuir*, **1997**, 13, 6485.
29. Gupta, A.; Akin, D.; and Bashir, R.; *Appl. Phys. Lett.*, **2004**, 84, 1976.
30. Ilic, B.; Czaplewski, D.; Craighead, H. G.; Neuzil, P.; Campagnolo, C.; and Batt, C., *Appl. Phys. Lett.*, **2000**, 77, 450.

31. Ilic, B.; Czaplewski, D.; Zalalutdinov, M.; Craighead, H. G.; Neuzil, P.; Campagnolo, C. and Batt, C., *J. Vac. Sci. Technol. B*, **2001**, 19, 2825.
32. Ilic, B.; Yang, Y.; and Craighead, H. G.; *Appl. Phys. Lett.*, **2004**, 85, 2604.
33. Ji, H-F; Yan, X.; Zhang, J.; and Thundat, T., *Expert Rev. of Mol. Diagn.*, **2004**, 4, 859.
34. Weeks, B. L.; Camarero, J.; Noy, A.; Miller, A. E.; Stanker, L.; and Yoreo, J.J. D., *Scanning*, **2003**, 25, 297.
35. Grogan, C.; Raiteri, R.; O'Connor, G. M.; Glynn, T. J.; Cunningham, V.; Kane, M.; Charlton, M.; Leech, D., *Biosens Bioelectron*, **2002**, 17, 201.
36. Kim, B. H.; Mader, O.; Weimar, U.; Brock, R.; Kern, D. P., *J. Vac. Sci. Technol. B*, **2003**, 21, 1472.
37. Alvarez, M.; Calle, A.; Tamayo, J.; Lechuga, L.; Abad, A.; Montoya, A.; *Biosens Bioelectron*, **2003**, 18, 649.
38. Kooser, A.; Manygoats, K.; Eastman, M.P.; Porter, T.L.; *Biosens. Bioelectron.*, **2003**, 19, 503.
39. Moulin, A. M.; S. J. O'Shea; R. A. Badley; P. Doyle; and M. E. Welland, *Langmuir*, **1999**, 15, 8776.
40. Subramanian, A.; Oden, P. I.; Kennel, S. J.; Jacobson, K. B.; Warmack, R. J.; Thundat, T.; Doktycz, M. J., *Appl. Phys. Lett.*, **2002**, 81, 385.
41. Pei, J.; Tian, F.; and Thundat, T., *Anal. Chem.*, **2004**, 76, 292.
42. Brown, M.A.; Brix, K. A.. *J. Appl. Toxicol.*, **1998**, 18, 393.
43. Ulman, A., *Ultrathin Organic Films*, Academic Press, **1991**.
44. Bain, C.; Troughton, B.; Tao, Y.; Evall, J.; Whiteside, G.; Nuzzo, R., *J. Am. Chem. Soc.*, **1989**, 111, 321
45. Wasserman, S.; Tao, Y.; Whiteside, G., *Langmuir*, **1989**, 5, 1074
46. Liedberg, B.; and Tengvall, T., *Langmuir*, **1995**, 11, 3821.
47. Creager, S.E.; Olsen, K.G., *Anal. Chem.*, **1995**, 307, 277.
48. Jaffrezic-Renault, N., *Sensors*, **2001**, 1, 60.

49. Boublik, Y.; Saint-Aguet, P.; Lougarre, A.; Arnaud, M.; Villatte, F.; Estrada-Mondaca, S.; Fournier, D., *Protein Eng.*, **2002**, 15, 43.
50. Chen, G. Y.; Thundat, T.; Wachter, E. A.; Warmack, R. J., *J. Appl. Phys.* **1995**, 77, 3618.
51. <http://ntri.tamuk.edu/immunology/proter.gif>
52. <http://129.128.91.75/de/immunology/70imm-rx.htm>
53. Tularemia, B., CRC Handbook Series in Zoonoses, volume two. CRC Press, Fl, USA, 1980, 161.
54. Wong, J.; Shapiro, F., *Manual of Clinical Microbiology, seventh edition*. ASM Press, 1999, 647.
55. Pomanskaia, L., *J. Microbiol. Epidemiol. Immunobiol.* **1957**, 28, 597.
56. Overholt, E.; Tigertt, W.; Kadull, P., *Am. J. Med.* **1960**, 30, 785.
57. Sandström, G.; Sjöstedt, A.; Johansson, T.; Kuoppa, K.; Williams, J.; *Microbiol. Immunol.* **1992**, 5, 201.
58. Sawyer, W.; Dangerfield, H.; Hogge, A.; Crozier, D.; *Bacteriol. Rev.*, **1966**, 30, 542.
59. White, J.; McGavran, M.; *JAMA*, **1965**, 194, 294.
60. Decher, G., *Science*, **1997**, 277, 1232.
61. Yoo, D.; Shiratori, S.; Rubner, M.; *Macromolecules*, **1998**, 31, 4309.
62. J.B. Schlenoff, S.T. Dubas, *Macromolecules*, **2001**, 34, 139.
63. Harris, J.J.; Stair, J.L.; Bruening, M.L.; *Chem. Mater.*, **2000**, 12, 1941.
64. Lvov, Y.; Lu, Z.; Zu, X.; Schenkman, J.; Rusling, J.; *J. Am. Chem. Soc.*, **1998**, 120, 4073.
65. Lvov, Y.; Ariga, K.; Ichinose, I.; Kunitake, T.; *J. Am. Chem. Soc.* **1995**, 117, 6117.
66. Ai, H.; Fang, M.; Jones, S.; Y. Lvov, *Biomacromolecules*, **2002**, 3, 560.
67. Ai, H.; Jones, S.; Villiers, M. De; and Lvov, J., *J. Controlled Release*, 2003, 86, 54.

68. Antipov, A.A.; Sukhorukov, G.B.; Möhwald, H.; *Langmuir*, **2003**, 19, 2444.
69. Lvov, Y.; Antipov, A.A.; Mamedov, A.; Möhwald, H.; Sukhoruhov, G.B.; *Nano Letters*, **2001**, 1, 125.
70. Radtchenko, I.L.; Sukhorukov, G.B.; H. Möhwald, *Int. J. of Pharm.*, **2002**, 242, 219.
71. Iler, R.; *J. Colloid & Interface Sci.*, **1966**, 21, 569.
72. Keller, S.; Kim, H-N.; and Mallouk, T.; *J. Am. Chem. Soc.*, **1994**, 116, 8817.
73. Decher, G. and Hong, J-D.; *Ber. Bunsenges. Phys. Chem.* **1991**, 95, 1430.
74. Lvov, Y.; Decher, G. and Möhwald, H.; *Langmuir*, **1993**, 9, 481.
75. Lvov, Y.; Decher, G. and Sukhorukov, G.; *Macromolecules*, **1993**, 26, 5396.
76. Lvov, Y.; Essler, F. and Decher, G.; *J. Phys. Chem.*, **1993**, 97, 13773.
77. Lvov, Y.; Haas, H.; Decher, G.; Möhwald, H.; and Kalachev, A.; *J. Phys. Chem.*, **1993**, 97, 12835.
78. Yoo, D.; Lee, J. and Rubner, M.; *Mat. Res. Symp. Proc.*, **1996**, 413, 395.
79. Cooper, T.; Campbell, A.; and Crane, R.; *Langmuir*, **1995**, 11, 2713.
80. Ariga, K.; Lvov, Y. and Kunitake, T.; *J. Am. Chem. Soc.*, **1997**, 119, 2224.
81. Lvov, Y.; Ariga, K.; Ichinose, I. and Kunitake, T.; *Langmuir*, **1997**, 13, 6195.
82. Lvov, Y.; Rusling, J.; Thomsen, D.; Papadimitrakopoulos, F.; Kawakami, T. and Kunitake, T.; *Chem. Commun.*, **1998**, 318, 1229.
83. Lvov, Y.; p. 125-136 in book: *"Protein Architecture: Interfacial Molecular Assembly and Immobilization Biotechnology"*, Editors: Y. Lvov and H. Möhwald, Marcel Dekker Publ., **2000**, NY;
84. Sano, M.; Lvov, Y. and Kunitake, T.; *Ann. Rev. Material Science*, **1996**, 26, 153.
85. Gibson, Quentin H.; Swoboda, Bennett E. P.; Massey, Vincent, *J. of Bio. Chem.*, **1964**, 239, 3927.
86. Duke, F. R.; Weibel, M.; Page, D.S.; Bulgrin, V.G.; and Luthy, J., *J. Am. Chem. Soc.*, **1969**, 91, 3904.



87. Klitzing, R. and Mohwald, H., *Macromolecules*, **1996**, 29, 6901.
88. Timoshenko, S.; **1925**, *J. Opt. Soc. Am.*, 11, 233.
89. Protein Data Bank, <http://www.rcsb.org/pdb/>
90. Amend, J. R.; Mundy, B. P.; Arnold, M. T.; "General, Organic and Biological Chemistry," Saunders College Publishing, **1993**, pp.772 – 777.
91. Higchi, A.; Ogawa, S.; Nakagawa, T.; *J. Chem. Faraday Trans.*, **1991**, 87, 695
92. Kulagina, N. V. and Micheal, A. C. *Anal. Chem.* **2003**, 75, 4875.
93. You, T.; Niwa, O.; Tomita, M. and Hirono, S.; *Anal. Chem.* **2003**, 75, 2080.
94. Hoshi, T.; Saiki, H.; Kuwazawa, S.; Tsuchiya, C.; Chen, Q. and Anzai, J.; *Anal. Chem.* **2001**, 73, 5310.
95. Matsubara, C.; Kawamoto, N.; Takamala, K.; *Analyst*, **1992**, 117, 1781.
96. Nyarady, A. S.; Barkley, R. M.; Sievers, R. E.; *Anal. Chem.* **1985**, 57, 2074.
97. Hamano, T.; Mitsuhashi, Y.; Yamamoto, S.; *J. Chromatography*, **1987**, 411, 423.
98. Wollenberger, U.; Wang, J.; Ozsoz, M.; Gonzalez-Romero, E.; Scheller, F.; *Bioelectrochem. Bioenerg.*, **1991**, 26, 287.
99. Hall, E.; in *Biosensors*, Edit by Milton Keynes, Prentice Hall.
100. Yu, X.; Sotzing, G. A.; Papadimitrakopoulos, F. and Rusling, J. F. *Anal. Chem.* **2003**, 75, 4565.
101. Raffa, D. K.; Leung, T. and Battaglini, F.; *Anal. Chem.* **2003**, 75, 4983.
102. Jia, J.; Wang, B.; Wu, A.; Cheng, G.; Li, Z.; and Dong, S.; *Anal. Chem.* **2002**, 74, 2217.
103. Yu, J. and Ju, H. *Anal. Chem.*, **2002**, 74, 3579.
104. Dunford, H. B. in *Peroxidase in Chemistry and Biology*, Edited by J. Everse, K. E. Everse, and M. B. Grisham, CRC Press, Boca Raton, FL, **1991**, Vol. 2, pp.1 - 24.
105. Gajhede, M.; Schuller, D. J.; Henriksen, A.; Smith, A. T. and Poulos, T. L. *Nature, Struct. Biol.*, **1997**, 4, 1032.

106. Henriksen, A.; Schuller, D. J.; Meno, K.; Welinder, K. G.; Smith A. T. and Gajhede, M.; *Biochemistry*, **1998**, 37, 8054.
107. Vianello, F.; Zennaro, L.; M. Paolo, L. D.; Rigo, A.; Malacarne C. and Scarpa, M., *Biotechnol. Bioeng.*, **2000**, 68, 488.
108. Gazaryan, I. G.; Chubar, T. A.; Ignatenko, O. V.; Mareeva, E. A.; Orlova, M. A.; Kapeliuch, Y.L.; Savitsky, P. A.; Rojkova, A. M. and Tishkov, V. I.; *Biochem. Biophys. Res. Commun.*, **1999**, 262, 297.
109. Tang, Y.; Fang, J.; Yan, X.; Ji, H-F, *Sens. Actuat. B-Chem.*, **2004**, 97, 109.
110. Calleja, M. Tamayo, J.; Johansson, A.; Rasmussen, P.; Lechuga, L.; and Boisen, A., *Sensor Lett.*, **2003**, 1, 1.
111. McFarland, A. W. Poggi, M. A. Bottomley, L. A. and Colton, J. S., *Rev. Sci. Instrum.*, **2004**, 75, 2756.
112. Lee, J. H.; Kim, T. S.; Yoon, K. H., *Appl. Phys. Lett.*, **2004a**, 84, 3187.
113. Lee, J. H.; Yoon, K. H.; Hwang, K. S.; Park, J.; Ahn, S.; Kim, T. S., *Biosens. Bioelectron.*, **2004b**, 20, 269.
114. Ren, Q.; Zhao, Y-P, *Microsystem Tech.*, **2004**, 10, 307.
115. Khaled, A.; Vafai, K., *J. Micromech. Microeng.*, **2004**, 14, 1220.
116. Khaled, A.; Vafai, K., Yang, M., Zhang, X., Ozkan, C. S., *Sensors Actuat B-Chem.*, **2003**, 94, 103.
117. Hou, M.; Chen, R., *J. Micromech. Microeng.*, **2004**, 14, 409.
118. Gunter, R. L.; Zhine, R.; Delinger, W. G.; Manygoats, K.; Kooser, A. and Porter, T. L. *IEEE Sensors J.*, **2004**, 4, 430.
119. Kooser, A.; Manygoats, K.; Eastman, M.P.; Porter, T.L.; *Biosens. Bioelectron.*, **2003**, 19, 503.